University of Naples, Federico II
PhD in Chemical science, XXXI cycle


# Structural characterisation of endotoxins from marine and halophilic bacteria

Clara Barrau

Tutor: Prof. Alba Silipo
Co-tutor: Prof. Antonio Molinaro
Supervisor: Dr. Angela Arciello

*If you can't fly, run,*
*if you can't run, walk,*
*if you can't walk, crawl,*
*but by all means, keep moving.*

- Martin Luther King Jr.

# Abstract

Gram-negative bacteria cell envelope is a complex structure that is constantly exposed to its environment. It is composed of an Inner-membrane (IM), a thin peptidoglycan layer and an Outer-membrane (OM)[a]. The main component of the OM are Lipopolysaccharides (LPS), also termed as endotoxins. Those molecules are composed of three main parts: a polysaccharide named the O-antigen, a core oligosaccharide and a Lipid A[b]. Endotoxins lacking the polysaccharide are termed Lipooligosaccharides (LOS).

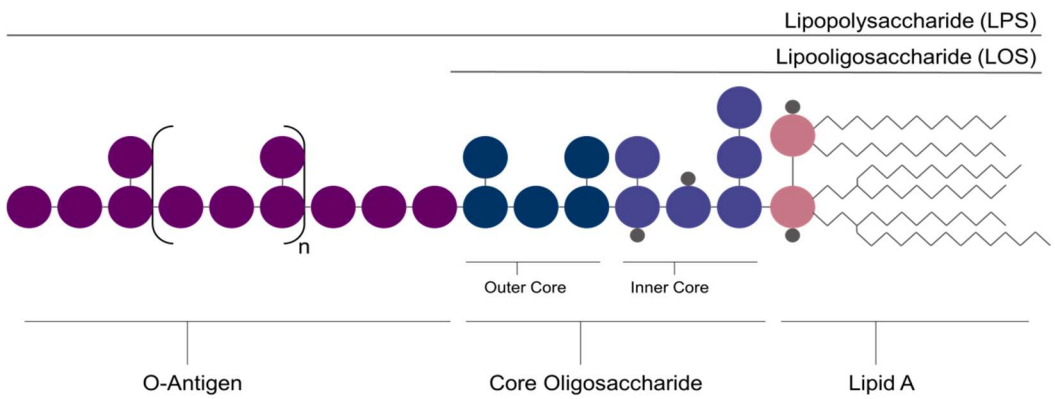


General structure of LPS and LOS

LPS are known to interact with mammal's innate immunity through the Toll-like receptor 4 (TLR4) and Myeloid Differentiation factor 2 (MD-2) receptorial complex[c]. Depending on their structure, and in particular on their

[a] Silhavy, T.J.; Kahne, D.; Walker S.; *Cold Spring Harb. Perspect. Biol.* **2010**, 2:a000414
[b] Raetz, C.R.H.; Whitfield C.; *Annu. Rev. Biochem.* **2002**, 71, 635–700
[c] Kieser, K.J.; Kagan J.C.; *Nat. Rev. Immunol.* **2017**, 17, 377-390

Lipid A, LPS can either have an agonist or an antagonist activity[d]. Discovering new LPS structure is hence necessary in order to develop new therapies, since agonist LPS can be used as vaccines adjuvant and antagonist as drugs against sepsis and septic shock.

In this context, LPS structures from various bacterial sources are currently under study. This project present the characterization of LPS and LOS extracted from marine and halophilic bacteria. As those organisms live in a particular environment, they developed specific strategies to adapt themselves and were hence investigated, as their LPS structure can be shaped by the adaptation to their environment[e]. In particular, the study of LPS from the following strains is here reported.

*Pseudoalteromonas sp1A1* is a sponge-pathogen bacterium isolated from *Suberites domuncula*[f]. The full structure of its LPS was resolved using NMR spectroscopy and Matrix assisted laser desorption (MALDI) Mass spectrometry (MS). Its O-antigen is a branched polysaccharide that have two remarkable features: (i) it possesses a pyruvate linked at 4,6-position of a Glucosamine and (ii) it possesses a 9-carbon ulosonic acid that is the 3-deoxy-D-*glycero*-D-*galacto*-nonulosonic acid (KDN).

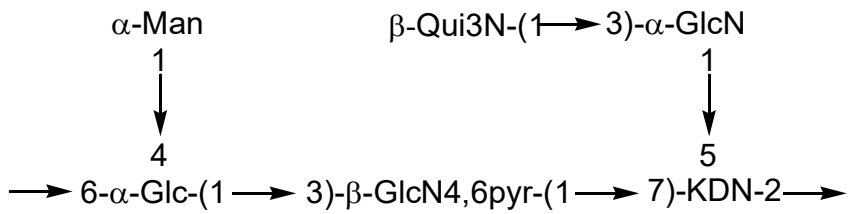


Structure of the O-antigen from *Pseudoalteromonas sp1A1*

[d] Molinaro, A; Holst, O; Di Lorenzo, F; Callaghan, M; Nurisso, A; D'Errico, G; Zamyatina, A; Peri, F; Berisio, R; Jerala, R; Jimenez-Barbero, J; Silipo, A; Martin-Santamaria, S.; *Chem. Eur. J.* **2015**, 21, 500 – 519
[e] Di Lorenzo, F.; Billod, J.M.; Martín-Santamaría, S.; Silipo, A.; Molinaro, A. *Eur. J. Org. Chem.* **2017**, 28, 4055–4073
[f] Gardères, J.; Bedoux, G.; Koutsouveli, V.; Crequer, S.; Desriac, F.; Le Pennec, G.; *Mar. Drugs* **2015**, 13, 4985-5006

The Lipid A from *Pseudoalteromonas sp1A1* was studied by MALDI MS. It is constituted of a mixture of tri- to penta-acylated species, among the penta-acylated Lipid A species, at *m/z* 1474.6 and 1446.6 were *bis*-phosphorylated species composed respectively of four C12:0 (3-OH) and one C12:0 and two C12:0 (3-OH), one C10:0 (3-OH), one C11:0 (3-OH) and one C13:0.

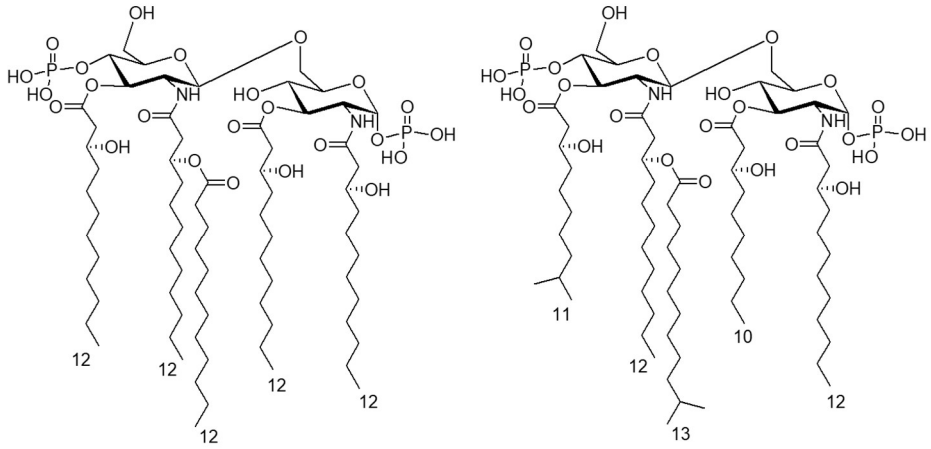

Structure *Pseudoalteromonas sp1A1* Lipid A species

The structure of the core oligosaccharide from *Pseudoalteromonas sp1A1* LPS was also resolved and turned out to be composed of a pentasaccharide containing one Kdo, one heptose, two galactoses and one glucose.

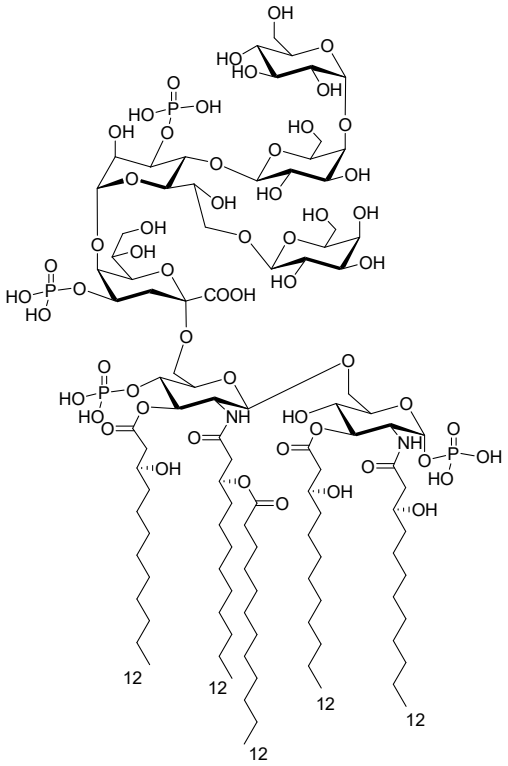

Structure of *Pseudoalteromonas sp1A1* LOS

*Pseudoalteromonas sp1A1* biological activity was assessed using ELISA and Quanti-blue assays. It was found that its LPS does not possess any significant immunostimulant activity on human and murine cell line. The Outer-Membrane properties of *Pseudoalteromonas sp1A1* were also studied through Molecular Dynamic (MD) simulation, that showed how the asymmetric repartition of *Pseudoalteromonas sp1A1* Lipid A influenced the properties of the phospholipid bilayer, increasing its flexibility. Finally, MD simulation was also performed with *Pseudoalteromonas sp1A1* LOS in water and in 0.5 M of NaCl, that is closed to the natural marine environment of the bacterium. Results showed that the presence of salts influenced the conformational behavior of the Kdo-Lipid A region.

The second bacterial strain studied was *Spiribacter salinus* M19-40$^T$, a halophile isolated from an intermediate salinity pound of a marine saltern in Spain, the structure of the Lipid A was resolved using MALDI MS and MS$^2$ experiment. It is a *mono*-phosphorylated and penta-acylated species bearing two C10:0 (3-OH), one C12:0, one C14:0 (3-OH) and one C14:0 (3-oxo). This structure possesses two interesting structural features: (i) the 2+3 symmetry that is unusual - as most penta-acylated Lipid A have a 3+3 symmetry and (ii) the occurrence of the C14:0 (3-oxo)[g].

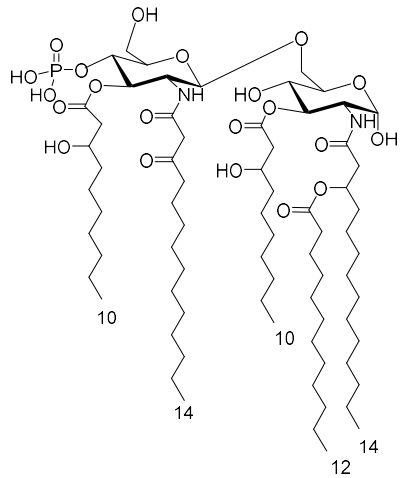


Structure of the Lipid A from *Spiribacter salinus* M19-40$^T$

*Halopeptonella vilamensis* is a halophilic bacterium that have been isolated from a saline lagoon in Argentina[h] whose Lipid A was characterized using MALDI MS and MS$^2$ experiments. Results showed that *H. vilamensis* has a highly heterogeneous mixture of Lipid A species, *mono*-phosphorylated and hexa-acylated, that differ for the length and saturation of their acyl chains. *H. vilamensis* main Lipid A species possesses two C10:0 (3-OH), two C12:0 (3-OH), one C12:0 and one C12:1.

[g] Barrau, C.; Di Lorenzo, F.; Javier Menes R.; Lanzetta R.; Molinaro A.; Silipo A.; Mar. Drugs 2018, 16, 124
[h] Menes, R.J.; · Viera, C.E.; Farías, M.E.; Extremophiles, 2016, 20, 19–25

Another major species possesses only saturated C12:0. Immunological assays were performed on murine and human cell lines with *H. vilamensis* LOS and demonstrated its slight immunopotency.

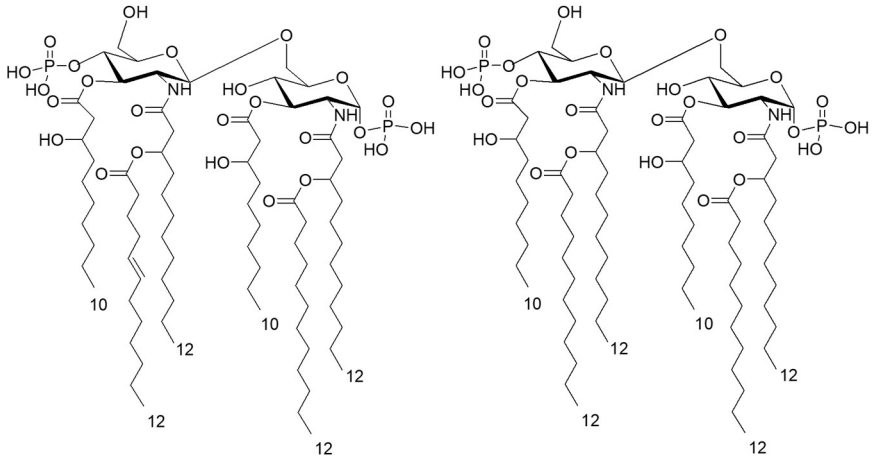

Structure of the Lipid A from *Halopeptonella vilamensis*

Finally, the characterization of cell envelope components of *Halomonas smyrnensis* was also attempted. *H. smyrnensis* is an Exopolysaccharide (EPS) producing halophile isolated from a Turkish salt lake[i]. It is known to be a high levan producer and two novel EPS were isolated. The first one is formed by α-(1→4)-Glc polymer and the second one by α-(1→3)-GlcNAc units.

[i] Poli, A.; Nicolaus, B. ; Denizci, A.A. ; Yavuzturk, B. ; Kazan, D. Int. J Syst. Evol. Microbiol. 2013, 63, 10-18

# Abbreviation

| | |
|---|---|
| BMDM | Bone marrow-derived macrophage |
| COSY | Correlation spectroscopy |
| CPS | Capsular polysaccharide |
| CWA | Cell-Wall associated protein |
| DFQ-COSY | Double-quantum filtered COSY |
| DOC | Sodium Deoxycholate |
| ELISA | Enzyme-linked immunosorbent assay |
| EPS | Exopolysaccharide |
| Gal | Galactose |
| GalNA | Galactaminuronic acid |
| GC-MS | Gas chromatography - Mass spectrometry |
| Glc | Glucose |
| GlcA | Glucuronic acid |
| GlcN | Glucosamine |
| HEK | Human Embryonic Kidney |
| HMBC | Heteronuclear multiple-bond correlation |
| HSQC | Heteronuclear single-quantum correlation |
| IL | Interleukin |
| IM | Inner membrane |
| IMP | Inner membrane protein |
| KDN | 3-deoxy-D-*glycero*-D-*galacto*-nonulosonic acid |
| KDO | 3-deoxy-D-*manno*-oct-2-ulosonic acid |
| LOS | Lipooligosaccharide |
| LPS | Lipopolysaccharide |

| | |
|---|---|
| LTA | Lipotechoic acid |
| MALDI | Matrix assisted laser desorption/ionization |
| Man | Mannose |
| MD-2 | Myeloid Differentiation factor 2 |
| MDS | Molecular dynamic simulation |
| MOMs | Monocyte-derived macrophages |
| MS | Mass spectrometry |
| MyD88 | Myeloid Differentiation primary response protein 88 |
| NF-κB | Nuclear factor-κB |
| NMR | Nuclear magnetic resonance |
| NOESY | Nuclear Overhauser effect spectroscopy |
| OM | Outer membrane |
| OMP | Outer membrane protein |
| PAGE | Polyacrylamide gel electrophoresis |
| PAMP | Pathogen associated molecular pattern |
| POPE | Palmitoyloleoyl Phosphatidylethanolamine |
| POPG | Palmitoyloleoyl Phosphatidylglycerol |
| PRR | Pattern recognition receptor |
| QuiN | Quinovosamine |
| SDS | Sodium dodecyl sulfate |
| SEAP | Secreted alcaline phophate |
| TH | T-Helper cell |
| TLR4 | Toll-like receptor 4 |
| TNF | Tumor necrosis factor |
| TOCSY | Total correlation spectroscopy |
| TOF | Time of flight |
| WTA | Wall techoic acid |

# INDEX

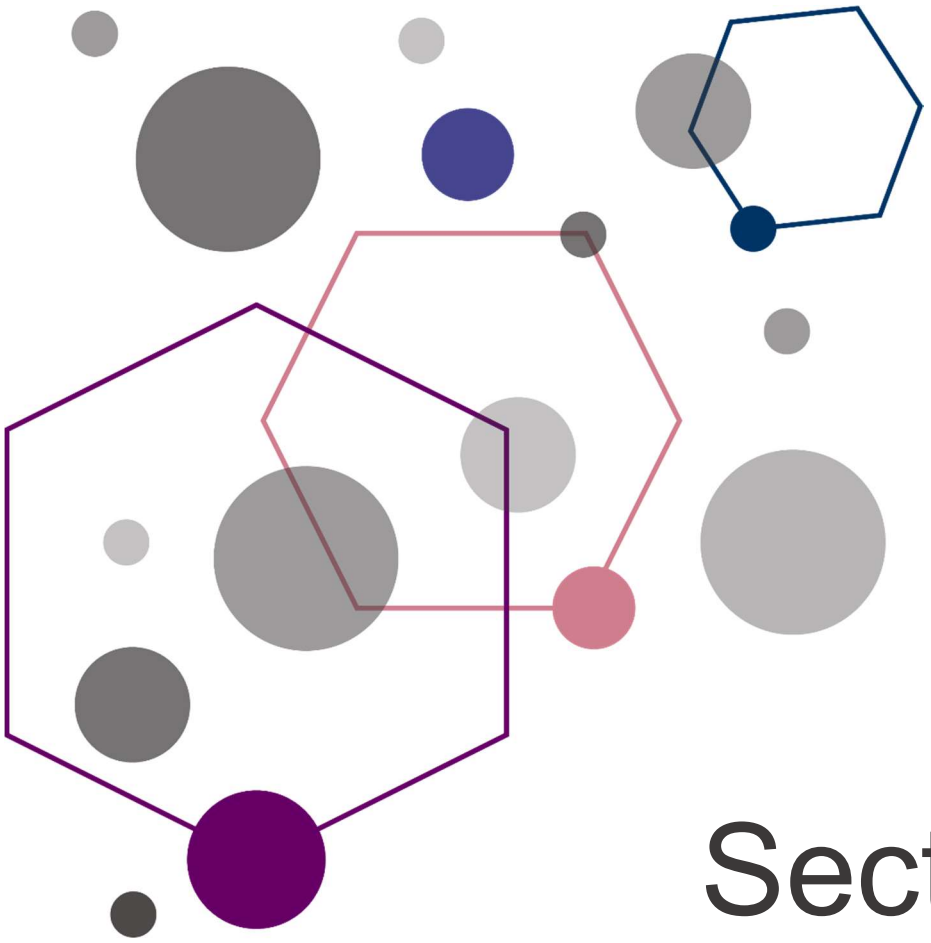

# Section I

## Introduction

# Chapter 1: Gram-negative bacteria

## 1.1. The bacterial cell

From microorganisms to complex plants and animals, life comprise a remarkable diversity and can be divided into a five-kingdom system that includes *Monera*, *Protista*, *Plantae*, *Fungi*, and *Animalia* (Figure 1). Around 30 year ago, Woese et al.[1] changed the previous system based on RNA analysis. They established the three-kingdom system and defined *Bacteria* as one of the three domains of life, with *Archaea* and *Eukarya* (Figure 1). *Eukarya* are uni- or pluricellular organisms that possess an internal cell compartmentation. Indeed, the presence of organelles within their cytoplasm is characteristic of this domain. *Archaea* are unicellular prokaryotic organisms devoid of cellular compartmentation. *Bacteria* are also prokaryotes but they differ from *Archaea*, *inter alia*, by the composition of their plasmatic membrane.

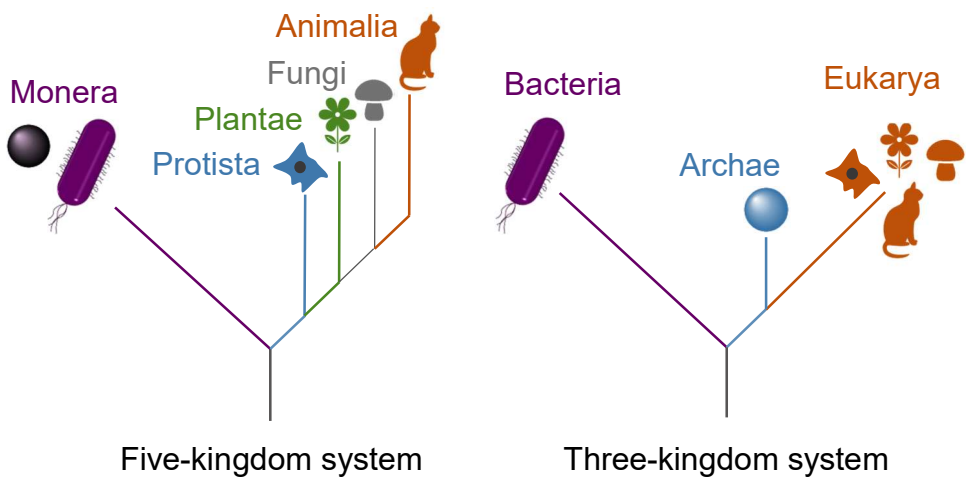


**Figure 1:** The five-kingdom and three-kingdom systems of life

Bacteria include a vast group of microorganisms that grow and reproduce in diverse environments. They comprise an impressive array of

sizes, shapes and arrangement[2]. Roughly, Bacteria can be divided on the basis of their cell morphologies, e.g. rod shape, spherical and curved cells are respectively called “bacillus”, “cocci” and “spirilli”[3]. Despite the great diversity, there are still general features among bacteria (Figure 2). Their cytoplasm comprises most bacteria metabolites and is the place where all transcription and replication of the DNA occurs. Exposed outside the bacteria, flagella and pili are involved in motility. They are anchored in the bacterial cell envelope, which possesses a sophisticated architecture.

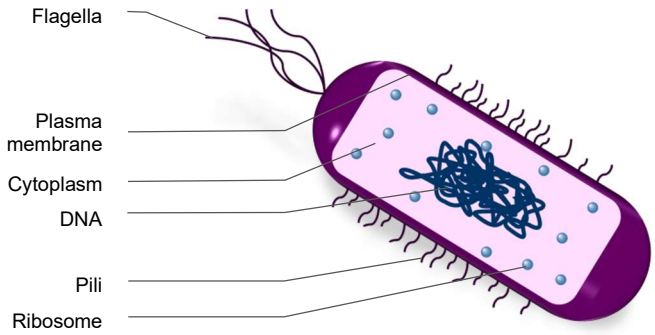


**Figure 2:** Schematic representation of general bacteria composition

## 1.2. Bacterial cell envelope

Bacterial cell envelope is a complex structure that evolved to adapt to the environment in which they live. Based on their cell external structure, two types of bacteria can be distinguished: Gram-positive and Gram-negative bacteria. Historically, those category were termed based on a colorimetric test developed in 1884 by Hans Christian Gram. Nowadays, this determination is still used to describe the bacterial cell envelope composition[4].

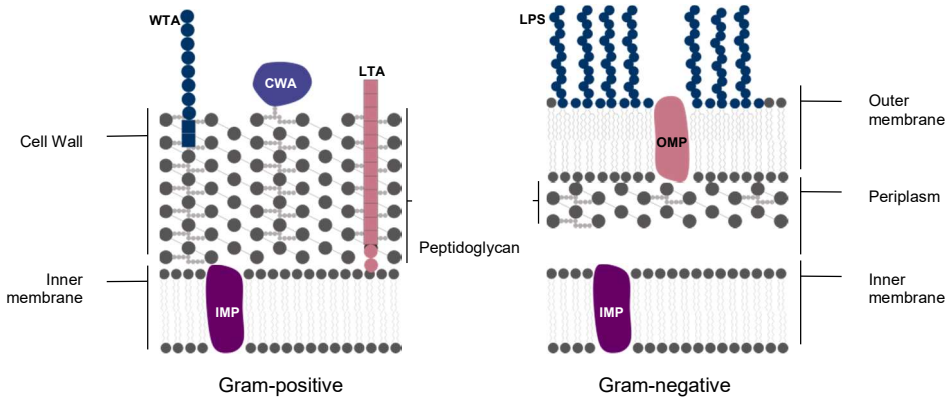


**Figure 3**: Schematic representation of Gram-positive and Gram-negative bacteria cell envelope. Abbreviations correspond to: Wall techoic acid (WTA), Lipotechoic acid (LTA), Lipopolysaccharide (LPS), Inner membrane protein (IMP), Cell-wall associated protein (CWA); Outer membrane protein (OMP)

Gram-positive cell envelope is composed of two main parts: the cell membrane and the cell wall (Figure 3). The cell membrane is a phospholipid bilayer. As bacteria do not possess any organelle, all membrane-related biosynthesis occur in the cell membrane, including the synthesis and transport of molecules composing the cell wall[5]. This bilayer also includes inner membrane proteins (IMP). Over this structure, and directly exposed to the environment, there is the cell wall that is composed of a thick layer of a glycopeptide polymer named peptidoglycans. On this structure are exposed different types of cell-wall glycopolymers[6]: Wall techoic acids (WTA) are linked to the peptidoglycan through phosphodiester linkages and lipotechoic acids (LTA) are anchored to the cytoplasmatic membrane through a glycerol phosphate unit. Cell-wall glycopolymer are diverse among bacteria species and strains and possess different ionic charges or number of repeating unit. They are essential for Gram-positive bacteria survival, playing a role in important functions as

protection, attachment and colonisation. There are also cell-wall associated proteins (CWA) that are exposed at the surface of the cell wall.

Differently from Gram-positive bacteria, Gram-negative cell envelope do not have its peptidoglycan exposed to the environment. It is composed of three parts: the inner membrane, the periplasm and the outer membrane (Figure 3). As for Gram-positive bacteria, the inner membrane is a phospholipid bilayer that plays a key role for the biosynthesis of Gram-negative other cell wall constituents[7]. Between the two membranes, the periplasm is composed of a peptidoglycan layer that is thinner than the one found in Gram-positive bacteria and in turn surrounded by the outer membrane (OM). The OM is a lipid bilayer that acts as a barrier between bacteria and their environment. The OM includes outer membrane proteins (OMP) that are β sheets anchored to the bilayer through hydrophobic residues. Contrary to the inner membrane, the outer membrane is an asymmetric bilayer. Its inner leaflet is still made of phospholipids but its outer leaflet is composed at 75% of Lipopolysaccharides (LPS). LPS are complex molecules that are crucial for the bacteria survival as they are constantly interacting with their environment.

## 1.3. Lipopolysaccharides and Lipooligosaccharides

### 1.3.1. General structure

Lipopolysaccharides (LPS) are heat-stable amphiphilic molecules. Initially referred as endotoxins, they are anchored in the bacterial cell membrane and are infamously known for their toxicity. LPS are composed of three main parts[8]: a repeating unit of polysaccharide termed the O-antigen, the core oligosaccharide, and the Lipid A (Figure 4). Smooth-type

LPS (S-LPS), or Lipopolysaccharides (LPS), are composed of all the three previously mentioned parts. Rough LPS (R-LPS), or Lipooligosaccharides (LOS), do not possess the O-antigen. The Smooth/Rough determination was originally adopted because of the appearance R-LPS and S-LPS give to their bacteria colonies.

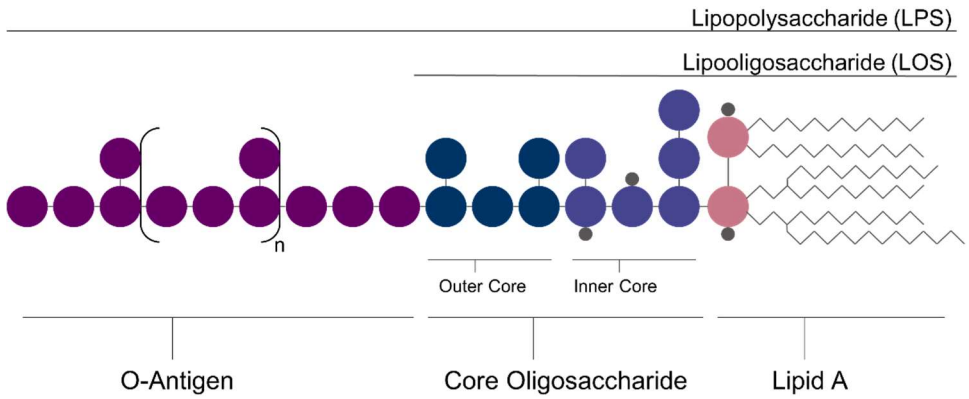


**Figure 4**: General structure of Lipopolysaccharides (LPS) and Lipooligosaccharide (LOS)

Lipopolysaccharides are essential for the bacterial survival. Indeed, they are crucial in many biological roles as adhesion, symbiosis and pathogenicity. In particular, their structure determines the relationships between bacteria and their host. Although LPS share the same broad architecture, each bacterial strain possesses their own variation. Those differences can be seen in the composition of the O-antigen, the core oligosaccharide and the Lipid A.

## 1.3.2. The O-antigen

The O-antigen is the most variable part of the LPS. It is a hydrophilic polymer that can be composed up to 50 units of from 1 up to 8 monosaccharides. O-antigens can be linear or branched polysaccharides, structural variation of the O-antigen occur in the nature of each

monosaccharide, their linkages and the presence of non-carbohydrate constituents. Non-stoichiometric modifications increase the heterogeneity of O-antigen structures. Differences between O-antigen can be observed between each bacterial strain (*inter*-strain specific) but also within the same bacterial strain (*intra*-strain specific). For example, *E. coli* has more than 170 O-serotypes. A single bacterium can synthetize O-antigen with different number of repeating units. The structure of O-antigen play a role in bacterial pathogenicity and symbiosis[9]. Its length also influences the adhesion properties of the LPS[10]. Interestingly, Gram-negative bacteria can shorten their O-antigen using a reversible process called phase-variation[11], allowing them to hide from the host immune defence.

### 1.3.3. The Core Oligosaccharide

The core Oligosaccharide has less chemical diversity than the O-antigen and is composed of two main parts: the Inner and the Outer core (Figure 4). The Outer Core is directly linked to the O-antigen and has the most structural variations. It is often made of negatively charged monosaccharides such as uronic acids. The Inner core is a more conserved part. It is typically made of 3-deoxy-D-*manno*-oct-2-ulosonic acid (Kdo) and L-*glycero*-D-mannoheptose (L,D-Hep)[12] (Figure 5); D-*glycero*-D-talo-oct-ulosonic acid (Ko) or D-*glycero*-D-mannoheptose (D,D-Hep). The Inner core is usually decorated with phosphates (P).

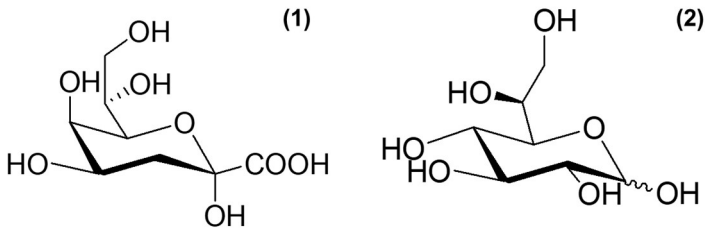


**Figure 5**: Structure of (1) 3-deoxy-D-*manno*-oct-2-ulosonic acid (Kdo) and (2) L-*glycero*-D-mannoheptose (L,D-Hep)

### 1.3.4. The Lipid A

The lipid A is the hydrophobic part of the LPS that anchors the molecule within the OM. It is composed by a phosphorylated and acylated β(1'→6) di-Glucosamine backbone (GlcN)[13] on which the core oligosaccharide is attached at C-6' position. The Lipid A can possess one or two phosphates linked on the C-4' position of the non-reducing GlcN (GlcN II) and on C-1 position of the reducing GlcN (GlcN I). Lipid As mainly differ on their degree of acylation and the nature of their fatty acids. They are acylated by primary fatty acids on C-2, C-3, C-2' and C-3' position through ester and amide bounds. They can also possess ester-linked secondary fatty acids that are attached on the hydroxyl group of primary-linked acyl chains. Finally, Lipid As can also possess substituents as phosphoethanolamine. The first resolved Lipid A structure was from *E. coli*. It is a *bis*-phosphorylated and penta-acylated structure with 4+2 symmetry. Many other Lipid As from various bacteria sources pathogen (Figure 6) were characterized revealing their highly diverse architectures[14,15,16,17]. The Lipid A structure is crucial for the survival of the bacteria and its pathogenicity. Indeed, this moiety is known to directly bind with a receptorial complex of mammal's innate immunity composed of Toll-like receptor 4 (TLR4) and myeloid differentiation factor 2 (MD-2).

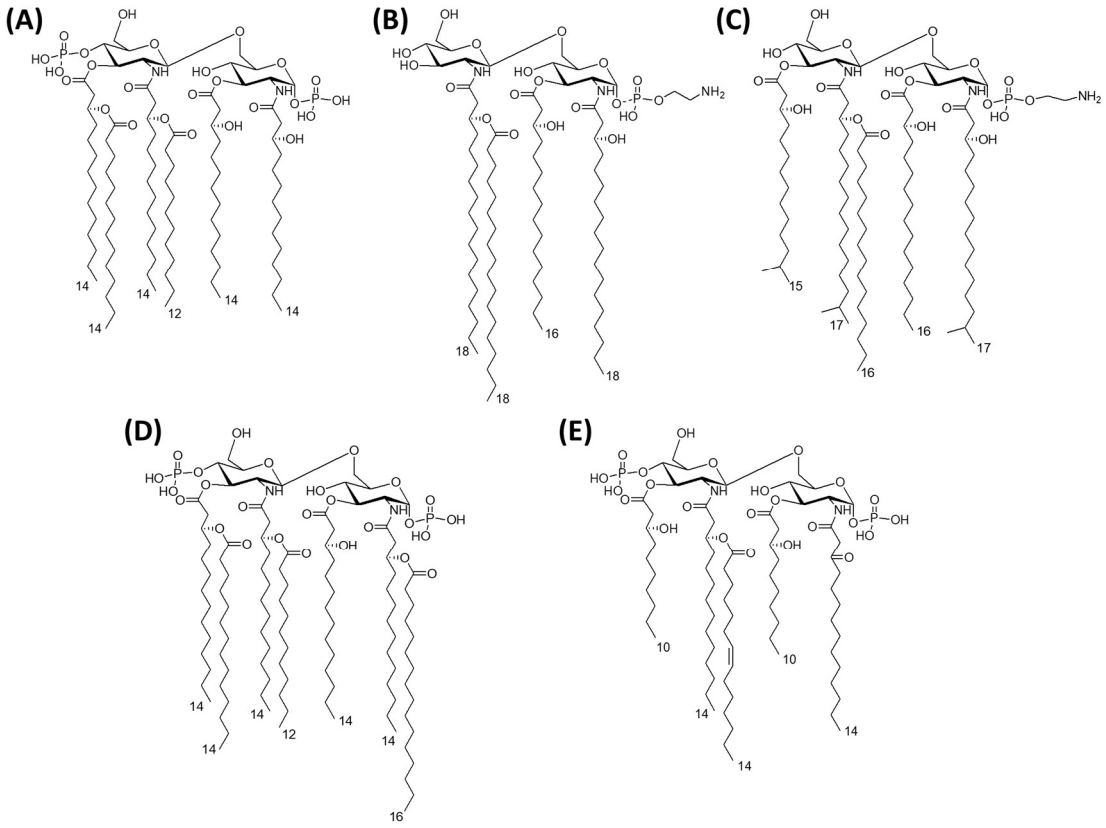


**Figure 6**: Structure of Lipid As from several bacteria, illustrating their structural diversity among Gram-negative bacteria. (A) *Escherichia coli* (B) *Helicobacter pyroli* (C) *Porphyromonas gingivalis* (D) *Salmonella minnesota* (E) *Rhodobacter sphaeroides*

# 1.4. Gram-negative bacteria and innate immunity

## 1.4.1. Innate and adaptive immunity

Living organisms develop ways to defend against threats in order to survive. Immunity is a complex system that allows the host to detect and supress the intruding pathogens. In 1989, Charles A. Janeway introduced the concept of innate and adaptive immunity[18]. The organism's ability to prevent infections is broadly based on adaptive immunity. This response is highly specific and is developed after a first encounter with a pathogen. However, around 7 days are needed to recruit the specialised cells during the first activation[19]. Therefore, a first line of defence is needed to protect the organisms against new pathogens. This is the role of innate immunity

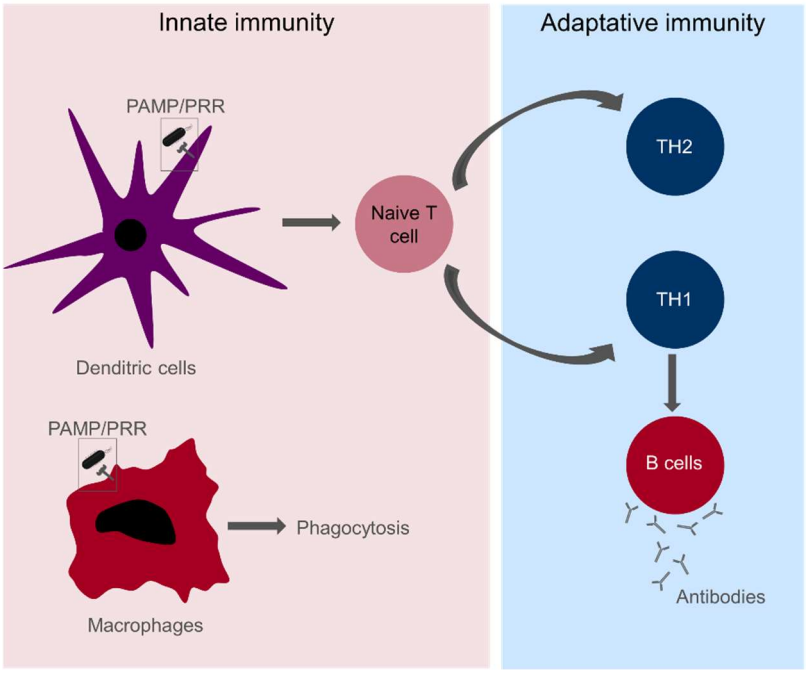


**Figure 7:** An overview of the innate and adaptive immunity. PAMP: Pathogen-associated Molecular patterns; PRR: Pathogen-Recognition Receptors; TH: T-helper cells

Part of the innate immune response is performed by macrophages via phagocytosis (Figure 7). However, dendritic cells (DC) play a key role in the innate immune recognition and the induction of adaptive immunity[20]. Briefly, their activation leads to the secretion of cytokines or direct cell contacts with naïve T cells that triggers the formation of T and B cells (Figure 7). The first step in the activation of the innate immunity is the recognition of the pathogen that is done through Pathogen-Recognition Receptors (PRR) that recognise Pathogen-associated Molecular patterns (PAMP)[21] on the surface of innate immune cells. PAMP are molecules that are not produced by eukaryotic cells, possess invariant structural features and are necessary for the microbe's survival. Their recognition by PRR is hence advantageous for the host. There are several PRR that evolved in order to interact with different PAMPs; among them, there is a receptor that is specialized in the recognition of LPS.

### 1.4.2. TLR4/MD-2 receptorial complex and inflammation

Firstly discovered in *Drosophila*, the Toll protein was known to control dorsal-ventral patterning in embryon and inflammatory response in adults. Its analogue was later on discovered in humans as a transmembrane protein related to NF-κB signaling[22]. Those proteins are now referred as Toll-like receptors (TLRs) and known to be part of human's innate immunity. To better fight infection, there are several types of TLRs that can each recognize a particular PAMP. For example, TLR2 interacts with lipoprotein and TLR5 with flagellin.

The first discovered TLR was TLR4 that was shown to specifically interact with LPS[23]. Further studies proved that TLR4 does not work alone. The presence of another protein, the Myeloid Differentiation factor 2 (MD-2) is necessary to respond to LPS infection[24]. MD-2 is associated to the extra-cellular domain of TLR4 and together they form the TLR4/MD-2 receptorial complex. Further studies enhanced the comprehension of TLR4/MD-2 activation and its related signalling pathway. LPS is firstly recruited by LPS Biding proteins (LBP) and is further transferred to the TLR4/MD-2 receptor through CD14. All those interaction spontaneously happen due to the existence of a thermodynamic funnel that prone the assembly of those molecules[25].

Once LPS is linked to TLR4/MD-2, it triggers the dimerization of the receptorial complex and further intra-cellular signalling. In brief, two main supramolecular structures can be formed after the dimerization, triggering different inflammations pathways[26] (Figure 8). When the Toll/interleukin-1 Receptor domain-containing Adaptor Protein (TIRAP) and Myeloid Differentiation primary response protein 88 (MyD88) are linked to the intracellular part of TLR4, an assembly called the Myddosome is formed. Further association with Interleukin-1 Receptor Associated Kinase (IRAK) triggers cytokine production with the activation of transcription factors that are Nuclear Factor-κB (NF-κB) and Activator Protein 1 (AP1). The second supramolecular complex, the Triffosome, is MyD88-independent and involves the assembly of TIR domain-containing adaptor protein inducing IFNβ (TRIF) and TNF receptor-associated factor 3 (TRAF-3). It activates NF-κB, AP1 and also interferon regulatory factor 3 (IRF-3). All the recruited transcription and regulatory factors can then modulate the expression of the host genome, leading to the inflammatory response[27].

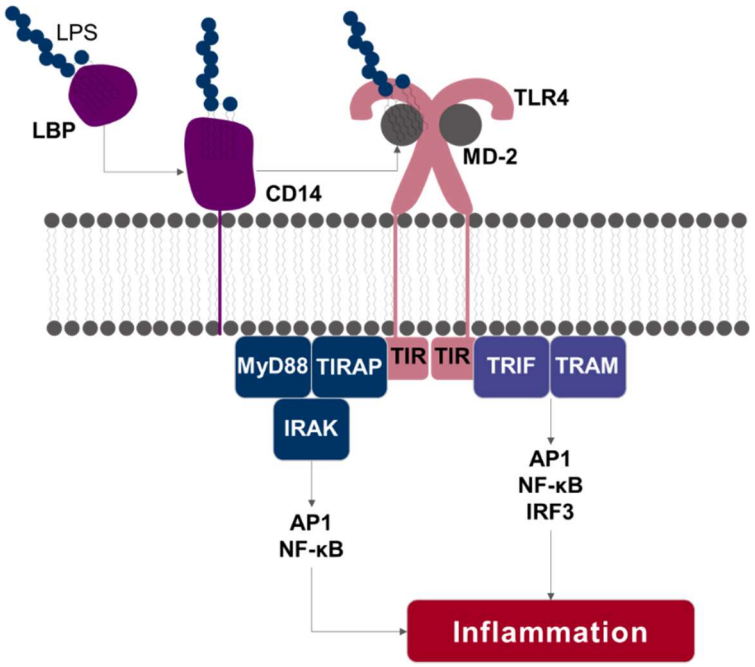


**Figure 8**: General description of TLR4/MD-2 signalling pathway

Inflammation is a physiological phenomenon that is necessary for the organism to protect itself. However, a dysregulation can lead to major deceases. Sepsis and septic shock are disorders that arise from an unbalanced inflammatory response. Those are significant cause of death among developed countries[28]. Better understanding TLR4/MD-2 mechanism and finding new regulators is essential to develop therapies. In this context, many bioactive compounds have been tested in order to modulate the innate immunity[29]. As natural activators of TLR4/MD-2, LPS play a key role in the exploration of new modulators. It is now widely known that the interaction between TLR4/MD-2 and LPS is driven by a structure dependent relationship.

### 1.4.3. Structure and function relationship

The idea that LPS structure would influence its endotoxic activity was already investigated 25 years ago[30]. The study of Lipid As conformation from several gram-negative bacteria lead to observation of a correlation between their three-dimensional structures and biological activity. Indeed, the Lipid A toxicity potency is linked to a non-lamellar supramolecular structure. Further researches confirmed the relationship between LPS shape and biological activity. The degree of acylation of the Lipid A and the length of its fatty acids influence its three-dimensional conformation. When the Lipid A has a high degree of acylation, as the hexa-acylated Lipid A from *E. coli*, it adopts a conical shape. Penta-acylated Lipid A, e.g. from *P. gingivalis*, have an intermediate shape and hypo-acylated Lipid As, as biosynthetic precursors Lipid Ia and Lipid IVa, adopt a strictly cylindrical shape (Figure 9)[31].

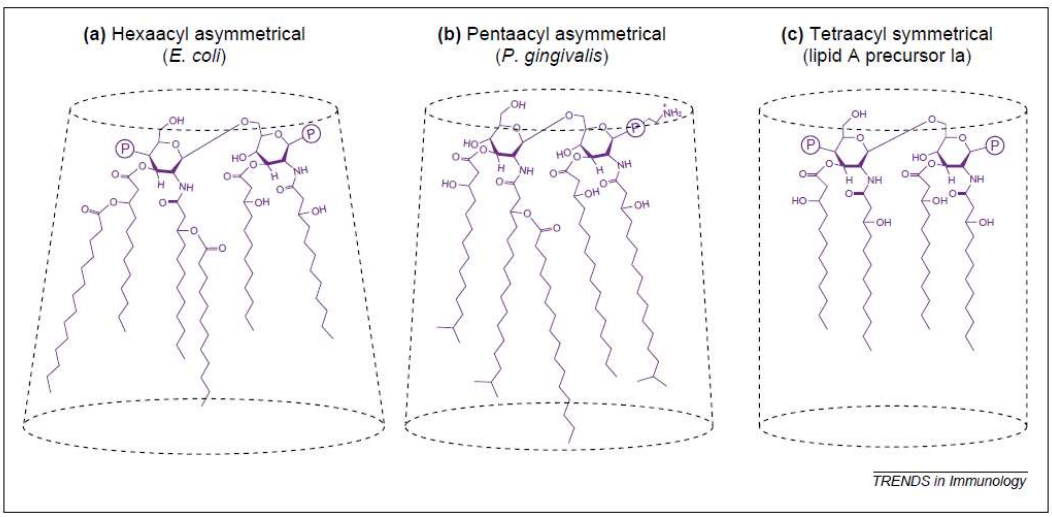


**Figure 9:** Three dimensional conformations of Lipid A with different degree of acylation[31]

It is known that *E. coli* LPS possesses a strong agonist activity towards TLR4/MD-2 receptorial complex and *P. gingivalis* LPS activity is less TLR4-dependent[32]. Lipid IVa has been identified as a slight agonist in mice and an antagonist towards human MD-2[33]. All those data confirm that conical supramolecular structures are correlated to agonist activity and cylindrical shapes to antagonist. Crystal structure of Lipid IVa linked to human MD-2 showed that all fatty acids of the antagonist Lipid A are inserted in the MD-2 binding pocket[34], and that this did not modify the conformation of MD-2. The interaction between *E. coli* agonist Lipid A and TLR4/MD-2 was also investigated by crystallography[35]. When the hexa-acylated Lipid A interacts with MD-2, one of its fatty acid does not enter the hydrophobic pocket and remains on the protein surface (Figure 10). The exposed fatty acid can then interact with the hydrophobic region of a second TLR4. As for Lipid IVa, the insertion of *E. coli* LPS in MD-2 does not change the size of the hydrophobic pocket. However, the di-glucosamine backbone of *E. coli* LPS adopts a different spatial conformation, compared to Lipid IVa. Such orientation of the Lipid A makes its phosphates groups interact with positively charged residues of both TLR4. This interaction, combined to hydrophilic and hydrophobic contacts, are crucial in order to generate the dimerization of TLR4/MD-2. Indeed, the fatty acid of *E. coli* Lipid A that is at the surface of the hydrophobic pocket can interact with two TLR4s, whereas Lipid IVa does not have fatty acid that mediates the heterodimer formation (Figure 10). As the dimerization of the receptorial complex is necessary for triggering an inflammatory response, those interactions explains why *E. coli* LPS has a strong agonist activity and Lipid IVa is an antagonist.

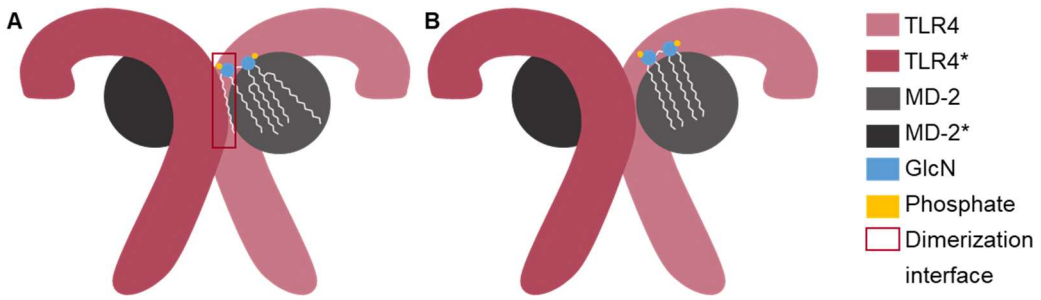


**Figure 10:** Representation of the interaction between *E. coli* Lipid A (A), Lipid IVa (B) and TLR4/MD-2 receptorial complex. Orientation of *E. coli* Lipid A triggers the dimerization of the receptor

Finally, Lipid IVa was also studied with murine MD-2[36]. It was shown that the different amino acids present in the hydrophobic pocket made the Lipid IVa adopt the same overall conformation than *E. coli* LPS. That explains the slight agonist activity of Lipid IVa in mice. Interactions between endotoxins and TLR4/MD-2 were studied not only by crystallisation but also using other techniques. A more recent investigation of LPS-TLR4 interaction was done by Single Molecule Localisation Microscopy (SMLM)[37]. With this technique, it was possible to detect monomeric and dimeric TLR4 molecules in presence of various LPS. In presence of LPS from *E. coli* and *S. minesotta*, most of TLR4 were detected in dimeric forms but in presence of LPS from *R. sphaeroides*, TLR4 remained in monomeric state.

Thus, the whole structure of the LPS may influence the interaction. Indeed, a lot of work have been dedicated to the Lipid A but other constituents, as the Kdo or heptoses of the core oligosaccharide, contribute to the biological activity[38]. In this context, discovering novel LPS structures is necessary to find new modulators for TLR4/MD-2 receptorial complex. Exploring particular environment where bacteria have specific adaptation strategy is a promising way to detect interesting molecular features.

## 1.5. Lipopolysaccharides from marine and extreme environment

### 1.5.1. Life at the extreme

From a human perspective, the optimal conditions for life are at neutral pH, temperature between 20 and 40 °C and at atmospheric pressure. However, life can also exist in conditions that are considered as hostile for many life forms. Organisms living in such conditions are termed extremophiles and their fascinating properties were studied for decades[39]. Extremophiles can be classified in several categories depending on the conditions in which they thrive. For example, **psychrophiles** can live below 15 °C and **thermophiles** above 60 °C, **barophiles** can support up to 80 MPa and **halophiles** can live in salinity environment with saturated NaCl (Figure 11). Some organisms are able to survive in several extreme conditions, as high pressure and high temperature, and are termed polyextremophile. There is still a lot to discover about extremophiles and current metagenomic analysis lead to the discovery of extremophiles new genus and species and a better understanding of their metabolism[40]. The study of extremophiles is also appealing for biotechnology. Indeed, those organisms can produce metabolites with unique properties that are studied for industrial applications[41]. Extremophiles Gram-negative bacteria also possess LPS on their OM and those molecule can have particular properties.

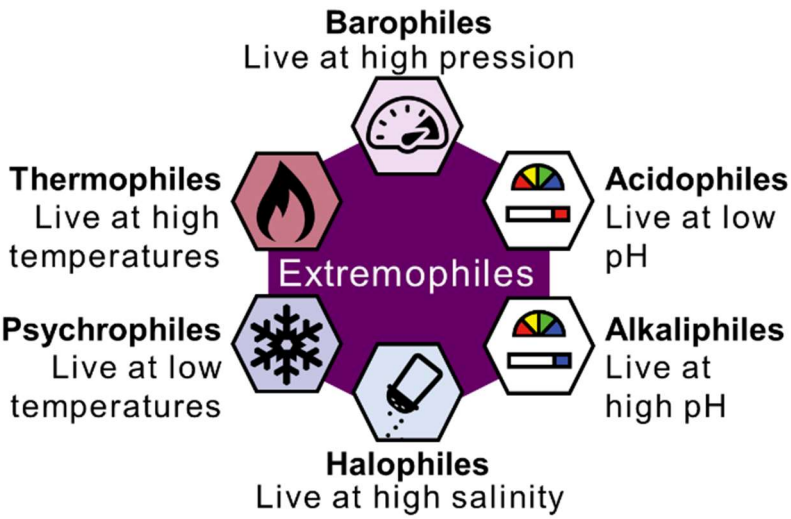


**Figure 11**: Representation of extremophiles diversity in different environments

### 1.5.2. LPS structures from marine bacteria and extremophiles

The ocean is the place where life could be created and it still includes a countless diversity of organisms. Marine microorganism adapted to their environment by creating a various number of metabolites. Their study lead to the discovery of bio-active compounds with large therapeutic interest, as anti-bacterial, anti-fungal and anti-tumoral molecules[42]. In particular, Gram-negative marine bacteria are omnipresent organism whose LPS can possess interesting immunological activity. Indeed, specific structural features can be observed in these environments[43]. O-antigen and core oligosaccharides of marine LPS are usually negatively charged with the presence of uronic acids and non-glycosidic substituents. As LPS are constantly exposed to the marine environment, the anionic residues links to the surrounding cations, strengthening the global membrane structure. This mechanism provides the bacteria higher stability towards its environment.

Several Lipid A from marine bacteria were also characterized and common features were observed. Short fatty acids – in comparison to *E. coli* Lipid A- are often found in marine bacteria with Lipid A containing 10 to 13 carbon acyl moieties. Marine bacteria also possess low acylated (penta and tetra-acylated) and phosphorylated (*mono*-phosphorylated) Lipid A. Those characteristic are associated with low-agonist and antagonist activity and encourage the exploration of new endotoxin structures in the oceans.

As a consequence of their adaptation, extremophiles also possess LPS with interesting structures[44]. As for marine bacteria in general, extremophiles often possess negatively charged O-antigen and their Lipid A usually have shorter acyl chains (Figure 12)[45,46,47]. They are a promising source of agonist and antagonists towards the TLR4/MD-2 receptorial complex. Characterizing LPS from bacteria that live in marine and extreme conditions is hence necessary in order to understand their adaptation process and to find new modulators of the innate immune system.

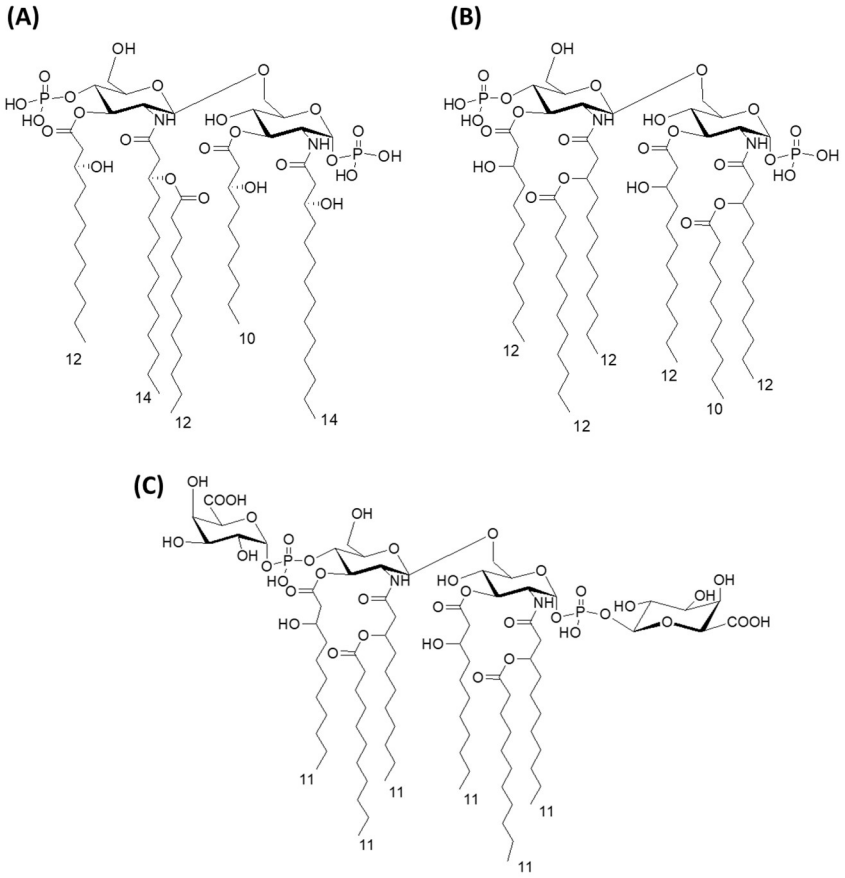


**Figure 12**: Structure of Lipid As from some marine and extremophile bacteria: (A) *Alteromonas aldita*, a marine bacterium (B) *Halomonas patelleriensis*, an haloalkaliphilic bacterium (C) *Thermomonas hydrothermalis*, a thermophile

# Chapter 2: Characterization of Lipopolysaccharides

## 2.1. Extraction and purification of Lipopolysaccharides

Extraction of LPS is the first step towards its structural elucidation. Two main procedures have been designed in order to isolate LPS. The first one is the PCP extraction in which bacterial cells are exposed to a mixture of Phenol/Chloroform/Petroleum ether (5:8:2). This methods is more suitable for the extraction of LOS as the extracted material can be found in the phenol phase. The other procedure is the Hot Phenol-Water extraction[48], in which the extraction is more convenient for LPS as they can be isolated in the aqueous phase. The extracted material is usually impure after this procedure. Indeed, cells contaminants such as proteins and nucleic acids can be also found in the same aqueous phase. In order to remove contaminants and purify the extracted material, the sample is further purified using an enzymatic treatment with several enzymes (Proteases, DNAses and RNAses); the sample then undergoes several Ultra-centrifugation or Size-Exclusion chromatography steps (Figure 13).

Once the extract is lyophilised, electrophoretic methods as Sodium Dodecyl-Sulfate polyacrylamide gel (SDS-PAGE) and Sodium Deoxycholate Polyacrylamide gel (DOC-PAGE) are performed. The use of subsequent silver staining procedure allows the detection of the LPS/LOS by revealing its saccharidic portion[49]. If the extract is an LOS, a large band is detected at the bottom of the gel. If it is an LPS, a ladder-like pattern is seen in the middle of the gel, showing the bacteria O-antigen length diversity. Performing electrophoresis with silver staining is a necessary step in the characterization of endotoxin structures. Indeed, typical stains provide a solid validation of the LPS/LOS nature of the extract.

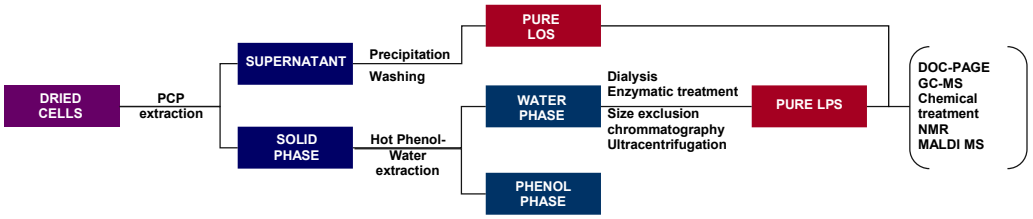


**Figure 13**: Usual procedure used for the extraction and purification of LPS and LOS

## 2.2. Chemical analysis of Lipopolysaccharides

GC-MS analysis of carbohydrate and fatty acids derivatives provide crucial information about the composition of the extracted and purified LPS. Several methods can be used in order to determine the carbohydrate composition of the core oligosaccharides and the O-antigen[50]. The first one is the Acetylated Methyl glycoside (MGA) procedure. This methods gives information about the nature of the monosaccharides present in the LPS. An aliquot of the extract is methylated at anomeric position in acidic conditions and then per-acetylated. The obtained derivatives are then analysed by GC-MS with a standard that is per-acetylated inositol. The nature of each monosaccharide is given by their retention time on the chromatogram combined with their MS data.

Once the monosaccharide composition of the LPS is assessed, their branching points are determined using the Partially Methylated Alditols Acetates (AAPM) method. In the present procedures, the polysaccharide is methylated at free hydroxyl positions in basic condition with further treatment by iodomethane ($CH_3I$)[51]. The linkages are then cleaved with Trifluoroacetic acid (TFA). A reduction with Sodium Borodeuteride ($NaBD_4$)

is then performed. This step is crucial because it leads to the ring opening and marks the anomeric position with deuterium atoms. The sample is then acetylated at its remaining free hydroxyls groups (Figure 14). The obtained monosaccharides derivatives are finally injected on GC-MS. It should be noted that with the present procedure, carbohydrates containing carboxylic acids (as uronic or ulosonic acid) cannot be detected. In order to analyse those monosaccharides, it is necessary to first reduce the carboxylic acid group before performing the hydrolysis with TFA (Figure 14). As for MGA, the determination of the branching points is done by analysing their retention time on the GC chromatogram and their fragmentation by MS.

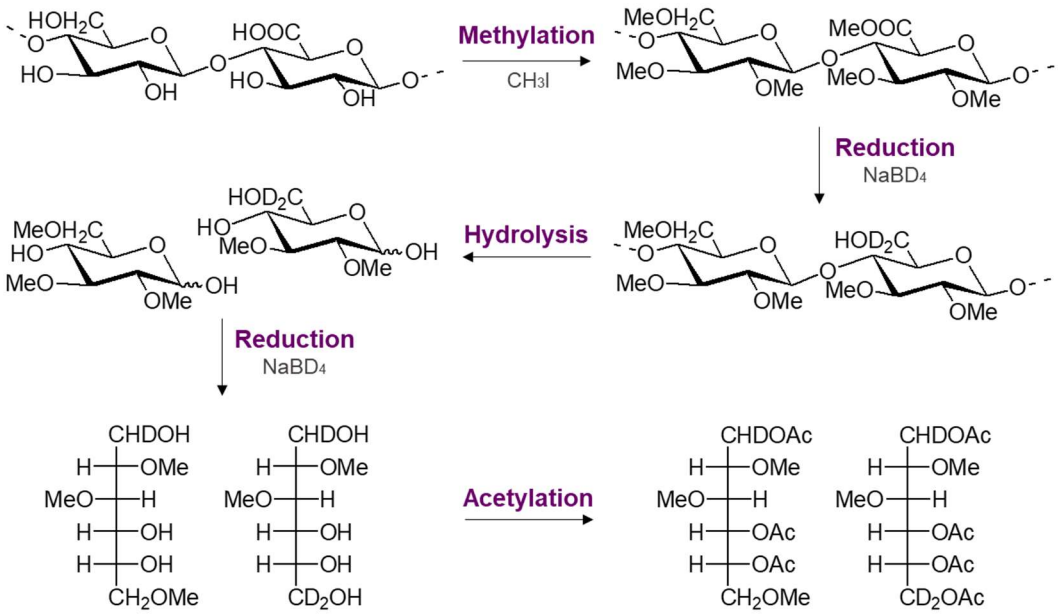


**Figure 14**: Protocol used for the AAPM derivatisation of carbohydrates

Fatty acid content of the LPS can also be analysed by GC-MS[52]. An aliquot of the LPS is methylated as described for the MGA procedure and then extracted with hexane. The obtained methyl-ester derivatives are then injected on GC-MS. Each fatty acid has a specific retention time and fragmentation pattern. It is hence possible to determine the composition of the sample by detecting fatty acids with different acyl chain length, hydroxylation and unsaturation.

Compositional analysis give crucial data for the structural analysis of the LPS. However, they are not sufficient to achieve the characterization of the exact structure. Different methods have to be used on the saccharidic part and the Lipid A. Several chemical treatments can be performed in order to separate and isolate those two moieties.

## 2.3. Isolation of poly- and oligo-saccharide and Lipid A portions

The Kdo is a particular monosaccharide that is most of the times found between the non-reducing glucosamine of the Lipid A and the core oligosaccharide. Due to the presence of carboxylic acid at anomeric position and the lack of hydroxyl substituent at its C3 position, it is highly labile in acidic position. This is a useful property when the Lipid A needs to be separated from the saccharidic moiety. When the LPS is treated in mild acidic conditions, a cleavage occurs between the non-reducing glucosamine of the Lipid A and the Kdo. The polysaccharide and Lipid A are then easily separated by centrifugation.

Another methods can be used for the isolation of the saccharide portion. It is the full deacylation of the LPS[53]. This procedure is typically used to separate the Lipid A from the core Oligosaccharide. In a first step,



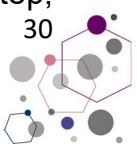

the sample is treated with hydrazine ($N_2H_4$), removing the O-linked acyl chains. Then a treatment in basic condition (using KOH) cleaves the remaining N-linked acyl chains. After desaltation and purification by column chromatography, the isolated oligosaccharide is ready to be fully characterized.

## 2.4. NMR of poly- and oligo-saccharides

Nuclear Magnetic Resonance (NMR) is a non-destructive technique that give information on the different nuclei present in a molecule and their atomic environment. There exist many NMR experiments that provide complementary data for structural characterization of polysaccharides[54]. $^1$H NMR experiment is a 1D spectrum where signals corresponding to each protons of the polysaccharides are recorded. Many information can be assessed with this experiment. Indeed, each region of the spectrum corresponds to a specific kind of proton. Anomeric protons are visible between δ 4.6 and 5.5 ppm, acetyl groups between δ 2.0 and 2.2 ppm and methyl groups between δ 1.0 and 1.3 ppm. Remaining protons are found in the bulk region between δ 2.6 and 4.6 ppm.

$^1$H NMR spectrum can also be used in order to measure anomeric coupling constant and hence determine each monosaccharide configuration. Indeed, $^3J_{H1\text{-}H2}$ is around 7-9 Hz for α-configured and 1-4 Hz for β-configured carbohydrates like glucose and galactose, respectively due to diaxial and equatorial-axial couplings. For D-mannose, different values are measured as its H2 is equatorial. Its β-configuration correspond to a $^3J_{H1\text{-}H2}$ around 1-2 Hz and α-configuration around 0-1 Hz.

To go deeper in the analysis, several 2D spectra must be recorded. Correlation Spectroscopy (COSY), and Total Correlation Spectroscopy



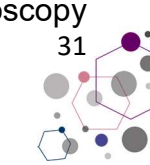

(TOCSY) are homonuclear through-bond experiments. Both of the axis in the spectra correspond to the same kind of atom ($^{1}H$) and the magnetization transfer is performed through bounds connections. Those experiments hence measure the correlations of protons among the same monosaccharide unit. All protons from a given unit hence belong to the same spin system. In COSY experiment, observed cross-peaks emerge from magnetization transfer to direct neighbours. This is convenient for the attribution of the precise proton sequences among the same spin system. TOCSY experiment give additional information by transferring the signal through several connections. The two previously described experiments allow the assignment of proton sequence within the same unit but do not give any information about the linkages between each monosaccharides. Nuclear Overhauser Spectroscopy (NOESY) is a homonuclear through-space experiment. Contrary to COSY and TOCSY, the magnetisation is transferred to proton that are spatially closed. With this experiment, it is hence possible to detect a correlation between an anomeric proton and the proton of the other unit to which it is linked (Figure 15).

Other structural data can be assed using heteronuclear 2D experiments. Heteronuclear Single-Quantum Correlation Spectroscopy (HSQC) shows correlations between carbons and protons that are directly linked. As for proton spectra, HSQC can be divided in different region in which the carbon chemical shift is characteristic of its environment. Anomeric carbon are usually found between δ 90-110 ppm, nitrogen-bearing carbons between δ 45-60 ppm, methyl groups around δ 10-20 ppm and sugar ring carbons between δ 60-80 ppm. Heteronuclear Multiple Bond Correlation (HMBC) gives signals between $^{13}C$ and $^{1}H$ that are correlated through several bounds (Figure 15).

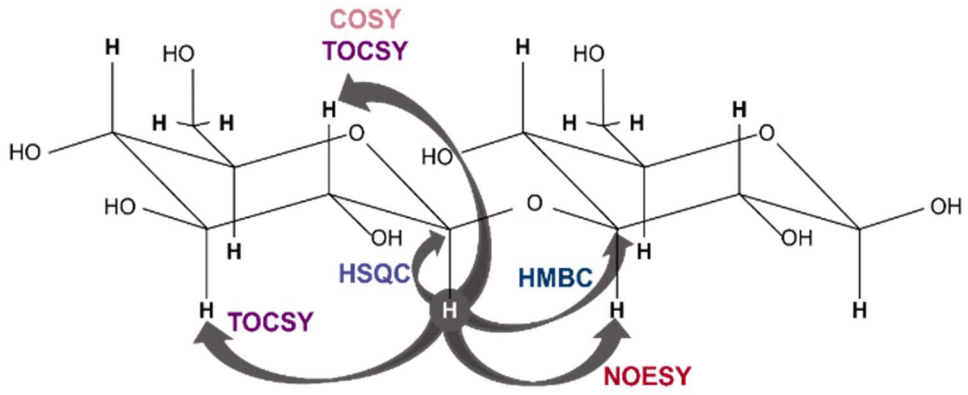


**Figure 15**: Representation of atom interactions with different 2D NMR experiments

## 2.5. Mass Spectrometry of the Lipid A

Mass Spectrometry (MS) is a technique that give information about molecular mass. It is a destructive methods that have the advantage to work with very little amount of sample. Several ionisation and fragmentation techniques can be used in MS. For big molecules, as peptides or Lipid A, MALDI ionisation coupled with Time Of Flight (TOF) separation is a suitable technique that is often used. MALDI/TOF MS of Lipid A can be recorded either in positive or negative ion mode.

Negative ion MALDI/TOF MS of Lipid A extracted in acidic conditions contains several clusters of peaks corresponding to species with different degree of acylation. Indeed, under-acylated species can be formed after mild acid hydrolysis and there can also naturally occur a mixture of Lipid A species in intact cells. The mass difference between each clusters usually corresponds to an acyl chain or a phosphate. The composition of the Lipid A, i.e. its phosphorylation, the number and nature of its acyl chains and the presence of other substituents, can be determined with this experiment.

However, MALDI/TOF MS analysis alone is not sufficient to obtain a detailed structure. Indeed, it is not possible with this technique to determine the linkage position of each phosphates and acyl chains on the di-glucosamine backbone. MS/MS analysis are then performed on several precursor ions. The fragmentation of the studied Lipid A species are analysed with those experiments. Those fragments can arise from the loss of phosphates and fatty acids but also from sugar ring and linkage cleavage. Those well-known events possess a specific nomenclature that was determined by Costello et al.[55] (Figure 16). The occurrence of those linkages and sugar ring fragmentation allow the detection of mass corresponding to each glucosamine. This experiment is hence necessary in order to establish the acyl chains repartition among the di-glucosamine backbone.

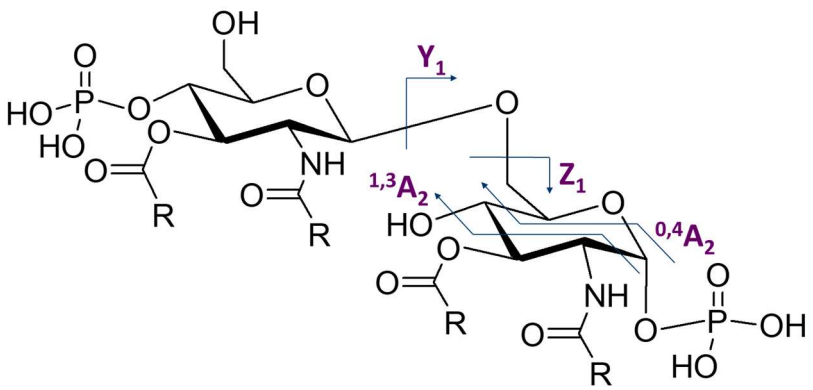


**Figure 16**: Main linkages and sugar ring fragmentation that can be observed during MS/MS of the Lipid A

Finally, the Lipid A should undergo an ammonium treatment to complete its structural analysis. Indeed, this procedure is necessary in order to determine if each acyl moieties in ester or amide-linked[56]. It is known that with this method secondary ester-linked are more labile than primary ester-linked acyl moieties and amide linked residues. MALDI/TOF MS performed after such extraction procedure hence lead to the detection of species which mass difference correspond to their ester-linked fatty acids. The analysis can be completed with MS/MS of ammonium treated Lipid As. The combination of all previously described MS experiments lead to the precise determination of the Lipid A architecture.

# Section II

## Pseudoalteromonas sp1A1: From endotoxin to Outer-Membrane

# Chapter 3: Structure and activity of Lipopolysaccharide of *Pseudoalteromonas sp 1A1*

## 3.1. *Pseudoalteromonas* spp. and their environment

The genus *Pseudomonas* is part of the 'gamma-proteobacteria' group and is composed of gram-negative aerobic and flagellated bacteria[57]. Based on 16S rRNA analysis, Gauthier et al. proposed a division of this group with the new genus *Pseudoalteromonas*[58]. Since then, *Pseudoalteromonas spp.* is widely studied for its capacity to produce biologically active molecules such as antibiotics and compounds against fungi[59]. These properties give *Pseudoalteromonas spp.* the ability to survive and coexist in its complex environment[60]. It can indeed significantly influence its ecosystem with several mechanisms as the production of biofilms, anti-fouling and anti-algae agents[61].

*Pseudoalteromonas spp.* encloses several marine species, some known to interact as symbiont or pathogens with eukaryotic organisms including marine sponges[62]. Within this ecosystem, sponges developed molecular strategy to recognize and defend themselves against pathogenic microbes, as the case of *Suberites domuncula* which developed a molecular immune response towards bacterial infection[63]. As gram-negative bacteria, *Pseudoalteromonas spp* possess LPS in their OM (See Section 1). The LPS isolated from different *Pseudoalteromonas* strains were shown to be penta-acylated with low-immunostimulatory and antagonist properties in murine cells[64]. For *S. domuncula*, LPS is recognized by a specific receptor named *S. domuncula* LPS interacting protein (SLIP) and then activates the MyD88-dependent pathway of TLR4/MD-2 receptorial complex[65].

The present chapter reports the investigation of the structure and immunological activity of the LPS from *Pseudoalteromonas sp1A1*. It is a sponge-pathogen bacterium isolated from *S. domuncula*[66]. Further analysis of the properties of the LPS were made in order to understand *Pseudoalteromonas sp1A1* behaviour in its ecosystem and to dissect its immunopotential.

## 3.2. Extraction and compositional analysis

The LPS was extracted using hot phenol-water procedure and purified by enzymatic treatment. SDS-PAGE confirmed the presence of LPS in the purified water phase with the occurrence of a ladder-like pattern on the gel (Figure 17).

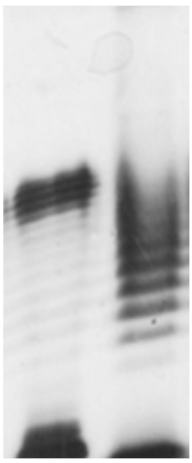

**A** **B**

**Figure 17**: SDS-PAGE 13.5% **A**. LPS from *E. coli* standard; **B.** LPS from *Pseudoalteromonas sp1A1*, water phase

Compositional analysis (MGA) showed the presence of D-3-deoxy-3-amino-Quinovose (D-QuiN), D-Mannose (D-Man), D-Glucose (D-Glc), D-Glucosamine (D-GlcN), 3-deoxy-D-*manno*-oct-2-ulopyranosonic acid (D-Kdo) an another Ulosonic acid identified as 3-deoxy-D-*glycero*-D-*galacto*-nonulosonic acid (KDN)[67] (Figures 18 and 19). Combined with previous MGA experiment, AAPM analysis showed that *Pseudoalteromonas sp1A1* LPS is composed of terminal Qui3N, terminal Man, 4,6-subsituted-Glc, 3-substituted-GlcN and 3,4,6-substituted-GlcN.

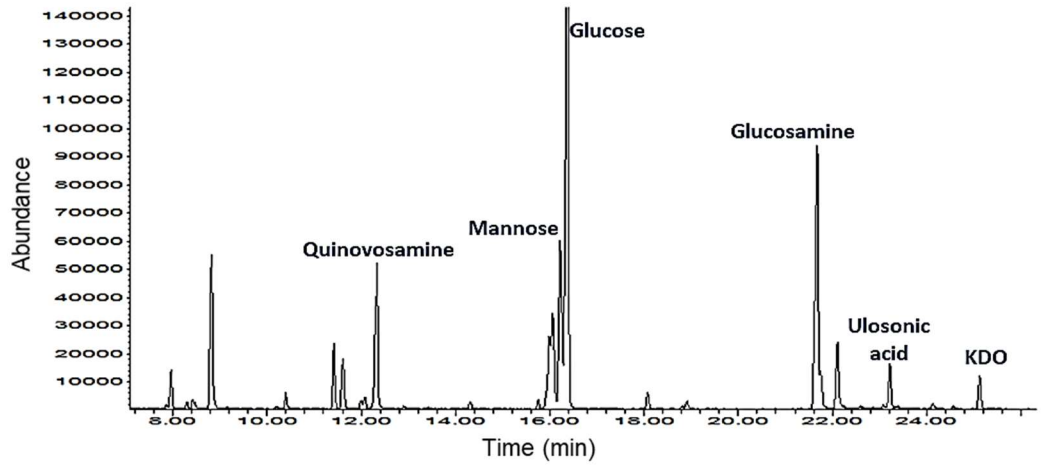


**Figure 18**: GC-MS chromatogram of MGA derivative of *Pseudoalteromonas sp1A1* LPS

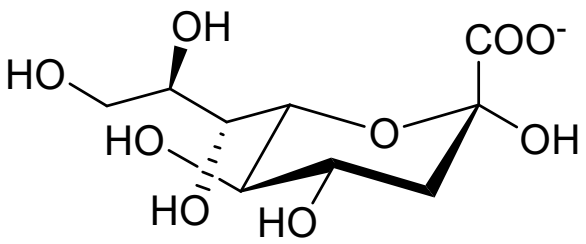


**Figure 19**: Structure of as 3-deoxy-D-*glycero*-D-*galacto*-nonulosonic acid (KDN)

Fatty acid analysis revealed the occurrence of *(R)*-3-hydroxydodecanoic acid [12:0(3-OH)], *(R)*-3-hydroxydecanoic acid [10:0 (3-OH)], *(R)*-3-hydroxyundecanoic acid [11:0 (3-OH)], *(R)*-3-hydroxytridecanoic acid [13:0 (3-OH)] as primary acyl chains, both in amide and ester linkage, and, as secondary acyl chain, of dodecanoic acid (12:0), decanoic (10:0), undecanoic acid (11:0), tridecanoic acid (13:0), dodecenoic (12:1) and tridecenoic (13:1).

## 3.3. Structure of *Pseudoalteromonas sp 1A1* O-antigen

*Pseudoalteromonas sp1A1* LPS was fully de-acylated and its O-antigen was characterised via NMR spectroscopy. A combination of homo- and heteronuclear 2D NMR experiment (DQF-COSY, TOCSY, ROESY, NOESY, $^{1}$H-$^{13}$C HSQC, $^{1}$H-$^{13}$C HMBC) was executed to assign all the spin systems and to define the saccharidic sequence. Complete assignment of the spin systems was obtained attributing the proton resonances by DQF-COSY and TOCSY spectra, and subsequently correlating each proton to its related carbon atom through the HSQC spectrum. The anomeric configuration of each monosaccharide unit was assigned on the basis of $^{3}J_{H\text{-}1,H\text{-}2}$ coupling constant obtained by the DFQ-COSY.

A magnitude of $^{3}J_{H\text{-}1,H\text{-}2}$ with values of 7–9 Hz was associated with the diaxial coupling of a β-configured sugar unit, whereas 2–4 Hz was indicative of an equatorial-axial coupling of α-configured residues. Six different units were detected in *Pseudoalteromonas sp1A1* O-antigen (Figure 20).

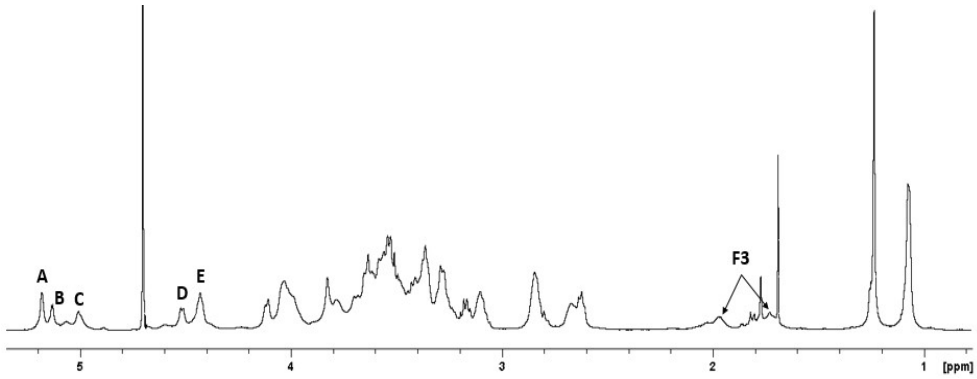


**Figure 20:** $^{1}$H spectra of deacylated O-antigen from *Pseudoalteromonas sp1A1*

| Unit | 1 | 2 | 3 | 4 | 5 | 6 | 7 | 8 | 9 |
|---|---|---|---|---|---|---|---|---|---|
| **A α-GlcN** | 5.18 *99.37* | 2.80 *56.21* | 3.54 *80.66* | 3.29 *74.67* | 4.04 *72.57* | 3.63-3.51 *64.01* | -- | -- | -- |
| **B α-Glc** | 5.13 *99.18* | 3.36 *72.96* | 3.51 *72.57* | 3.17 *69.60* | 3.61 *72.26* | 3.65-3.52 *60.47* | -- | -- | -- |
| **C α-Man** | 5.00 *97.97* | 3.58 *72.10* | 3.47 *71.10* | 3.23 *69.99* | 3.365 *71.71* | 3.69-3.52 *60.70* | -- | -- | -- |
| **D β-GlcN** | 4.51 *98.31* | 2.62 *55.87* | 3.36 *84.0* | 3.27 *75.76* | 3.43 *69.54* | 3.78-3.82 *56.94* | -- | 1.24 *24.37* | -- |
| **E β-Qui3N** | 4.43 *103.41* | 3.10 *72.80* | 2.67 *57.26* | 2.84 *73.89* | 3.35 *69.15* | 1.07 *16.65* | -- | -- | -- |
| **F KDN** | -- | -- | 1.72-1.98 *34.6* | 3.99 *65.53* | 3.83 *73.5* | 4.11 *69.77* | 4.03 *62.7* | 3.40 *85.72* | 3.65-3.41 *64.01* |

**Table 1:** $^{1}$H and $^{13}$C (italic) chemical shifts (ppm) of de-acylated O-antigen from *Pseudoalteromonas* sp1A1

Spin systems **A**, **B**, **D**, **E** were *gluco*-configured residues as indicated by the large $^{3}J_{H,H}$ ring coupling constant values of their ring protons (8-10Hz). Residues **A** and **D** (H1 respectively at *δ* 5.18 ppm and *δ* 4.51 ppm,

table 1) were identified as α-GlcN and β-GlcN based on their nitrogen-bearing C-2 respectively at *δ* 56.21 and *δ* 55.87ppm. Residue **B** was recognized as α-Glc (H1 at *δ* 5.13ppm, table 1). Residue **E** was identified as β-Qui3N according to the value of its C-3 (*δ* 57.26 ppm) indicative of a nitrogen-bearing carbon and its downfield H-6/C-6 (*δ* 1.07/16.65 ppm) corresponding to the methyl group.

Residue **C** (H1 at *δ* 5.00ppm, table 1) was attributed as α-mannose. The *manno* configuration was established by $^{3}J_{H\text{-}1,H\text{-}2}$ and $^{3}J_{H\text{-}2,H\text{-}3}$ values (below 3 Hz), the α-configuration was assigned either by the *intra*-residual NOE contact of H-1 with H-2 and by chemical shift value of its C1 (*δ* 97.97 ppm, table 1). Finally, residue **F** was identified as KDN, in accordance with the compositional analysis. Indeed, it possesses characteristic diastereotopic methylene signals at H-3 (*δ* 1.72/1.98 ppm, table 1) and a 9-carbon sequence.

Moreover, the proton at 1.24 ppm (with corresponding carbon at *δ* 24.03 ppm) gave NOE contacts with protons H-4 (*δ* 3.27 ppm) and H-6 (*δ* 3.78-3.82 ppm) of unit **D**. It was attributed to a methyl group of a pyruvate that is linked to the β-GlcN.

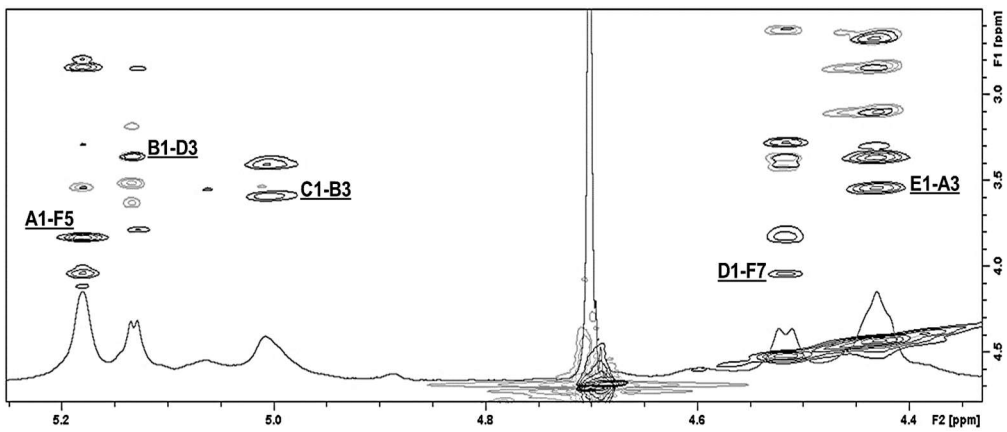


**Figure 21:** NOESY (black) and TOCSY (grey) spectra of the anomeric region of the O-antigen of *Pseudoalteromonas sp1A1*

NOESY (Figure 21) and HMBC spectra allowed the determination of the sugar sequence in the polysaccharide and was consistent with previous compositional analysis. Spin system **F** was substituted at O-5 by residue **A** and O-7 by residue **D**, as shown by NOE contacts found between H-1 **A** (*δ* 5.18 ppm) and H-5 **F** (*δ* 3.83 ppm) and between H-1 **D** (*δ* 4.51 ppm) and H-7 **F** (*δ* 4.03 ppm). Spin system **A** was in turn glycosylated by residue **E** as indicated by NOE contact between H-1 **E** (*δ* 4.43 ppm) and H-3 **A** (*δ* 3.54 ppm). Spin system **D** was substituted at O-3 by residue **B** as shown by NOE correlations between H-1 **B** (*δ* 5.13 ppm) and H-3 **D** (*δ* 3.36 ppm). Finally, spin system **B** was glycosylated at O-3 by residue **C** as proven by NOE contacts between H-1 **C** (*δ* 5.00 ppm) and H-3 **B** (*δ* 3.51 ppm) (Figure 21). Combined with previous methylation analysis, the full sequence of *Pseudoalteromonas* sp1A1 O-antigen was elucidated as a branched polysaccharide and its structure is represented in Figure 22.

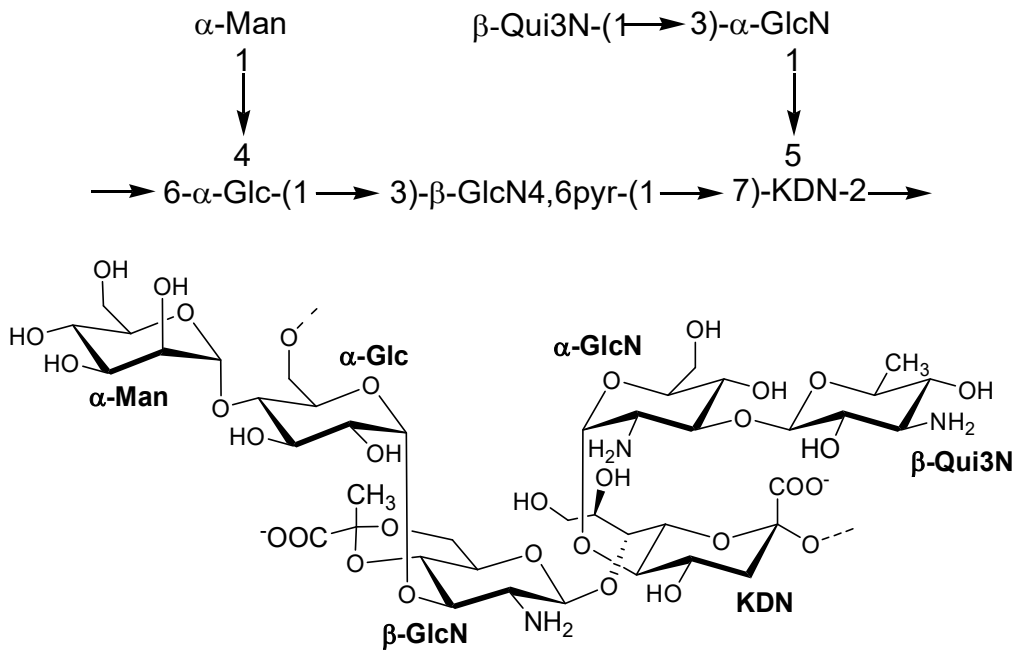


**Figure 22:** Structure of the O-antigen from *Pseudoalteromonas* sp1A1

## 3.4. Structure of *Pseudoalteromonas sp1A1* Lipid A

Negative-ion MALDI-TOF MS of *Pseudoalteromonas sp1A1* was performed on the mild acid hydrolysis product and is shown in Figure 23. The very heterogeneous composition of the Lipid A could be clearly seen, in accordance to previous compositional analysis and other *Pseudoalteromonas spp.* LPS Lipid A species[68,69,70.]. The mass spectrum showed multiple sets of *pseudomolecular* ion peaks $[M-H]^-$ comprised in the mass range *m/z* 1000-1500 Da (Figure 23). Within those clusters, the occurrence of mass differences of 14 amu was attributable to methylene units and thus referred to Lipid A species having different acyl chain lengths.

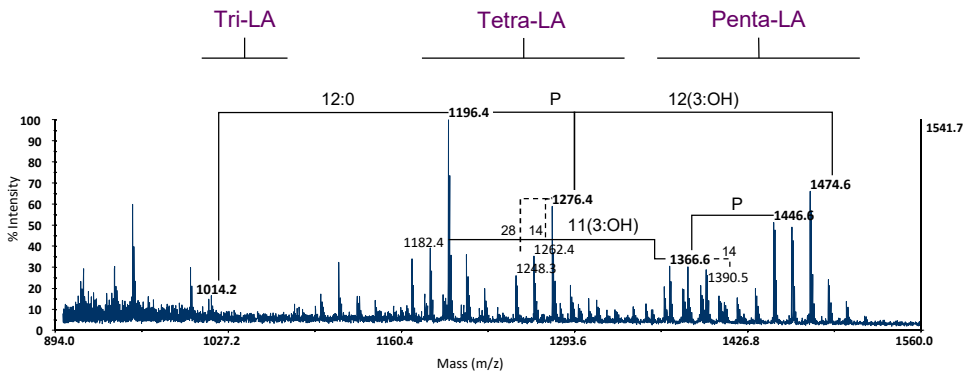


**Figure 23:** Negative-ion MALDI-TOF mass spectrum of the isolated lipid A fraction from *Pseudoalteromonas sp 1A1* LPS. Assignment of the lipid A species as Tri LA (tri-acylated lipid A species), Tetra LA (tetra-acylated lipid A species), Penta LA (penta-acylated lipid A species) and the relative groups of ions lacking one phosphate is also indicated

The *bis*-phosphorylated and penta-acylated species were detected in the cluster around *m/z* 1474.6 (Figure 23), this last corresponding to a lipid A species carrying four 12:0 (3-OH) primary acyl substituent and one 12:0 as secondary acyl moiety. The species at *m/z* 1446.6 matched with a lipid A containing two 12:0 (3-OH), one 11:0 (3-OH), one C10:0 (3-OH) and one

C13:0. Its corresponding *mono*-phosphorylated lipid A could be detected at *m/z* 1366.6 (Δ*m/z* = 80). Fragments at *m/z* 1276.4 and 1262.4 matched with tetra-acylated species that have respectively lost C12:0 (3-OH) or C11:0 (3-OH) moieties (Figure 23, Table 2). The most abundant peak, at *m/z* 1196.4, corresponded to a *mono*-phosphorylated and tetra-acylated Lipid A species bearing three 12:0 (3-OH) and one 12:0 (Figure 23, Table 2).

| Observed ion peak (m/z) | Acyl Substitution | Proposed Fatty acid/phosphate composition |
|---|---|---|
| 1474.6 | Penta-acyl | $HexN^2P^2$ [C12:0 (3OH)]$^4$[C12:0] |
| 1446.6 | Penta-acyl | $HexN^2P^2$[C12:0 (3OH)]$^2$[C11:0 (3OH)] [C10:0 (3OH)] [C13:0] |
| 1366.6 | Penta-acyl | $HexN^2P$[C12:0 (3OH)]$^2$[C11:0 (3OH)] [C10:0 (3OH)] [C13:0] |
| 1276.4 | Tetra-acyl | $HexN^2P^2$ [C12:0 (3OH)]$^3$[C12:0] |
| 1262.4 | Tetra-acyl | $HexN^2P^2$ [C12:0 (3OH)]$^2$[C10:0 (3OH)] [C13:0] |
| 1248.4 | Tetra-acyl | $HexN^2P^2$[C12:0 (3OH)][C11:0 (3OH)] [C10:0 (3OH)] [C13:0] |
| 1196.4 | Tetra-acyl | $HexN^2P$[C12:0 (3OH)]$^3$[C12:0] |
| 1182.4 | Tetra-acyl | $HexN^2P$[C12:0 (3OH)]$^2$[C10:0 (3OH)] [C13:0] |
| 1014.2 | Tri-acyl | $HexN^2P$ [C12:0 (3OH)]$^3$ |

**Table 2:** Proposed interpretation of main peak ions of MALDI-TOF MS (Figure 23)

*Pseudoalteromonas sp 1A1* hence possesses the same mixture of Lipid A species that are represented on Figure 24. The *bis*-phosphorylated and penta-acylated Lipid A species is acylated by four C12:0 (3-OH) in amide linkages and as primary ester-linked fatty acids and one C12:0 as secondary fatty acid. The other penta-acylated Lipid A species is also *bis*-phosphorylated and penta-acylated and possesses one C10:0 (3-OH), one C11:0 (3-OH) and one C12:0 (3-OH) as primary linked fatty acid and one C13:0 as secondary linked fatty acid. It should be noted that odd numbered fatty acids – C11:0 (3-OH) and C13:0 – likely possesses isopropyl groups

at their extremity. The obtained data are in accordance with the study of *Pseudoalteromonas sp 2A*, a commensal bacterium also isolated from *S. domoncula*[71].

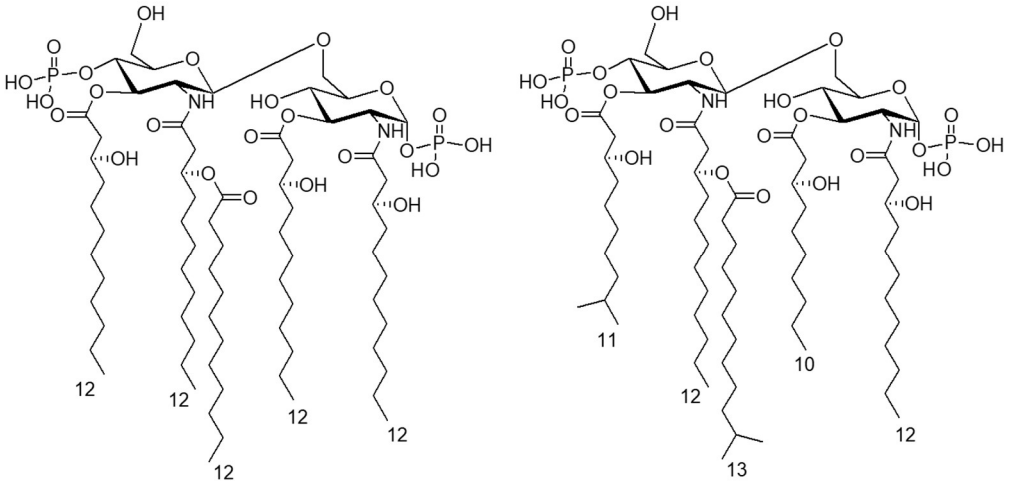

**Figure 24:** Structure of *Pseudoalteromonas sp1A1* Lipid A species

Gardères et al.[66] previously analysed *Pseudoalteromonas* sp 1A1 Lipid A and found mono-phosphorylated and penta-acylated Lipid A species, bearing four 12:0 (3-OH) one 12:0 units. However, they did not detected the bis-phosphorylated species and concluded that the secondary fatty acid on the non-reducing glucosamine was linked on the acyloaxyl ester instead of the acyloxyamide. They possibly detected fragments of the lipid A that got degraded.

## 3.5. Structure of *Pseudoalteromonas* sp 1A1 LOS

The full LOS structure has also been resolved using MALDI-TOF MS (Figure 25). Clusters corresponding to the native LOS could be seen between *m/z* 2300 and 3000. In source regiospecific cleavage (β-elimination) of the labile linkage involving the Kdo enables both the detection of the core oligosaccharide ions (B-type ions, *m/z* 1000-1200) and the Lipid A ions (Y ions, *m/z* 1400-1500)[72]. Several species were detected in the higher mass region, corresponding to the native LOS composed by the Lipid A with four C12:0 (3-OH) and one C12:0 (Figure 24). Peak at *m/z* 2531.7 was attributed to the LOS with a core oligosaccharide composed of one Kdo, one heptose and three hexoses. The minor peak at *m/z* 2369.7 corresponded to the LOS that lacks one hexose unit. Another LOS species constituted by four hexoses was detected at *m/z* 2693.6. The ion at *m/z* 2487.7 originated from the loss of a neutral $CO_2$ on the Kdo unit. Finally, the minor peak at *m/z* 2423.5 was attributed to the native LOS devoid of a phosphate group and constituted by the Lipid A with one C10:0 (3-OH), one C11:0 (3-OH), two C12:0 (3-OH) and one C13:0 (Figure 24).

The main *Pseudoalteromonas sp1A1* core oligosaccharide is composed of three hexoses, one heptose, the Kdo and two phosphates. The hexoses comprise one terminal glucose, one terminal galactose and one 4-substituted galactose. The heptose is 4,7-substituted and possesses a phosphate group at its 3-position. Finally, the Kdo is 5-substituted and possesses another phosphate group at its 4-position (Figure 26). Those data match the analysis of another *Pseudoalteromonas* strain that present the very similar LOS structure[73].

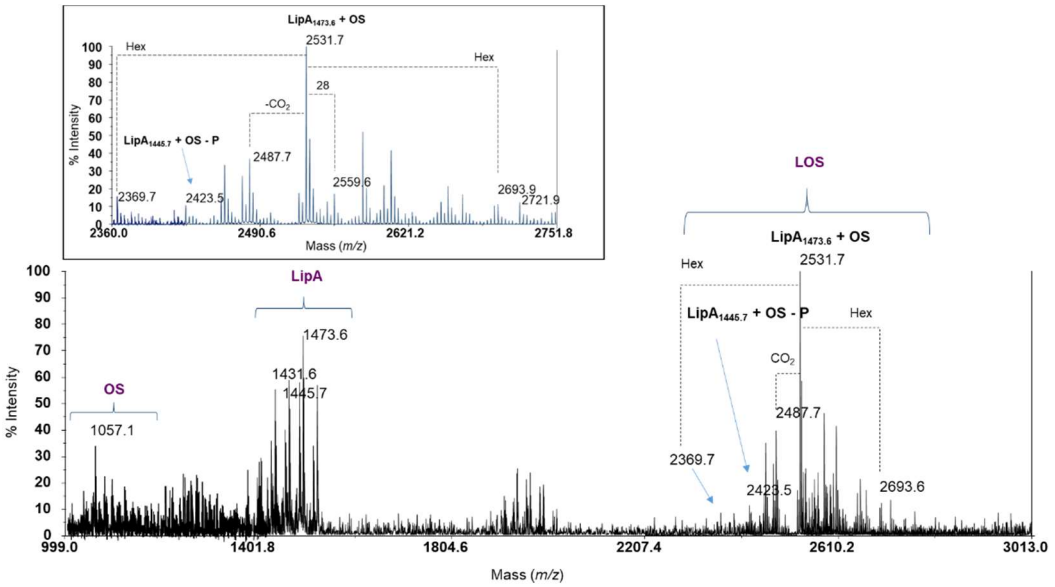


**Figure 25:** MALDI TOF MS analysis of total LOS from *Pseudoalteromonas sp1A1*; Zoom on the whole LOS fragmentation is reported in the inset

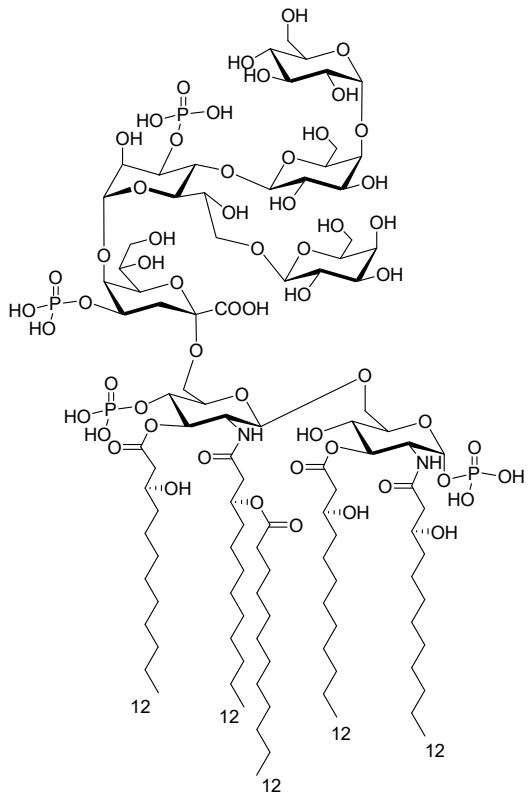

**Figure 26:** Structure of *Pseudoalteromonas sp1A1* LOS

## 3.6. Immunological assays

Biological assays were performed to determine the effect of *Pseudoalteromonas sp 1A1* on mammal's innate immune system. This work was performed within Prof. Bayeart's team at VIB, Ghent, Belgium. Human homocytic cell line THP1 was used to test agonist activity. Cells were stimulated with different concentrations of *Pseudoalteromonas sp1A1* and *E. coli* LPS or were left untreated. The quantity of secreted TNF was measured by ELISA. Results shows that, although a slight immunostimulant effect can be observed, *Pseudoalteromonas sp1A1* do not possess interesting agonistic activity compared to *E .coli* LPS (Figure 27 a).

Antagonist activity of *Pseudoalteromonas sp1A1* lipid A was assessed with a competitive test. The experiment was performed with Raw-Blue-hTLR4 murine cell line. Treatment with *E. coli* LPS and untreated cells were used as control. After incubation of cells with 100 ng/mL of *E. coli* LPS and different concentrations of *Pseudoalteromonas sp1A1* LPS, Secreted Alcaline Phophate (SEAP) was measured by absorbance. Its concentration is directly linked to the immunostimulant activity of the tested compound or its mixture. The results demonstrates that *Pseudoalteromonas sp1A1* do not inhibit the activity of *E. coli* LPS (Figure 27 b). In conclusion, *Pseudoalteromonas sp1A1* LPS do not possess any agonist or antagonist properties toward the mammal immune system.

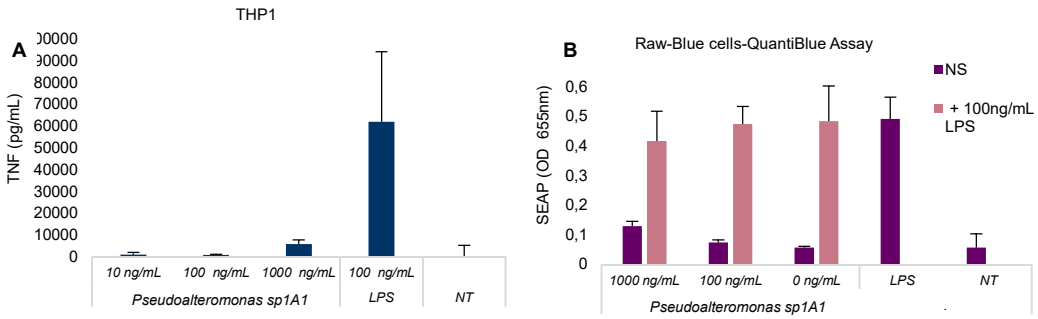


**Figure 27:** Immunological assays with *Pseudoalteromonas* sp 1A1 LPSs. (A) Measurement of TNF production by ELISA with THP1 human cell line and (B) measurement of SEAP absorbance by Quanti-blue assay with Raw-Blue-hTLR4 murine cell line. Cells were incubated with the indicated amounts of *Pseudoalteromonas sp1A1* and *E. coli* 0111:B4 LPS. Error bars represent the standard deviation of the mean of biological triplicates. Graph is representative of at least three independent experiments

## 3.7. Conclusion

This chapter reports the full structural characterization of *Pseudoalteromonas sp. 1A1* LPS. Its O-antigen is composed of a branched repeating unit that includes specific features as the presence of KDN and the linkage with a pyruvate. Its core oligosaccharide is composed of a phosphorylated pentasaccharides, with heptose and Kdo residues linked to the lipid A. Finally, *Pseudoalteromonas sp1A1* possesses a mixture of Lipid A species, bis-phosphorylated and differently acylated, the penta-acylated with a 3+2 symmetry. It is also interesting to note that *Pseudoalteromonas sp1A1* actually possesses the same Lipid A mixture as *Pseudoalteromonas sp2A*[71]. Indeed, *Pseudoalteromonas sp1A1* is a pathogenic bacterium for *S. domoncula* and *Pseudoalteromonas sp2A* is an opportunistic bacterium. This different properties, despite the similar structure, can be explained by

the fact that *Pseudoalteromonas sp1A1* does not influence sponge TLR-related pathway, contrary to *E. coli* Lipid A[66]. The activation of *S. domoncula* immunity may be triggered by other PRR/PAMP interactions.

Concerning the immunostimulant activity in human and mice, this study revealed no significant agonist or antagonist properties of *Pseudoalteromonas sp1A1* LPS that have hence no significant interaction with TLR4/MD-2 signaling either in mammals or with sponges in its natural environment.

# Chapter 4: In silico study of the outer-membrane of *Pseudoalteromonas sp1A1*

## 4.1. Molecular dynamic simulation of Gram-negative bacteria OM

The envelope of Gram-negative bacteria (Outer Membrane, OM) is a complex structure (See Section I), and the elucidation of its properties is important in order to gain insight about its interaction with its environment. In this context, Molecular Dynamic Simulations (MDS) of Gram-negative cell envelope have increasingly been performed during the last decade. The first designed asymmetric OM was from *Pseudomonas aeruginosa PA01*[74]. Other MDS of Gram-negative cell envelope lead to a better understanding of its structure and dynamics. This knowledge is a useful tool for the development of antibiotics and the prediction of new compounds for immunotherapy[75]. Investigations done with of *E. coli* OM showed the importance of the presence of LPS in the OM simulations. Indeed, LPS are involved in several membrane properties as its permeability and its interaction with OMPs[76].

It is now known that the LPS composition of an OM influence its overall properties. Indeed, a coarse-grain model of an asymmetric membrane showed that the presence of LPS is related to a diminution of the membrane melting point and an increase of its area per lipids[77]. Another study was performed with several homogeneous LPS bilayer at atomic level and highlighted several point as: (i) the area per lipid of a membrane is correlated to the number of acyl chains of its LPS and (ii) its hydrophobic thickness is linked with the length of the acyl chains[78].

In this context, the present chapter reports *in silico* study of *Pseudoalteromonas sp1A1* OM at atomic level. The experiments were designed in order to see if the OM was influenced by the Lipid A structure previously characterized (See Section II). Additionally, the properties of the



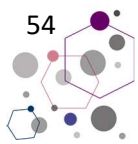

LOS itself were studied in order to understand if the presence of salts can modulate its structural conformation.

## 4.2. Molecular dynamic simulation of *Pseudoalteromonas sp1A1* OM

In order to understand *Pseudoalteromonas sp1A1* Outer-Membrane (OM) behaviour, several systems were built *in silico.* Three kind of bilayers were studied (i) an homogeneous POPE:POPG (3:1) bilayer (Figure 28), similar to the inner membrane of Gram-Negative bacteria[79], (ii) the same system with a single inserted Lipid A and (iii) an asymmetric lipid A containing bilayer. The goal was to determine if the properties of the OM could be influenced by the presence of a Lipid A.

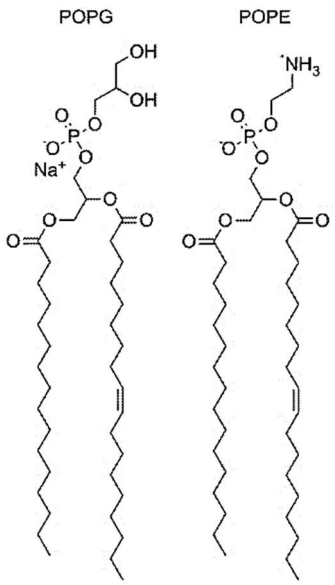


**Figure 28:** Structure of Palmitoyloleoyl Phosphatidylglycerol (POPG) and Palmitoyloleoyl Phosphatidylethanolamine (POPE)

To do so, a POPE:POPG (3:1) bilayer containing 128 lipids was generated using CHARMM-GUI[80] (Figure 29 A). Molecular dynamic simulation of this membrane was performed during 100 ns using AMBER Lipid11[81] and Lipid14[82] force fields. After the simulation, its hydrophobic thickness and area per lipid were calculated using CPPTRAJ software[83], giving the properties of a homogeneous bilayer. Meanwhile, *Pseudoalteromonas sp1A1* Lipid A was built calculating electrostatic charges of each of its residues (Figure 29 B). This study was focused on the main Lipid A species with homogeneous C12:0(3-OH) acylation (See Figure 24). This molecule was built with negatively charged phosphate groups and inserted in an octahedral TIP3P water box. Then molecular dynamic simulation was done for 100 ns, allowing the fatty acid chains to gather due to the hydrophobic effect (Figure 29 C). Then, using PyMOL software, a single Lipid A was inserted in the previous POPE:POPG bilayer (Figure 29 D). Another molecular dynamic simulation was performed during 100 ns and hydrophobic thickness and area per lipid were once again calculated, giving the properties of bilayer with a single inserted Lipid A.

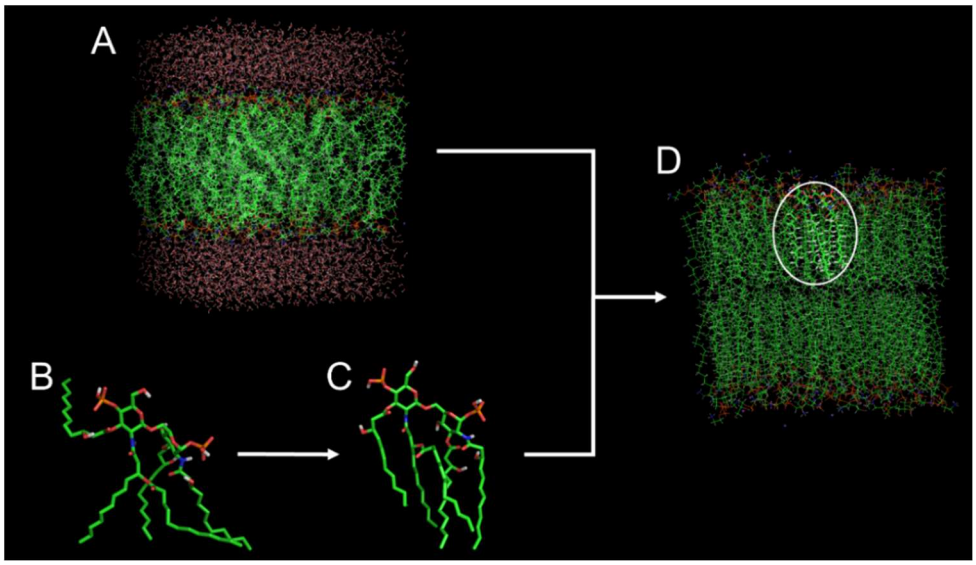


**Figure 29:** Snapshot from the molecular dynamic simulation of a single Lipid A from *Pseudoalteromonas sp1A1* in a POPE:POPG (3:1) bilayer. A: POPE:POPG (3:1) bilayer built with CHARMM-GUI. B: *Pseudoalteromonas sp1A1* Lipid A. C: *Pseudoalteromonas sp1A1* Lipid A after 100ns of MDS in explicit water. D: *Pseudoalteromonas sp1A1* Lipid A inserted in POPE:POPG (3:1) bilayer

Finally, to better mimic the real OM of gram-negative bacteria, an asymmetric bilayer was studied. The inner leaflet was composed of POPE:POPG (3:1) and the outer leaflet of 75% of Lipid A and 25% of POPE:POPG (3:1). Both leaflets were generated separately. The inner leaflet was created from of a 168 POPE:POPG (3:1) bilayer generated with CHARMM-GUI. The outer leaflet was generated manually. Firstly, the Lipid A was extracted after its MDS in POPE:POPG (3:1) bilayer (Figure 29 D). Then it was duplicated until a 30 Lipid A grid was obtained (Figure 30 A). Using PYMOL, the Lipid As were reorganized in order to leave place for other lipids (Figure 30 B). Then 8 POPE and 2 POPG were added (Figure 30 C). The obtained Lipid A / POPE:POPG proportions are consistent with the ones used in previous studies[77].

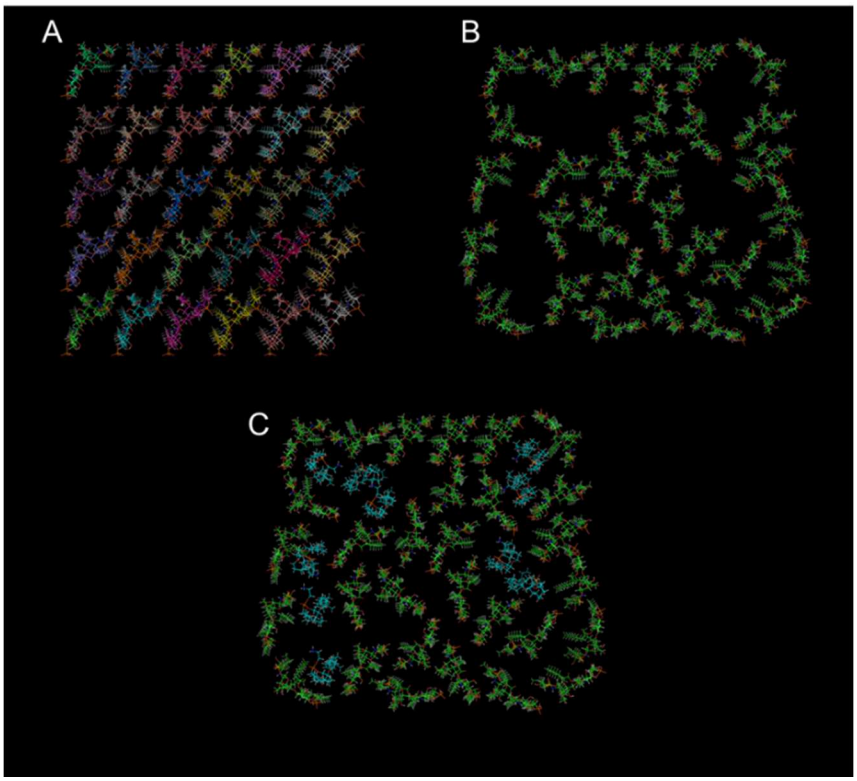


**Figure 30:** Top-view snapshot of the generation of *Pseudoalteromonas sp1A1* outer leaflet. A: generation of a 30 Lipid A grid; B: re-organisation of the grid; C: insertion of 8 POPE and 2 POPG

Finally, both inner and outer leaflet were combined using PyMOL (Figure 31 A). Molecular dynamic simulation of this new system was performed for 100ns. During the simulation, the membrane equilibrated reaching a stable conformation (Figure 31 B) and area per lipid and electron density were calculated. Some differences could be observed during the comparison of the properties of the 3 different membranes (bilayer without Lipid A, bilayer with single Lipid A and asymmetric bilayer, Figures 29 A, 29 D, and 31 B). Although the hydrophobic thickness was constant, the area per lipid of the asymmetric membrane was lower than the ones of the other bilayers. The electron density always showed a

hydrophobic thickness of 40 Å (Figure 32, C-D) but an asymmetric profile could be clearly seen with the third membrane (Figure 32 D). Moreover, the area per lipid stabilised around 52 $Å^2$ for homogeneous bilayers (Figure 32 A) and fluctuated around 67 $Å^2$ for the asymmetric membrane (Figure 32 B). Such system give *Pseudoalteromonas sp1A1* OM a higher flexibility.

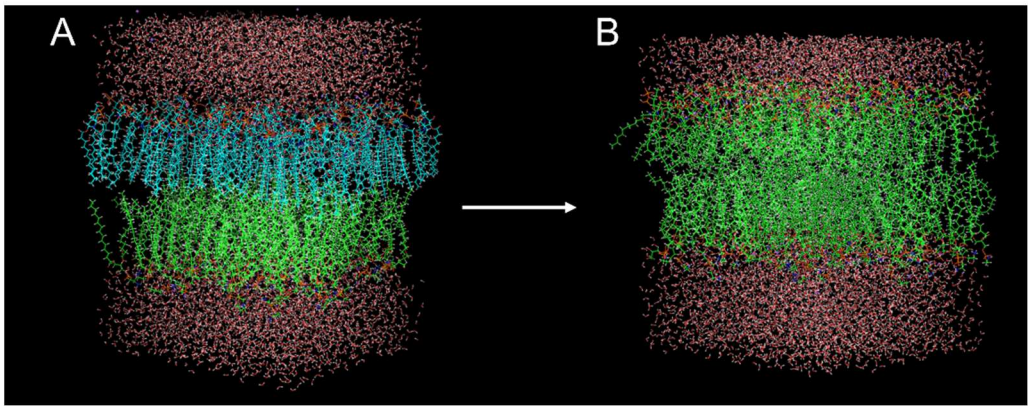


**Figure 31:** Assymetric bilayer before (A) and after (B) MDS for 100ns. Inner leaflet is composed of POPE:POPG (3:1) and Outer Leaflet is composed of 75% Lipid A and 25% POPE:POPG (3:1)

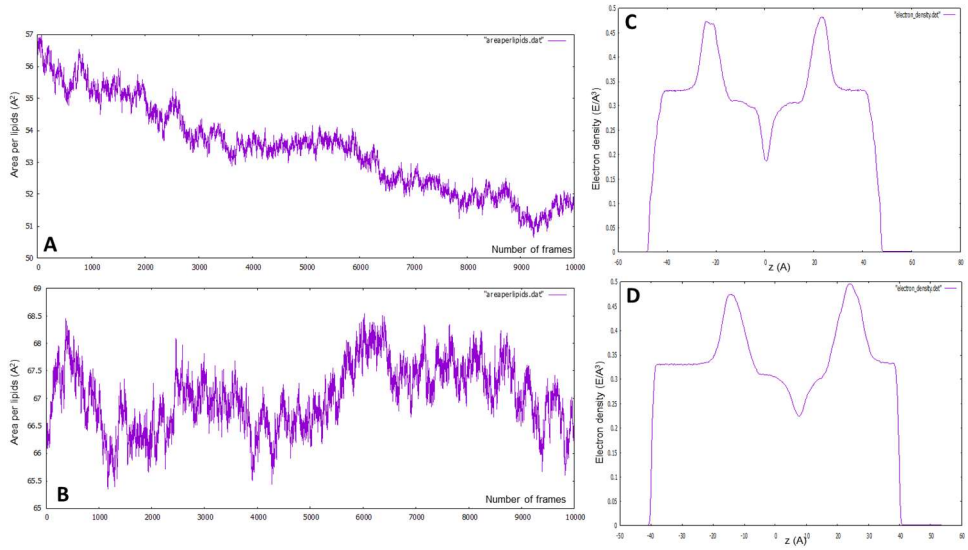


**Figure 32:** Area per lipids and electron density of POPE:POPG (3:1) bilayer with single-inserted Lipid A (A,C) and asymmetric bilayer (B,D)

Finally, dihedral angles of the glucosamine backbone from *Pseudoalteromonas sp 1A1* Lipid A were calculated after each simulations (Figure 33). No difference was detected compared to the free lipid A. The insertion of the molecule in a membrane do not influence its conformation.

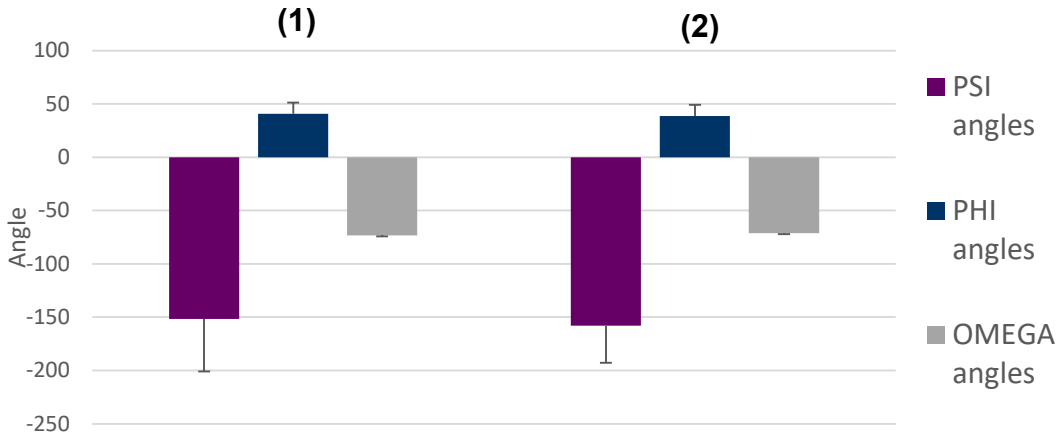


**Figure 33:** Conformational angles of the di-glucosamine backbone of *Pseudoalteromonas sp1A1* Lipid A (1) in water and (2) inserted in POPE:POPG (3:1) bilayer

## 4.3. Molecular dynamic simulation of *Pseudoalteromonas sp1A1* LOS

Another set of experiment was performed with *Pseudoalteromonas sp1A1* LOS (See Figure 26). The goal was to study its oligosaccharide conformation in different environments. The oligosaccharide from *Pseudoalteromonas sp1A1* was generated with GLYCAM and then inserted on the previously studied Lipid A (Figure 34).

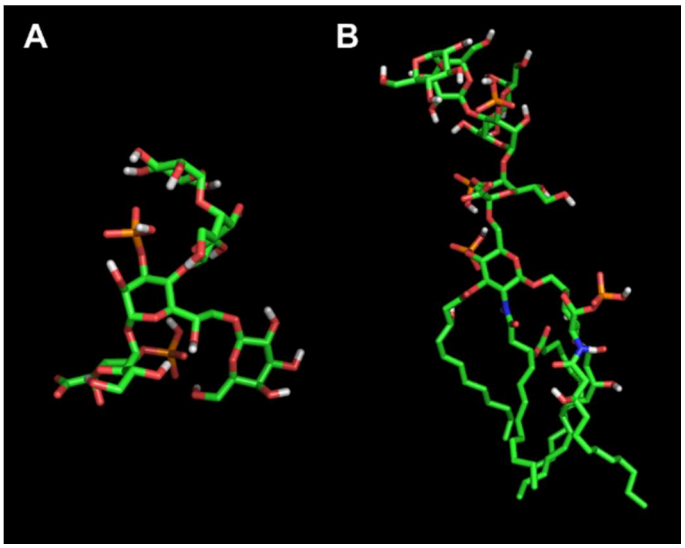


**Figure 34:** Snapshot of the oligosaccharide (A) and LOS (B) from *Pseudoalteromonas* after 100ns MDS in explicit water

Molecular dynamic simulation were performed during 50 ns in explicit water and 0.5 M of NaCl, that is closed to the salt concentration of its natural marine habitat. After simulations, dihedral angles between each monosaccharides were calculated and compared. Interesting feature was observed for the ω torsional angle between the Kdo from the core oligosaccharide and its linked glucosamine from the Lipid A. Indeed, during the simulation this angle was rotating between two values (Figure 35), one positive angle around 50° and another negative angle around -50°. When the LOS was in water, the positive value was preponderant but in salt the negative one predominated. This shows that salty environment have an influence on LOS conformation.

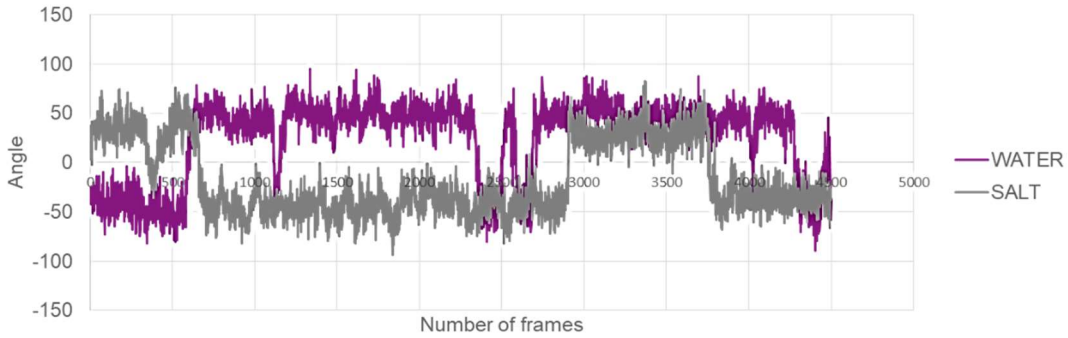


**Figure 35:** Omega tortional angle between the Kdo and reducing glucosamine of the LOS from *Pseudoalteromonas sp1A1*

## 4.4. Discussion

Molecular dynamic simulation allowed a better understanding of *Pseudoalteromonas sp1A1* properties. The influence of the Lipid A repartition was investigated. It was found that asymmetric membrane with 75% of Lipid A on one of their leaflet had higher area per lipid (67 $Å^2$) than homogeneous POPE:POPG (3:1) membranes (52 $Å^2$). Such repartition of Lipid A confer a higher flexibility to the OM. Those data are consistent with previous study with other membranes. Indeed, a coarse-grain model of LPS enriched OM also found an area per lipid of 0.67 $nm^2$ for a membrane containing 70% of LPS and 0.55 nm2 for a membrane containing 10% of LPS[77]. The presented results are hence another confirmation that the presence of LPS indeed influence the membranes properties.

This study also showed that the presence of salt in the environment could influence the conformation of the oligosaccharide and in particular the linkage between GlcN from the Lipid A and Kdo from the core oligosaccharide. This could be due to the interaction between $Na^+$ cations

and the negatively charged phosphate groups present on those sugars. This work was made in collaboration with Prof. Martin-Santamaria at CSIC in Madrid, Spain, whose team is currently making further investigation.

# Section III

## Structure and activity of Lipid A from halophiles

# Chapter 5: Stucture of the Lipid A from *Spiribacter salinus M19-40$^T$*

## 5.1. Halophilic micro-organisms

Halophiles are extremophiles that can live in hypersaline environment (See Section I, 1.5.1.). Halophilic bacteria comprise various species that can be found in diverse habitat, as salt lakes, saltern pounds and deep sea brines[84]. Halophiles developed two main strategy in order to survive in high salt concentration. In the “salt-in” strategy, halophiles produce proteins with a high proportion of negatively charged amino acids[85]. Such metabolites allow them to balance their osmotic pressure by accumulating $Na^+$ and $K^+$ counter-ions in their cytoplasm. The other strategy, called the “salt-out” strategy, consist in the production and accumulation of large amount of organic solutes in order to maintain the osmotic balance. The osmolytes are highly diverse and can be used for industrial applications[86]. Indeed, halophiles are appealing microorganisms for biotechnology. They are currently studied for their ability to produce metabolites with particular properties. For example, their protease can function in low-water environment and tolerate organic solvent[87]. They also produce other enzymes, as amylase, chitinase and lipase, and exopolysaccharides that can have practical applications[88].

Recent metagenomics analysis of hypersaline environment allowed the isolation and characterization of new halophiles genus and species[89]. It is the case of *Spiribacter spp.* that now comprise several organisms as *Spiribacter curvatus*[90] and *Spiribacter roseus*[91]. *Spiribacter salinus* M19-40$^T$ is the first isolated species of this genus. It is a halophilic Gram-negative gamma-proteobacterium identified as a new genus based on metagenomics analysis with close phylogenetic similarities with species of the genera *Alkalilimnicola*, *Alkalispirillum* and *Arhodomonas* within the family *Ectothiorhodospiraceae*[92]. It has been firstly isolated from an



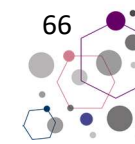

intermediate-salinity pound of a marine saltern located in Isla Cristina, Huelva, southwest Spain. It is now known that *S. salinus* M19-40$^T$ adapts to its environment with the "salt-out" strategy, producing osmolytes as ectoine and glycine betaine[93].

As a gram-negative bacterium, *S. salinus* M19-40$^T$ produce LPS that can have interesting structure and properties (See Section I). The present chapter reports the structural characterization of *S. salinus* M19-40$^T$ Lipid A. This is achieved by merging information that was attained from the compositional analyses performed on pure LPS with information from a MALDI MS and MS$^2$ investigation executed on the isolated lipid A fraction.

## 5.2. Extraction, purification and compositional analysis

LPS material was extracted from dried bacterial cells using the hot phenol/water procedure. The LPS material was found only in the water phase and underwent an enzymatic treatment in order to remove cell contaminants. A DOC-PAGE, followed by silver nitrate staining, was performed, revealing the rough nature (R-LPS) of the extracted material. An additional purification step was performed by ultracentrifugation, followed by size-exclusion chromatography. The compositional analysis executed on R-LPS revealed that *S. salinus* M19-40$^T$ lipid A was mainly composed of *(R)*-3-hydroxydecanoic acid (10:0 (3-OH)), *(R)*-3 hydroxytetradecanonic acid (14:0 (3-OH)), 3-oxo-tetradecanonic acid (14:0 (3-oxo)), and dodecanoic acid (12:0). Decanoic (10:0), undecanoic (11:0), tridecanoic (13:0), tetradecanoic (14:0), and tetradecenoic (14:1) acids were also detected as minor species.

The presence of the 14:0 (3-oxo) fatty acid was confirmed by the analysis of the fragmentation pattern of its methyl ester derivative (Figure 36) as it follows: (i) the presence of the molecule-ion peak at *m/z* 256 and (ii) the presence of the base peak at *m/z* 116, which clearly proved the beta cleavage to the oxo group with rearrangement of one hydrogen atom[94]. Moreover, (iii) the minor peak at *m/z* 183 $[M-73]^+$, which was indicative of the alpha cleavage to the oxo group, was also identified[95]. The occurrence of the 14:0 (3-oxo) fatty acid could not be shown using the typical procedure to define the total fatty acid, most likely because of decarboxylation. On the contrary, liberation of fatty acids by methanolysis with methanol/hydrochloric acid revealed the occurrence of 14:0 (3-oxo).

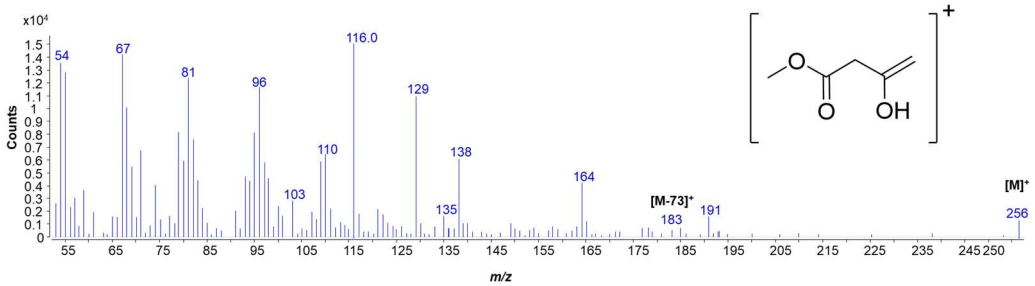


**Figure 36:** Mass spectrum of the methyl 3-oxotetradecanoic acid ester

## 5.2. Mass spectrometry of the Lipid A

An aliquot of pure R-LPS underwent a mild acid hydrolysis with an acetate buffer in order to selectively cleave the acid labile linkage between the core oligosaccharide and the lipid A. The isolated lipid A fraction then underwent a detailed MALDI MS and $MS^2$ investigation. The reflectron MALDI mass spectrum, which was recorded in negative polarity, is

presented in Figure 37. The spectrum clearly indicated—in the range *m/z* 1039.6–1499.9—a complex pattern of peaks relative to deprotonated $[M-H]^-$ lipid A species, which differed in both the nature and number of fatty acids and in phosphate content. Three main clusters of peaks were detected and matched with penta-, tetra-, and tri-acylated lipid A species, whose heterogeneous nature was also clearly visible because of the presence of mass differences of 14 ($–CH_2–$ unit) and/or 28 amu ($–CH_2CH_2–$ unit), which are diagnostic for lipid A species that differ in the length of their acyl chains, in accordance with compositional analysis data. In detail, the cluster of peaks at approximately *m/z* 1391.9 and *m/z* 1471.9 were assignable to mono- and *bis*-phosphorylated penta-acylated lipid A species (Figure 37, Table 3) carrying two 10:0 (3-OH), one C14:0 (3-OH), one C14:0 (3-oxo), and one C12:0. In the mass range *m/z* 1193.8-1301.7, tetra-acylated lipid A species were identified: the peak at *m/z* 1301.7 matched with *bis*-phosphorylated tetra-acylated lipid A species carrying one 10:0 (3-OH), one 14:0 (3-OH), one 14:0 (3-oxo), and one 12:0. The corresponding *mono*-phosphorylated form was assignable to the peak at *m/z* 1221.8. In the same mass range, *mono*-phosphorylated lipid A species that differed in the length of the acyl chains were clearly visible because of the occurrence of mass differences of 14 and 28 amu, as stated above. Finally, *mono*-phosphorylated tri-acylated lipid A species that were lacking in both 10:0 (3-OH) and 12:0, with respect to the penta-acylated lipid A species at *m/z* 1391.9, were also visible at *m/z* 1039.6 (Figure 37, Table 3).

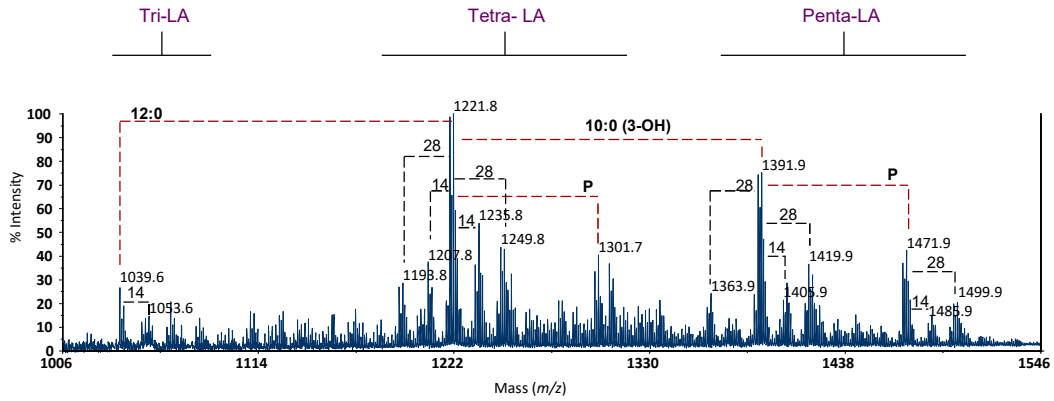


**Figure 37:** Reflectron MALDI mass spectrum, recorded in negative polarity, of lipid A from *S. salinus* M19-40$^{T}$ LPS obtained after acetate buffer treatment. Only deprotonated ions [M-H]- are formed in these conditions. The lipid A species are indicated.

| Observed ion peak (m/z) | Acyl Substitution | Proposed Fatty acid/phosphate composition |
|---|---|---|
| 1471.9 | Penta-acyl | HexN$^{2}$P[C10:0 (3-OH)]$^{2}$ [C12:0] [C14:0 (3-OH)] [C14:0 (3-oxo)] |
| 1391.9 | Penta-acyl | HexN$^{2}$[C10:0 (3-OH)]$^{2}$ [C12:0] [C14:0 (3-OH)] [C14:0 (3-oxo)] |
| 1301.7 | Tetra-acyl | HexN$^{2}$P[C10:0 (3-OH)] [C12:0] [C14:0 (3-OH)] [C14:0 (3-oxo)] |
| 1221.8 | Tetra-acyl | HexN$^{2}$[C10:0 (3-OH)] [C12:0] [C14:0 (3-OH)] [C14:0 (3-oxo)] |
| 1039.6 | Tetra-acyl | HexN$^{2}$[C10:0 (3-OH)] [C14:0 (3-OH)] [C14:0 (3-oxo)] |

**Table 3:** Proposed interpretation of main peak ions of MALDI-TOF MS (Figure 37)

To define the detailed structure of *S. salinus* M19-40$^{T}$ lipid A, unveiling the location of the acyl moieties with respect to the glucosamine disaccharide backbone, an MS$^{2}$ analysis on several peaks was performed. In detail, the negative-ion MS$^{2}$ spectrum of the precursor ion at *m/z* 1391.9 (Figure 38), corresponding to a *mono*-phosphorylated penta-acylated lipid A species, showed an intense peak at *m/z* 1203.7. This was attributed to an ion derived from the loss of a 10:0 (3-OH) fatty acid. A less intense peak was also observed at *m/z* 1191.7 and was assigned to a fragment that

originated from the loss of one 12:0 unit. Further minor peaks at m/z 1003.5 and m/z 1015.6 were identified and assigned as follows: (i) the ion at *m/z* 1003.5 matched with a fragment originated from the sequential loss of one 10:0 (3-OH) and one 12:0 unit, whereas (ii) the ion at *m/z* 1015.6 corresponded to a lipid A piece lacking two 10:0 (3-OH) moieties. The observation of both of these fragmentations was fundamental for the structural characterization. Indeed, the presence of a fragment that originated from a sequential loss of 10:0 (3-OH) and 12:0 from the precursor ion—in addition to the absence of fragmentations that referred to the loss of a whole unit of a hydroxylated fatty acid bearing a secondary acyl substituent — concurred to indicate that the secondary 12:0 was bound to an N-linked primary fatty acid. Moreover, the occurrence of the ion at *m/z* 694.1, originating from the sugar ring fragmentation ($^{0,4}A_2$), was crucial to establish the nature of the primary fatty acids that decorated the non-reducing glucosamine unit (that is, one 10:0 (3-OH) and one 14:0 (3-oxo)), and thus to locate the secondary acyl chain 12:0 only at the reducing glucosamine unit.

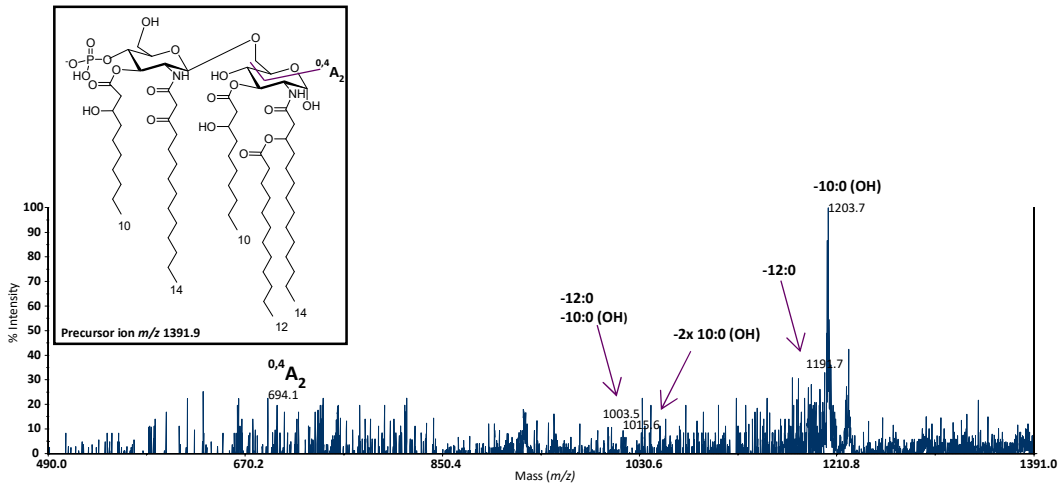


**Figure 38:** MALDI MS/MS spectrum of the mono-phosphorylated penta-acylated lipid A species at m/z 1391.8 from *S. salinus* M19-40$^{T}$ LPS. Fragment assignments are reported. The proposed structure for the penta-acylated lipid A species is reported in the inset.

The MS$^2$ analysis of the precursor ion at *m/z* 1221.8 (Figure 39), corresponding to a tetra-acylated and *mono*-phosphorylated species, indicated an intense peak at *m/z* 1021.6, which was attributed to an ion derived from the loss of the 12:0 moiety. A subsequent rearrangement of the ion at m/z 1021.6, promoted by the free 3-OH group on the 14:0, gave a loss of 184 mass units ($C_{12}H_{24}O$), resulting in the ion at *m/z* 837.4 (Figure 39)[96]. This fragmentation was helpful to establish that the primary 14:0 (3-OH) was sitting at position 2 of the reducing glucosamine. Moreover, the observation of such fragmentation, which occurred only when the secondary 12:0 unit was absent, suggested that the latter could be linked to the 14:0 (3-OH) moiety. A further intense peak, at *m/z* 923.4, was assigned to a fragment devoid of both the 12:0 unit and the phosphate group. A minor peak was also observed at *m/z* 1033.6, matching with a fragment that originated from the loss of a 10:0 (3-OH) acyl moiety (Figure 39). Two ions, derived from sugar ring fragmentations $^{0,4}A_2$ (*m/z* 694.3) and $^{1,3}A_2$ (*m/z*

754.1), were also detected. In particular, cross-ring fragmentation $^{1,3}A_2$ (*m/z* 754.1), which only took place when the hydroxyl group at position 3 of the reducing glucosamine was not substituted, further confirmed that the missing 10:0 (3-OH) acyl chain was placed in that position, and thus that 14:0 (3-OH) and 12:0 were located at position 2 of the same glucosamine as the primary and secondary fatty acids, respectively.

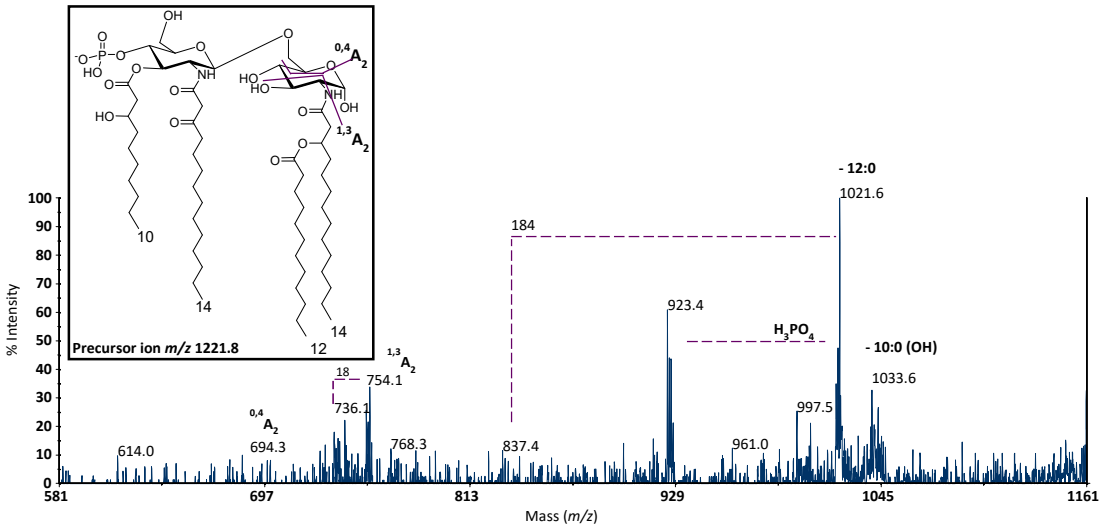


**Figure 39:** MALDI MS/MS spectrum of the *mono*-phosphorylated tetra-acylated lipid A species at m/z 1221.8 from *S. salinus* M19-40$^T$ LPS. Fragment assignments are reported. The proposed structure for the tetra-acylated lipid A species is reported in the inset.

The $MS^2$ analysis of the precursor ion at *m/z* 1301.7 (Figure 40), relative to a *bis*-phosphorylated tetra-acylated lipid A species, confirmed the structural characterization. This was because the occurrence of both the $Y_1$ ion (*m/z* 666.3)—which originated from the cleavage of the glycosidic linkage of the glucosamine backbone—and the ring fragmentation-derived ion $^{1,3}A_2$ (*m/z* 834.6) clearly indicated that the reducing glucosamine was decorated by 14:0 (3-OH) and 12:0, whereas the non-reducing glucosamine was acylated by 10:0 (3-OH) and 14:0 (3-oxo). Once again, the loss of 184

mass units was detected only from a fragment that was lacking in the secondary 12:0 unit.

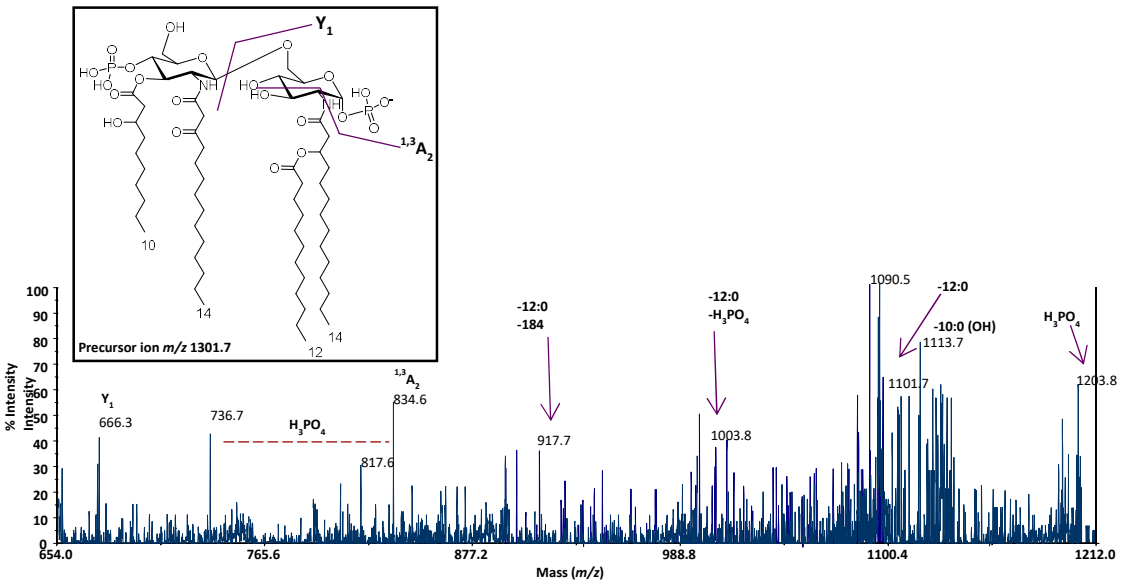


**Figure 40:** MALDI MS/MS spectrum of the *bis*-phosphorylated tetra-acylated lipid A species at *m/z* 1301.8 from *S. salinus* LPS. Fragment assignments are reported. The proposed structure for the tetra-acylated lipid A species is reported in the inset.

The positive-ion MALDI MS spectrum confirmed the presence of the molecular mass of the lipid A species with $Na^+$ counterions. A very diagnostic peak for structural elucidation was detected at *m/z* 636.3 (Figure 41) and attributed to the oxonium ion. This important fragment ion arose from the cleavage of the glycosidic linkage and was indicative of the substitution on the non-reducing glucosamine unit, which confirmed that it bore one 14:0 (3-oxo) and one 10:0 (3-OH). Finally, a further peak at *m/z* 466.2 was identified and assigned to the oxonium ion that was lacking the 10:0 (3-OH) unit (Figure 41).

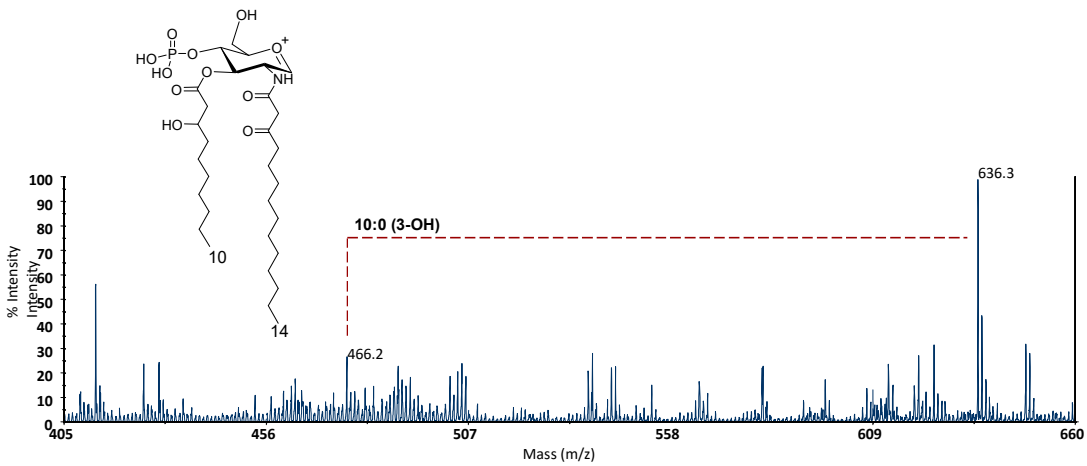


**Figure 41:** Section of the reflectron MALDI mass spectrum, recorded in positive polarity, of lipid A from *S. salinus* M19-40$^{T}$ LPS obtained after acetate buffer treatment. The oxonium ion structure is also sketched.

Finally, in order to unambiguously define the composition and position of the secondary fatty acids, an aliquot of lipid A underwent an ammonium hydroxide hydrolysis. The negative-ion MALDI mass spectrum (Figure 42) of the ammonium-treated lipid A displayed the following peaks that were important for the structural assessment, particularly in the mass range *m/z* 869.1–1051.2: (i) the ion at *m/z* 1051.2, which was explained as a *mono*-phosphorylated tri-acyl residue that was composed of both the primary N-linked 14:0 (3-OH) and 14:0 (3-oxo), with the former carrying the secondary 12:0 unit, and (ii) the ion at *m/z* 869.1, which was attributed to the *mono*-phosphorylated di-acyl residue that was composed only of the N-linked primary acyl moieties 14:0 (3-OH) and 14:0 (3-oxo). The occurrence of both of these peaks further corroborated the nature of the amide-bound acyl moieties and the occurrence of 12:0 as a secondary fatty acid in an acyloxyacyl amide moiety.

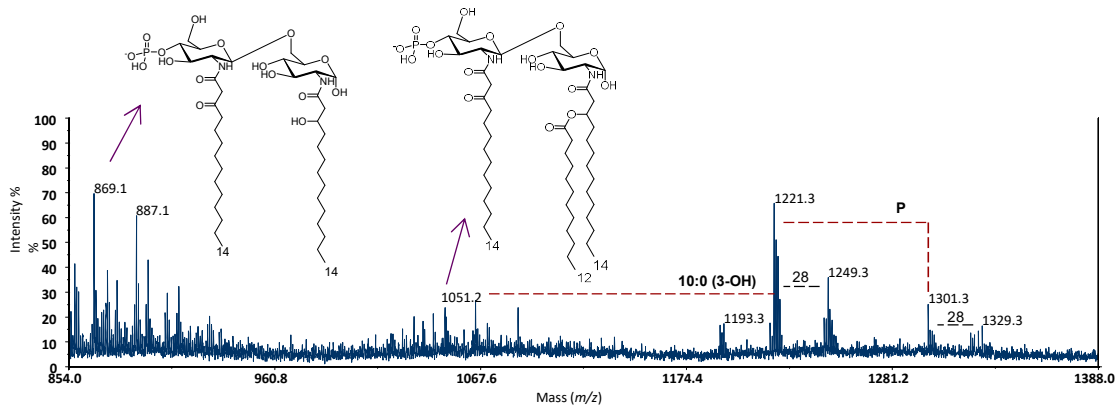


**Figure 42:** Negative ion MALDI mass spectrum of the lipid A from *S. salinus* M19-40$^T$ LPS obtained from 10 % $NH_4OH$ hydrolysis. The proposed structures of the product are reported in the figure.

Thus, through a combination of analytical organic chemistry, and the merging of MS and $MS^2$ data of the mild acid hydrolysis and the ammonium hydroxide-treated products with those from the compositional analysis, it was possible to define the *S. salinus* M19-40$^T$ LPS as expressing a complex blend of the lipid A species—of which the component with the highest acylation degree is sketched in Figure 43.

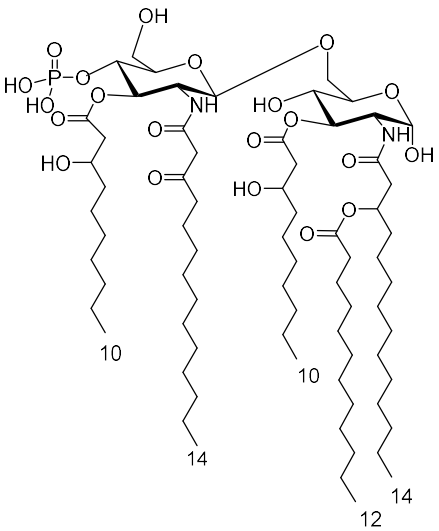

**Figure 43:** Structure of *Spiribacter salinus* M19-40$^T$ Lipid A

## 5.3. Discussion

The adaptation mechanisms of marine bacteria to the different chemical, physical, and biological conditions that are encountered in marine environments have led to the evolution of highly diverse microbes. The adaptation phenomena typically involve the chemical modification of the bacterial membrane system in order to reinforce the overall cell envelope to resist the mutable conditions of the saline habitats. The structure of the LPS from halophilic microbes often presents unusual chemical characteristics, which help the bacterium in maintaining membrane integrity. In particular, the nature and distribution of the fatty acids composing the lipid A moiety may change according to the external habitat. In this paper, the characterization of the structure of the lipid A moiety of the R-LPS that was isolated from the slightly halophilic bacterium *S. salinus* M19-40$^T$ is reported. The structural elucidation was performed, through MALDI MS and $MS^2$ analysis, on the isolated lipid A. In parallel, a detailed fatty acid compositional analysis was executed on the LPS, providing the chemical constituents of the lipid A, which are essential to interpret the information derived from the MALDI MS investigation.

*S. salinus* M19-40$^T$ appeared to possess an R-LPS with a heterogenous lipid A, characterized by a mixture of tri-, tetra-, and penta-acylated species, and decorated by one or two phosphate groups. In general, the 14:0 (3-OH) fatty acid was always found to be acyloxyamide linked to the reducing glucosamine; whereas 14:0 (3-oxo) was always found to be acyloxyamide decorating the non-reducing glucosamine; position 3 and 30 were substituted with 10:0 (3-OH); and finally, the 12:0 unit was identified as a secondary substituent only of the reducing glucosamine. As indicated in Figure 43, the main penta-acylated lipid A

species exhibits a 2 + 3 symmetry. Such an uncommon fatty acid distribution is interesting as most of the penta-acylated lipid A species—whose structure has been characterized to date—show a 3 + 2 asymmetry.

The unusual distribution of acyl substituents over the backbone resembles that of the lipid A of two psychrophilic and moderately halophilic bacteria, namely *Marinomonas vaga*[97] and *Marinomonas communis*[98], even though the chain length of the fatty acids is different. Moreover, *M. vaga* and *M. communis* possess only *mono*-phosphorylated species, and their 2 + 3 asymmetry is given by both the occurrence of a secondary acyl substitution on the acyloxyamide of the non-reducing glucosamine and by the absence of the primary ester-bound fatty acid decorating the same glucosamine unit.

Even more interestingly, *S. salinus* M19-40$^T$ lipid A presented the rare amide-linked 14:0 (3-oxo), whose presence is consistent with the close phylogenetic similarities with species within the family *Ectothiorhodospiraceae*. Indeed, previous studies revealed that the LPS isolated from the extremely halophilic *Ectothiorhodospira halophila* also expresses the amide-bound 14:0 (3-oxo) fatty acids. Moreover, similarities with other *Ectothiorhodospira* species in lipid A fatty acid composition have been highlighted[99].

Given that, depending on the nature and distribution of the acyl chains, the lipid A may induce a TLR4/MD-2 agonistic or antagonistic activity after interaction with the host immune cells' receptors, it is worth emphasizing that the presence of the 3-oxo fatty acids has also been shown for lipid As from *Rhodobacter sphaeroides* and *R. capsulatus*, two phototrophic bacteria that are of enormous importance in the LPS research field. Indeed, these bacteria exhibited a penta-acylated lipid A with strong TLR4/MD-2 antagonistic activity against toxic LPS and were used as an inspiration model for synthesis of the analogue Eritoran: a well-tolerated,



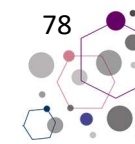

synthetic lipid A mimetic, acting as a TLR4/MD-2 antagonist, which reached phase III clinical trials as an antisepsis agent[100].

Therefore, given the peculiar elucidated structure, the immunological activity of the lipid A from *S. salinus* M19-40$^T$ LPS is also worth being investigated, since it can potentially provide interesting activities in the perspective of the development of analogues with an immunomodulatory action on the immune system.

# Chapter 6: Stucture and activity of the Lipid A from *Halopeptonella vilamensis*

*Halopeptonella vilamensis* is a halophilic Gram-negative gamma-proteobacterium isolated from a hypersaline lake, Laguna Vilama, in Argentina[101]. It was identified as a new genus and species that have phylogenetic similarities with species of the genera *Alkalilimnicola*, *Alkalispirillum*, *Arhodomonas* and *Spiribacter* within the family *Ectothiorhodospiraceae*. *Halopeptonella vilamensis* is the first, and at present time, only member of the *Halopeptonella* genus.

## 6.1. Extraction, purification and compositional analysis

Extraction of the LPS content was done using the hot phenol/water procedure. LPS material was only found in the water phase and was further purified by enzymatic treatment, in order to remove cell contaminants as nucleic acids and proteins. A DOC-PAGE with subsequent silver nitrate staining was carried out. It showed that the extracted material was a LOS, with a characteristic single band at the bottom of the gel (Figure 44). It was further purified using size-exclusion chromatography.


**Figure 44:** DOC-PAGE; A: LOS from *Halopeptonella vilamensis,* water phase; B; LPS from *E. coli* standard

The compositional analysis of purified LOS from *H. vilamensis* revealed that its oligosaccharide was composed of D-Glucuronic acid (D-GlcA), D-Mannose (D-Man), D-Galactose (D-Gal), D-Glucose (D-Glc), D-Galacturonic acid (D-GalNA), D-Glucosamine (D-GlcN) and Kdo. Its Lipid A was composed of *(R)*-3-hydroxydecanoic acid (C10:0 (3-OH)), *(R)*-3-hydroxydecenoic acid (C10:1 (3-OH)), dodecanoic acid (C12:0), dodecenoic acid (C12:1), *(R)*-3-hydroxydodecanoic acid (C12:0 (3-OH)), tridecanoic acid (C13:0), tetradecanoic acid (C14:0) and tetradecenoic acid (C14:1). This heterogeneous mixture of fatty acids is shown in Figure 45.

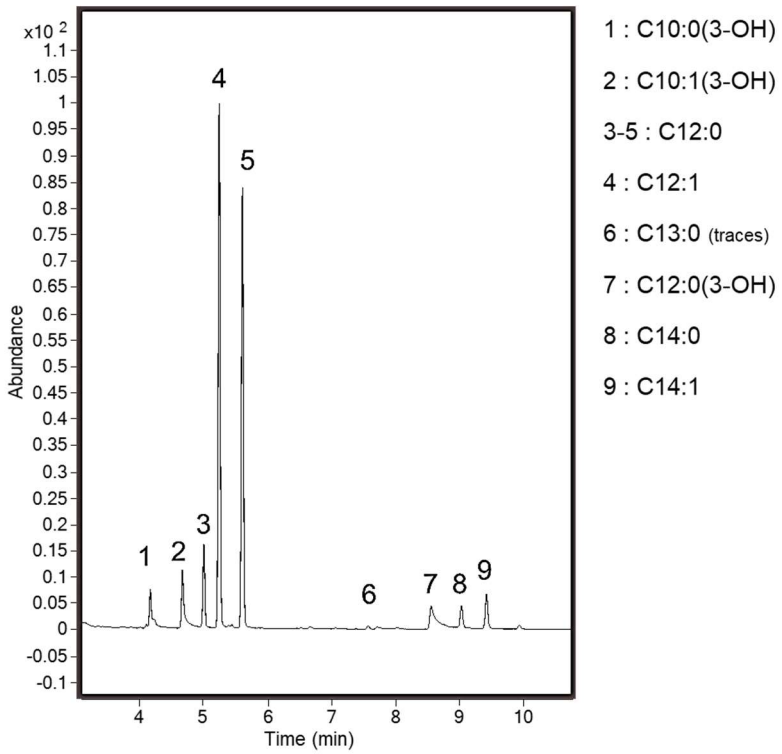


**Figure 45:** GC-MS chromatogram of methyl-ester derivates of fatty acids from *H. vilamensis*

## 6.2. Mass spectrometry of the Lipid A

The Lipid A was isolated from the pellet of the mild acid hydrolysis performed on the LOS. It was then studied by MALDI MS and $MS^2$ analysis. The reflectron negative-ion MALDI MS is represented in Figure 46. A complex pattern of ion peaks $[M-H]^-$ was detected in the mass range *m/z* [997.6-1597.9]. Four clusters of peaks were detected, corresponding to hexa, penta, tetra and tri-acylated Lipid A species (Figure 46, Table 4). The occurrence of mass difference of 14 (-$CH_2$-unit) and 28 amu (-$CH_2$-$CH_2$-unit) showed that *H. vilamensis* possesses a highly heterogeneous mixture of Lipid As, differing by the length of their fatty acids. Differences of 2 amu were also observed within the clusters, showing that there is a mixture of species bearing saturated and unsaturated acyl chains. This heterogeneity was also detected in the previous compositional analysis (Figure 46).

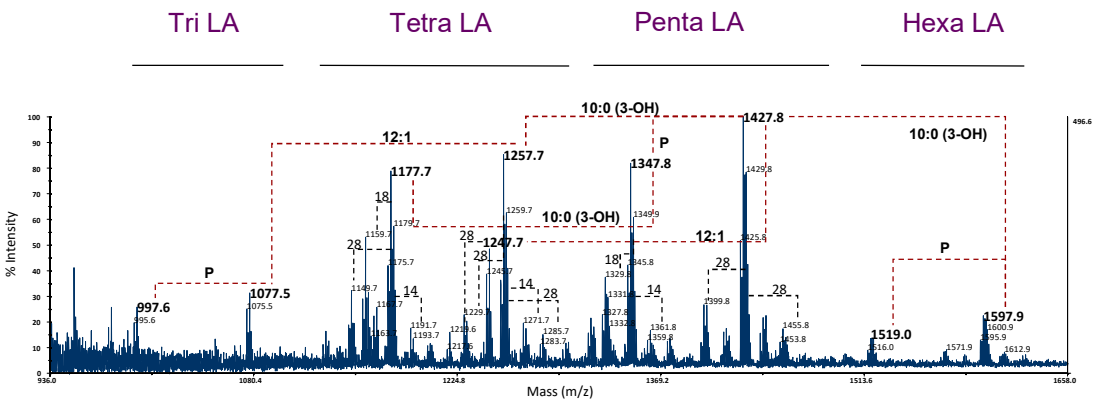


**Figure 46:** Reflectron MALDI mass spectrum, recorded in negative polarity, of lipid A from H. vilamensis LPS obtained after acetate buffer treatment. Only deprotonated ions [M-H]- are formed in these conditions. The lipid A species are indicated.

In detail, the set of peaks at *m/z* 1597.9 and 1519.0 matched with *bis*- and *mono*-phosphorylated hexa-acylated species carrying two C10:0 (3-OH), two C12:0 (3-OH), one C12:0 and one C12:1. The *bis*- and *mono*-phosphorylated penta-acylated species lacking one C10:0 (3-OH) were respectively detected at *m/z* 1427.8 and 1347.8. Clusters at *m/z* 1257.7 and 1177.7 corresponded to *bis*- and *mono*-phosphorylated tetra-acylated species lacking two C10:0 (3-OH). Finally, sets of peaks at *m/z* 1077.5 and 977.6 matched with *bis*- and *mono*-phosphorylated tri-acylated species bearing two C12:0 (3-OH) and one C12:0 (Figure 46, Table 4).

| Observed ion peak (m/z) | Acyl Substitution | Proposed Fatty acid/phosphate composition |
|---|---|---|
| 1597.9 | Hexa-acyl | $HexN^2P^2$ [C10:0 (3-OH)]$^2$ [C12:0 (3-OH)]$^2$ [C12:0] [C12:1] |
| 1519.9 | Hexa-acyl | $HexN^2P$ [C10:0 (3-OH)]$^2$ [C12:0 (3-OH)]$^2$ [C12:0] [C12:1] |
| 1427.8 | Penta-acyl | $HexN^2P^2$ [C10:0 (3-OH)] [C12:0 (3-OH)]$^2$ [C12:0] [C12:1] |
| 1347.8 | Penta-acyl | $HexN^2P$ [C10:0 (3-OH)] [C12:0 (3-OH)]$^2$ [C12:0] [C12:1] |
| 1257.7 | Tetra-acyl | $HexN^2P^2$ [C12:0 (3-OH)]$^2$ [C12:0] [C12:1] |
| 1247.7 | Tetra-acyl | $HexN^2P^2$ [C10:0 (3-OH)]$^2$[C12:0 (3-OH)]$^2$ [C12:0] |
| 1177.7 | Tetra-acyl | $HexN^2P$[C12:0 (3-OH)]$^2$ [C12:0] [C12:1] |
| 1077.5 | Tri-acyl | $HexN^2P^2$ [C12:0 (3-OH)]$^2$ [C12:0] |
| 997.6 | Tri-acyl | $HexN^2P$ [C12:0 (3-OH)]$^2$ [C12:0] |

**Table 4:** Proposed interpretation of main peak ions of MALDI-TOF MS (Figure 46)

In order to determine to position of the acyl moieties regarding the di-glucosamine backbone, several $MS^2$ analysis were carried out. The $MS^2$ spectrum of the precursor ion at *m/z* 1177.7 is shown in Figure 47. The analysed species matched with a mono-phosphorylated tetra-acylated Lipid A containing two C12:0 (3-OH), one C12:0 and one C12:1 (table 4). Ion peak at *m/z* 1077.6 matched with the loss of a phosphate group. Clusters at *m/z* 977.4 and 799.1 corresponded to the lipid A lacking respectively one



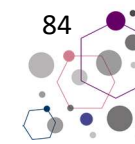

C12:0 and one C12:0 (3-OH). More interestingly, an ion peak from the $^{1,3}A_2$ ring fragmentation could be observed at *m/z* 738.2. It showed that the non-reducing unit was composed of one C12:0 (3-OH) and one C12:1.

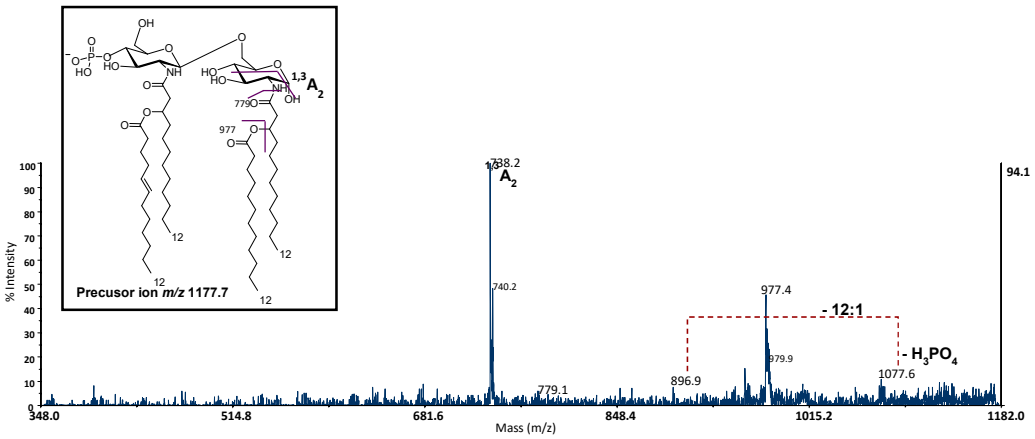


**Figure 47:** MALDI MS/MS spectrum of the *mono*-phosphorylated tetra-acylated lipid A species at *m/z* 1177.7 from *H. vilamensis* LOS. Fragment assignments are reported. The proposed structure for the tetra-acylated lipid A species is reported in the inset.

This analysis was confirmed by another $MS^2$ analysis done on the precursor ion *m/z* 1258.7 that corresponded to the *bis*-phosphorylated tetra-acylated species bearing two C12:0 (3-OH), one C12:0 and one C12:1 (Figure 48). The most abundant ion peak at 1160.1 matched with a loss of a phosphate group. Cluster at 1059.9 corresponded to the loss of a C12:0, with a further loss of phosphate at *m/z* 963.8. Finally, the $^{1,3}A_2$ ring fragmentation was visible at *m/z* 818.5 with a loss of a phosphate group at *m/z* 720.6. The ring cleavage $Y_1$ was also detected at *m/z* 638.1. Those specific fragmentations confirmed the determined repartition of the acyl moieties along the di-glucosamine backbone. Each unit is composed of one C10:0 (3-OH) and one C12:0 (3-OH), C12:1 is anchored on the non-reducing glucosamine whereas C12:0 is on the reducing unit.

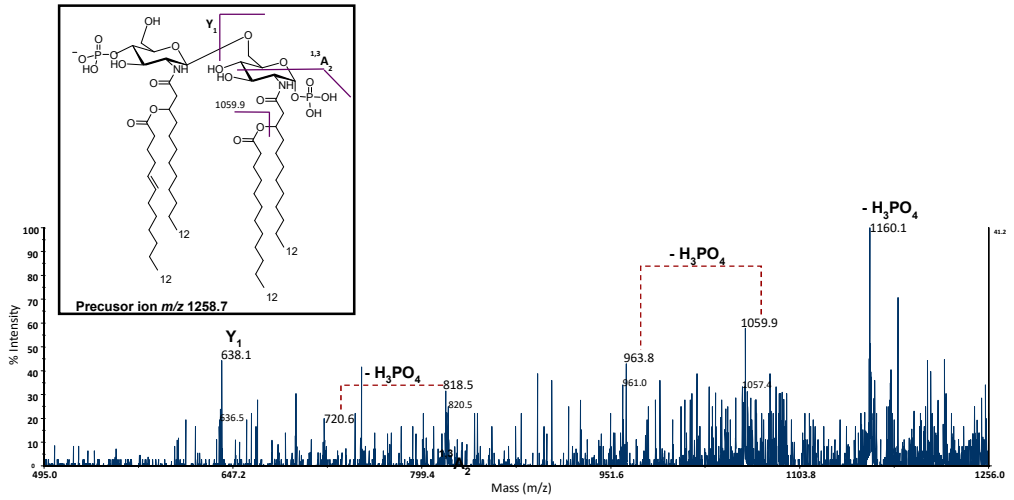


**Figure 48:** MALDI MS/MS spectrum of the *mono*-phosphorylated tetra-acylated lipid A species at *m/z* 1258.7 from *H. vilamensis* LOS. Fragment assignments are reported. The proposed structure for the tetra-acylated lipid A species is reported in the inset.

Finally, other $MS^2$ analysis showed consistent data. Indeed, the experiment performed on the precursor ion at *m/z* 1347.8 lead to the same conclusion about the structure of *H. vilamensis* Lipid A (Figure 49). The studied species corresponded to the *mono*-phosphorylated and penta-acylated Lipid A carrying one C10:0 (3-OH), two C12:0 (3-OH), one C12:0 and one C12:1. Peaks arising from the loss of phosphate groups were detected at *m/z* 1245.1 and the loss of C10:0 (3-OH) and C12:0 could respectively be seen at *m/z* 1159.8 and *m/z* 1147.5. $^{1,3}A_2$ and $Y_1$ fragmentations were also detected at *m/z* 908.2 and *m/z* 556.0. They showed that the reducing glucosamine was bearing the C12:0 and C12:0 (3-OH) and all the other acyl chains were on the non-reducing unit. Those data corroborate the previously defined repartition of the acyl chains among the di-glucosamine backbone.

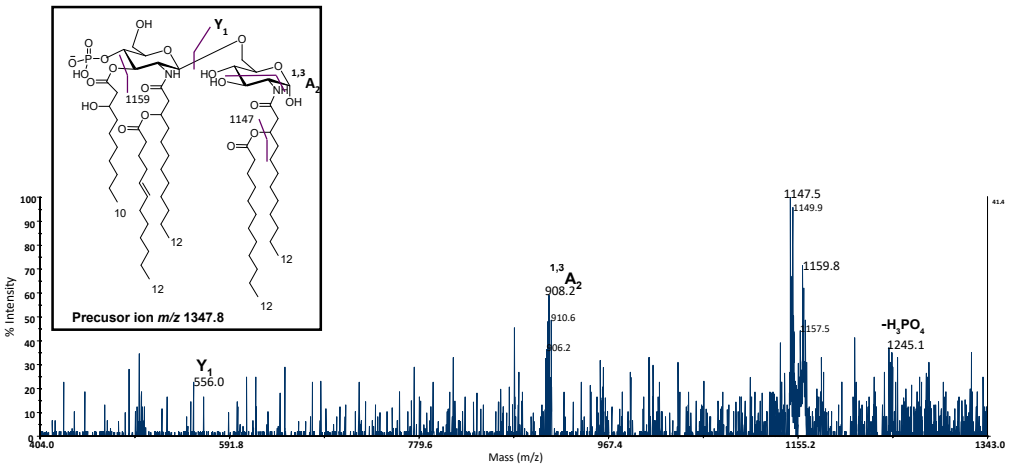


**Figure 49:** MALDI MS/MS spectrum of the *mono*-phosphorylated Penta-acylated lipid A species at *m/z* 1347.8 from *H. vilamensis* LOS. Fragment assignments are reported. The proposed structure for the penta-acylated lipid A species is reported in the inset

In order to precisely establish the nature of the ester or amide linkage, an aliquot of the Lipid A was treated with ammonium hydroxide hydrolysis. The negative ion MALDI MS (Figure 50) showed several cluster of peaks in the mass range *m/z* 1281.8-1059.6. As for previous MALDI MS (Figure 46), the heterogeneity of *H. vilamensis* Lipid A could be clearly seen with mass differences of 14 and 16 amu. The most abundant ion peak at *m/z* 1257.8 matched with *bis*-phosphorylated and tetra-acylated species lacking two C10:0 (3-OH). It confirmed that those two fatty acids are directly linked to the di-glucosamine backbone through ester linkages. Loss of phosphates could be observed at *m/z* 1177.6 and 1097.6. Finally, peaks at *m/z* 1077.7 and 1075.6 were crucial to determine the position of secondary fatty acids. Indeed, they correspond to *bis*-phosphorylated and tri-acylated species with two C12:0 (3-OH) and either one C12:0 or one C12:1. This clearly shows that the C12:0 (3-OH) are linked to the di-glucosamine

backbone through amide linkages, in turn esterified at the hydroxyl groups by C12:0 and C12:1.

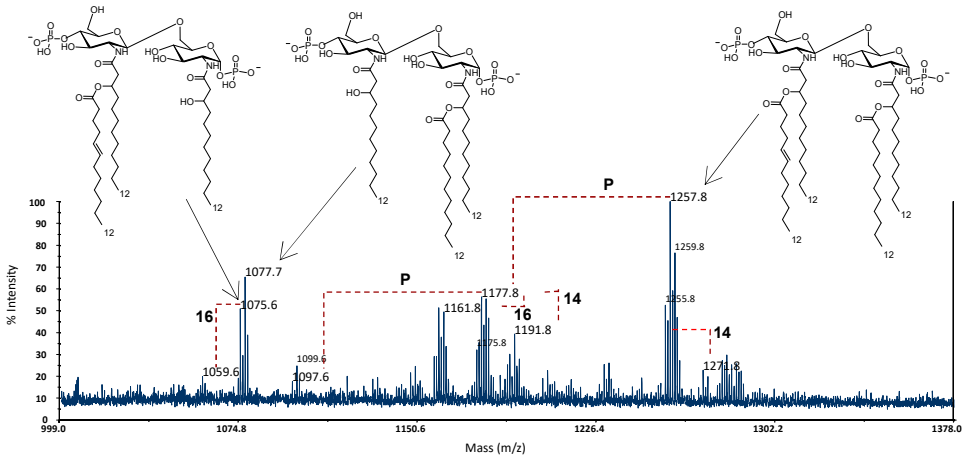


**Figure 50:** Negative ion MALDI mass spectrum of the lipid A from *H. vilamensis* LOS obtained from 10 % $NH_4OH$ hydrolysis. The proposed structures of the product are reported in the figure

Combining all those data, it was possible to determine *H. vilamensis* Lipid A structures. It possesses a *bis*-phosphorylated *hexa*-acylated Lipid A with a 3+3 symmetry that is shown on Figure 51. The present analysis describe the data relative to the species bearing two C10:0 (3-OH) as primary ester-linked fatty acids, two C12:0 (3-OH) as amide-linked acyl chains, and one C12:0 and one C12:1 as secondary fatty acid. However, the high heterogeneity of MALDI mass spectra clearly demonstrated that *H. vilamensis* lipid A was characterised by a mixture of several species. The occurrence of 2 amu within each cluster (Figure 46) showed that *H. vilamensis* also possesses species with unsaturated acyl chains, as C12:1 on the non-reducing unit or on both glucosamines. Finally, the compositional analysis (Figure 45) and the occurrence of 28 amu in the

negative-ion MALDI MS spectrum (Figure 46) also showed the presence of species bearing C14:0 and C14:1 instead of C12:0 and C12:1.

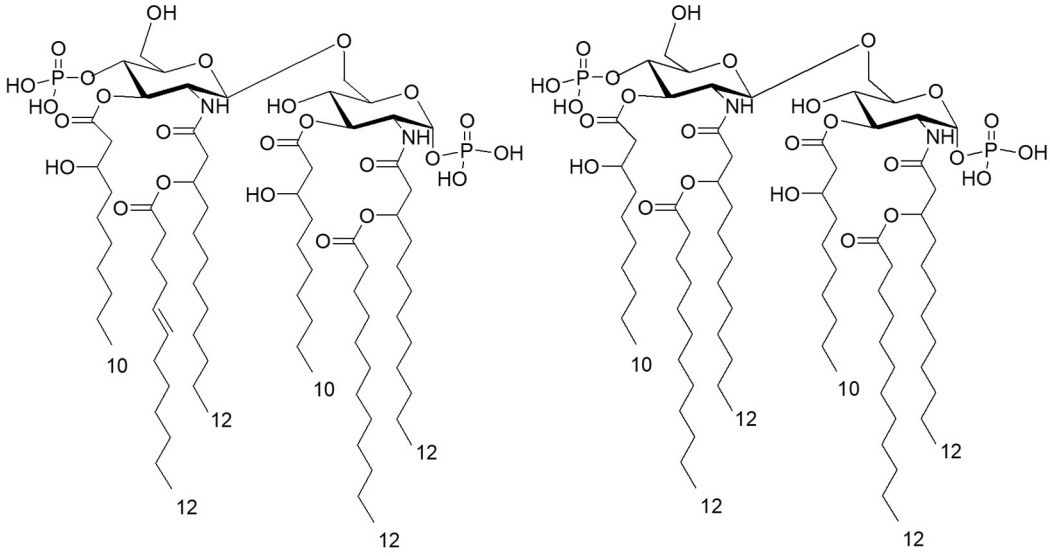

**Figure 51:** Structure of *Halopeptonella vilamensis* hexa-acylated Lipid A species

## 6.3. Immunological assays

To evaluate the immunological impact of *H. vilamensis* LOS a first analysis was done at different concentrations (1, 10, and 100 ng/mL) in the HEK293 cell line[102], stably transfected with human CD14/MD-2/TLR4. Similar concentration of the hexa-acylated, highly stimulatory LPS of *E. coli* O111:B4 and the synthetic lipid IVA were used as agonistic and antagonistic controls, respectively. Likewise, untreated cells were considered as the negative control in all the experiments shown. Stimulation of HEK293 hTLR4 was carried out for 6 h (Figure 52, A-B). It was observed that stimulation of HEK293 hTLR4 with *H. vilamensis* LOS elicited a poor NF-κB activation and CXCL-8 production, which were

significantly lower with respect to the values induced by *E. coli* LPS stimulation.

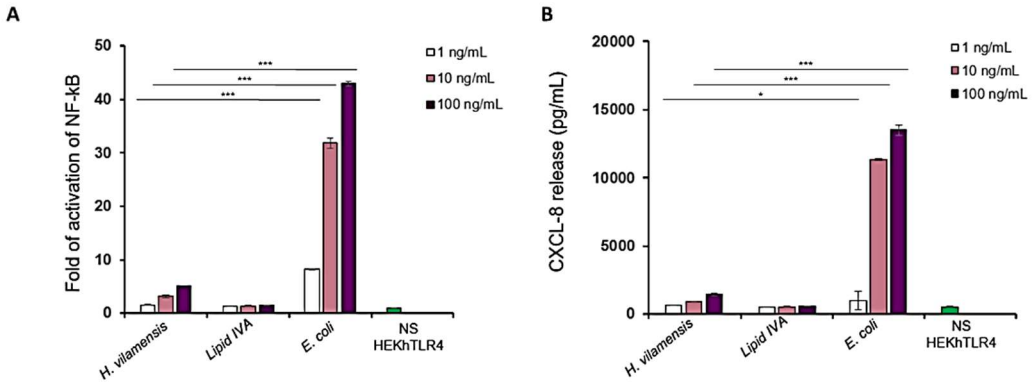


**Figure 52:** Analysis of immunopotential of *H. vilamensis* LOS in HEK293 hTLR4 cell line. Activation of nuclear factor kappa B **(A)** and CXCL-8 production **(B)** in HEK 293 hTLR4/MD2-CD14 stimulated with *H. vilamensis* LOS at the concentration of 1, 10, and 100 mg/mL for 6 h. Commercial hexa-acylated *Escherichia coli* LPS or synthetic lipid IVA were used at the same concentrations as positive and negative control, respectively. Data are expressed as mean ± SD of three independent experiments in triplicate. *$p < 0.05$, **$p < 0.01$, and ***$p < 0.001$, after Student's *t*-test.

In order to confirm its low immunological impact, *H. vilamensis* LOS was also tested in human Monocytes-derived Macrophages (MoMs), which naturally expresses TLR4. Cells were exposed to *H. vilamensis* LOS at the concentration of 1, 10 and 100 ng/mL for 12 h. *E. coli* LPS was tested in parallel at same concentrations. Untreated cells and stimulation with Lipid IVa were used as negative control. The release of the pro-inflammatory cytokines TNF, interleukin-6 (IL-6) and interleukin-10 (IL-10) was assessed as readout. The results are shown in Figure 53. In agreement to what observed in the HEK293 hTLR4 cell model, with *H. vilamensis* LOS the release of these cytokines were significantly lower than those elicited by *E. coli* LPS at 10 and 100 ng/mL. However, the immunological activity was

significantly higher than *E. coli* LPS at 1 ng/mL and greater Lipid IVa at all concentration. This result demonstrate that *H. vilamensis* LOS possess a low immunostimulatory property.

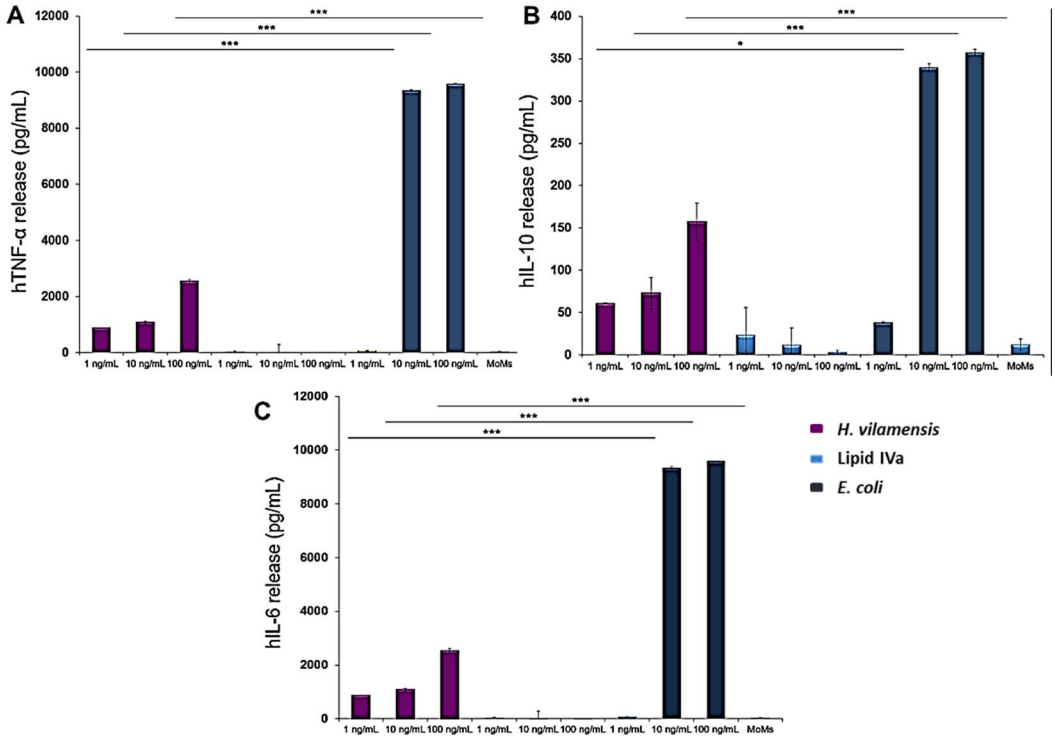


**Figure 53:** Analysis of immunopotential of *H. vilamensis* LOS in MOMs. Activation of tumor necrosis factor TNF **(A)**, IL-6 **(B)** and IL-10 **(C)** release in cell-free supernatants of monocytes stimulated with *H. vilamensis* LOS at the concentration of 1, 10 and 100 mg/mL for 12 h. Commercial hexa-acylated *Escherichia coli* LPS or synthetic lipid IVA were used at the same concentrations as positive and negative control, respectively. Abbreviation: NS: not stimulated. Data are expressed as mean ± SD of three independent experiments in triplicate. *$p < 0.05$, **$p < 0.01$, and ***$p < 0.001$, after Student's *t*-test.

A complementary experiment with Bone marrow-derived macrophages (BMDMs) from C57BL/6 wild-type mice was performed in order to gain information about the signalling pathway activated by *H. vilamensis* LOS (Figure 54. A-B). BMDMs were exposed to *H. vilamensis* LOS at 1, 10, and 100 ng/mL. *E. coli* LPS and Lipid IVa were used respectively as positive and negative control, at the same concentrations as above. Untreated cells were also considered as the negative control. After 6 h stimulation, TNF and Interferon inducible protein 10 (IP-10) production were quantified. As IP-10 is known to be induced by the TRIFF pathway[103] (See Section I), its release is indicative of a non-dependent MyD88 signalling activation. The results obtained with the TNF release (Figure 54. A) are in accordance with the immunostimulatory activity observed with HEK293 hTLR4 and MoMs cell lines. However *H. vilamensis* LOS did not induce any significant release of IP-10, compared to the negative control Lipid IVa (Figure 54 B). This result suggest that *H. vilamensis* LOS slight agonist activity is not related to the TRIFF related signalling pathwatys and hence should be linked to an activation of the MyD88-dependent pathway.

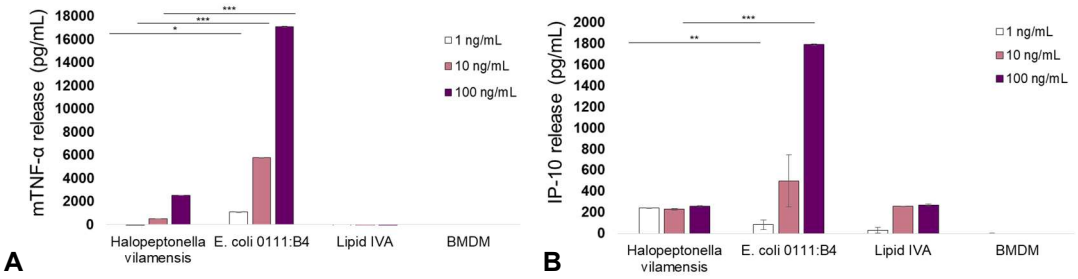


**Figure 54:** Analysis of immunopotential of *H. vilamensis* LOS in BMDMs. TNF **(A)** and IP-10 **(B)** production stimulated with *H. vilamensis* LOS at the concentration of 1, 10, and 100 mg/mL for 6 h. Commercial hexa-acylated *Escherichia coli* LPS or synthetic lipid IVA were used at the same concentrations as positive and negative control, respectively. Abbreviation: NS: not stimulated. Data are expressed as mean ± SD of three independent experiments in triplicate. *$p < 0.05$, **$p < 0.01$, and ***$p < 0.001$, after Student's *t*-test.

## 6.4. Investigation of *Halopeptonella vilamensis* core oligosaccharide region

A mild acid hydrolysis was performed in order to separate the Lipid A from the oligosaccharide portion. The supernatant was then further purified by size exclusion chromatography. The sample was then analysed through NMR experiments. The proton spectrum revealed that the obtained product was a complex saccharide mixture containing up to 10 different units (Figure 55).

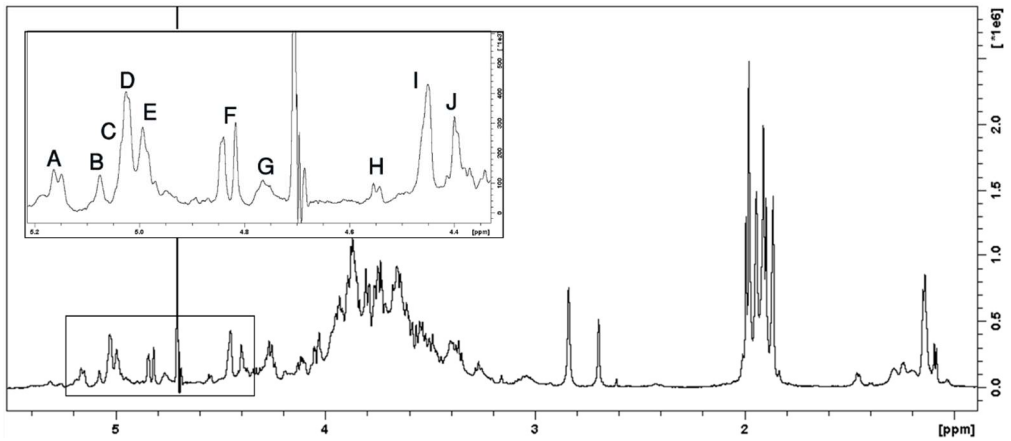


**Figure 55:** $^{1}$H NMR spectrum of *H. vilamensis* saccharidic product. Zoom of the anomeric region is reported in the inset

2D NMR spectra were analysed and showed that the oligosaccharide from *H. vilamensis* LOS could still not be resolved. Indeed, the present saccharide was in fact a mixture of several compounds. Moreover, no Kdo was detected during the analysis. Further attempts to isolate the oligosaccharide are currently ongoing.

## 6.5. Discussion

The present study showed the characterisation of *H. vilamensis* LPS structure with the elucidation of its immunological activity. *H. vilamensis* is a strictly aerobic gamma-proteobacterium isolated from a hypersaline lake in Argentina. DOC-PAGE analysis of the extracted and purified content revealed that *H. vilamensis* possesses an LOS. Combining compositional analysis, MALDI-MS and MS/MS, it was possible to elucidate the structure of its Lipid A species. Careful analysis of the MALDI-MS revealed that *H.*

*vilamensis* actually possesses a highly heterogeneous mixture of *bis*-phosphorylated Lipid As, differing in their acylation and the length of the acyl moieties *H. vilamensis* tri- to hexa-acylated Lipid As bearing C10:0 (3-OH) as primary ester-linked fatty acids, C12:0 (3-OH) as amide-linked acyl chains and C10:1 (3-OH), C12:0, C12:1, C13:0, C14:0 and C14:1, as secondary ester-linked fatty acids. This remarkable heterogeneity was observed in the compositional analysis (Figure 45) and confirmed by MALDI MS on the intact Lipid A (Figure 46). It is herein represented on Figure 56.

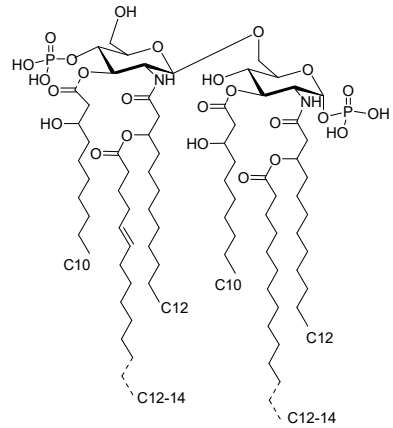


**Figure 56:** The complete structure of *H. vilamensis* Lipid A. Non stoichiometric substitution are denoted as dotted bonds

It is the first time that *H. vilamensis* Lipid A is reported. The hexa-acylated Lipid A species possess two structural feature that are shared among marine and halophiles[104,105]. Firstly, it has a 3+3 symmetry, contrary to the well-known Lipid A from *E. coli* that has a 4+2 symmetry. Secondly, it possess relatively short fatty acids chain. Indeed, *E. coli* fatty acids possess 12 to 14 carbons atoms and *H. vilamensis* acyl chains are composed of 10 to 12 carbon atoms.

The immunological assays demonstrated the slight agonist activity of *H. vilamensis* LOS. The symmetric repartition of the acyl chain and the occurrence of shorter fatty acids can explain why *H. vilamensis* LOS is less agonist than *E. coli* LPS. The biological assays also indicate that the activation of inflammatory response by *H. vilamensis* should follow the MyD88-dependent pathway. This work was performed in collaboration with Prof. Bernardini and complementary tests are being performed in order to fully understand *H. vilamensis* LOS immunological activity.

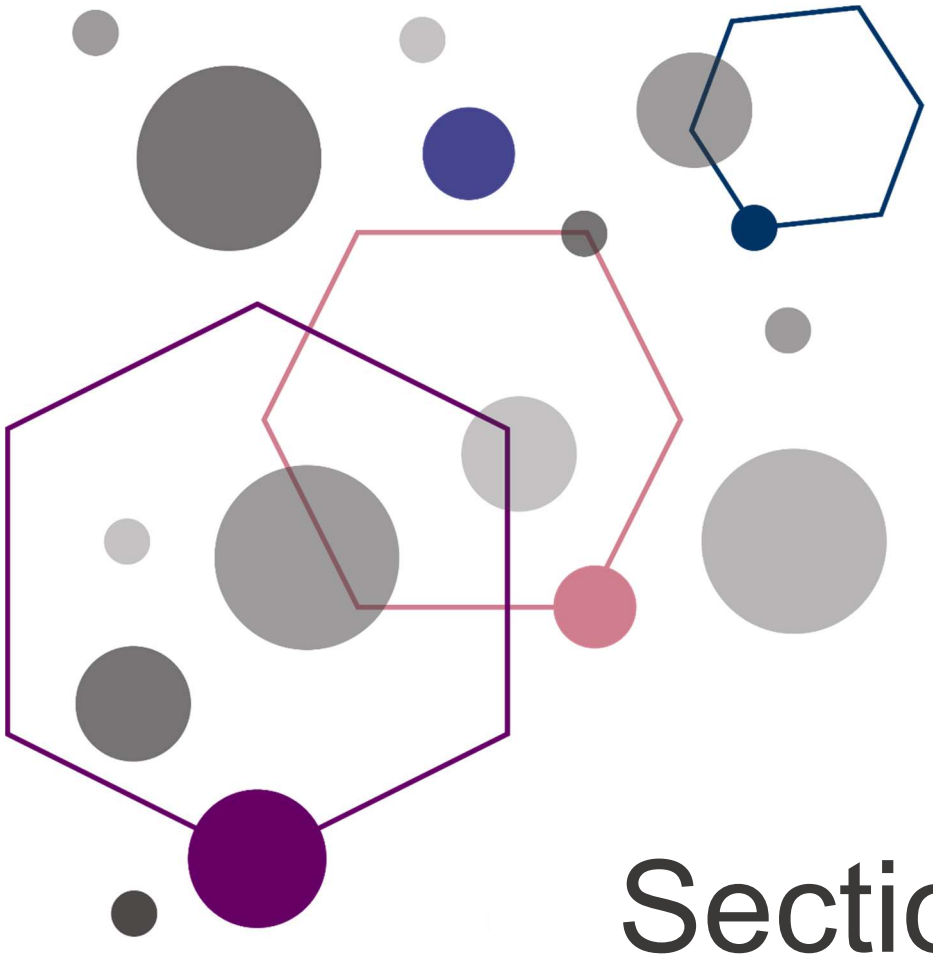

# Section IV

## Looking for endotoxins among exopolysaccharides: the case of *Halomonas smyrnensis*

# Chapter 7: Analysis of *Halomonas smyrnensis* polysaccharides

## 7.1. Sweet and salty: an exopolysaccharide producing halophile

Exopolysaccharides (EPS) are extra-polymeric substances secreted by various life forms, including bacteria. They are involved in many biological functions as aggregation, protection and symbiosis. Their diversity and particular properties made them appealing for several biotechnological applications as medicine and nutrition[106]. EPS from marine and extremophile micro-organisms have been extensively studied and bacteria from those ecological source possess a high variety of EPS structures[107]. In particular, halophiles (See Section III, 5.1) can produce particular EPS that can be used in industry as viscofier, gelling, emulsifying agents, therapy and bioremediation[108].

Among halophiles, bacteria belonging to the genus *Halomonas* are promising EPS producers. For example, *Halomonas mauran* produce a unique sulphated EPS that was called Mauran and studied for its biotechnological applications[109]. Discovered and isolated more recently Çamaltı Saltern Area in Turkey, *Halomonas smyrnensis* is a gamma-proteobacterium that was also shown to be an EPS producer[110]. Further genomic analysis revealed that *H. smyrnensis* produce Levan[111], a β-(2,6)-linked fructose that was already known for its biotechnological applications[112]. Given its promising Levan-producing properties, *H. smyrnensis* is currently studied and used in order to make it viable for industrial use[113].

The present chapter reports the study of *H. smyrnensis* exopolysaccharide content. The usual procedure for LPS extraction and purification (See Section I, 2.1) was used and obtained products were analysed using NMR and 2D NMR experiments.



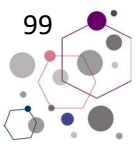

## 7.2. Extraction, purification and NMR spectroscopy

*H. smyrnensis* cell wall components were extracted using hot Phenol-Water procedure and further purified by enzymatic treatment, extensive dialysis, centrifugation and size-exclusion column chromatography. Compositional analysis showed that the water phase was composed of a highly heterogeneous mixture of polysaccharides, while LPS related constituents, as Kdo and fatty acids, were almost absent.

To further confirm that the LPS was present in a tiny amount, the water phase was treated by mild acid hydrolysis and its supernatant purified by size-exclusion column chromatography. Mass spectrometry of the pellet did not reveal the presence of the Lipid A. Chemical analysis was performed on the purified supernatant in order to determine the composition and branching points of its constituting polysaccharides. The GC-MS analysis of the partially methylated alditol acetates derivatives revealed that it was mainly composed of 4-glucose and 3-glucosamine. NMR experiments were then carried on the sample, in order to resolve the structure of this potential new exopolysaccharide.

A combination 1D and 2D NMR experiments was performed. $^{1}$H NMR spectra confirmed that the extract was composed of a mixture of polysaccharides, herein termed as **A** (H1 at *δ* 5,07ppm) and **B** (H1 at *δ* 4.99 ppm) (Figure 57).

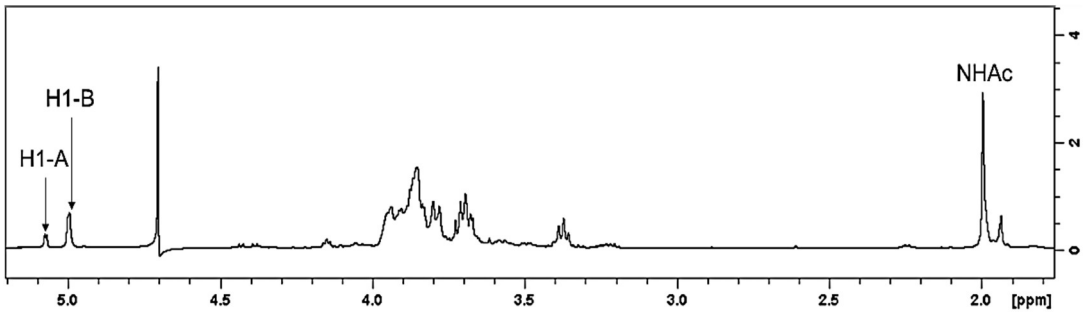


**Figure 57:** Proton spectra of the EPS isolated from *Halomonas smyrnensis*

COSY, TOCSY and HSQC experiments allowed the assignment of their respective spin systems (Table 5, Figure 58). **A** and **B** were both were considered as *gluco*-configured in the pyranose ring based on the large $^{3}J_{H,H}$ ring coupling constant and their $^{1}H$ and $^{13}C$ chemical shift value. **A** was identified as an α-glucose. **B** was attributed to an α –N-Acetyl-glucosamine, as its C-2 chemical shift is indicative of a nitrogen-bearing carbon (C-2 at *δ* 53.6 ppm) and gave its H-2 (*δ* 3,84 ppm) gave NOE contact with a methyl group (*δ* 1,99 ppm).

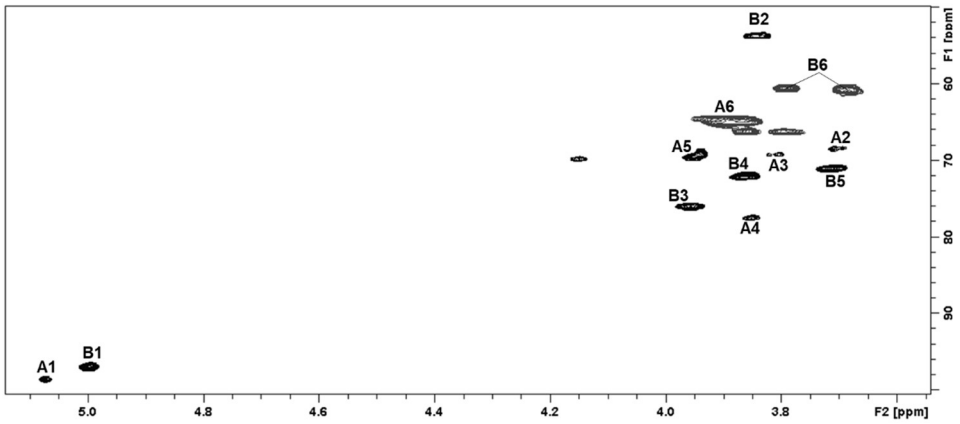


**Figure 58:** $^{1}H$-$^{13}C$ HSQC NMR spectra of EPSs isolated from *H. smyrnensis*

| Unit | 1 | 2 | 3 | 4 | 5 | 6 |
|---|---|---|---|---|---|---|
| **A α-Glc** | 5.07/*98.6* | 3.70/*68.4* | 3.82/*69.1* | 3.85/*77.5* | 3.94/*69.4* | 3.86-3.91/*64.5* |
| **B α-GlcNAc** | 4.99/*96.8* | 3.84/*53.6* | 3.96/*75.9* | 3.86/*72.2* | 3.71/*71.1* | 3.68-3.78/*60.5* |

**Table 5:** $^{1}H$ and $^{13}C$ (italic) NMR Chemical shift of EPSs isolated from *H. smyrnensis*. Additional chemical shifts: NAc at δ 1.99/22.3 ppm (CH3), 174,5 ppm (CO)

Branching points between each monosaccharide unit were analysed by HMBC and NOESY spectra. It revealed that **A** and **B** were not each other connected and represented hence two separate homoglycans. Indeed, HMBC spectrum in anomeric region clearly showed signals that corresponded to ring closure and linkages within the same spins systems (Figure 59). Those linkages were consistent with previous GC-MS analysis. Moreover, the upfield shift of carbone resonance is indicative of glycosylation at those position (Table 5). **A** would hence be a homopolymer constituted of α-(1→4)-Glc and **B** constituted of α-(1→3)-GlcNAc (Figure 60).

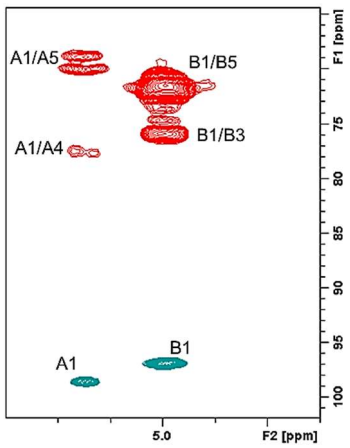


**Figure 59:** $^{1}H$-$^{13}C$ HSQC (Blue) and $^{1}H$-$^{13}C$ HMBC (Red) NMR spectra of EPSs isolated from *H. smyrnensis.*

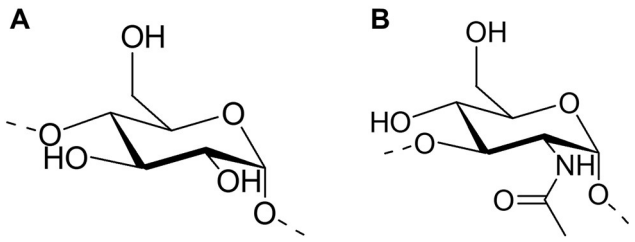


**Figure 60:** Structure of α-(1→4)-Glucose (A) and α-(1→3)-GlcNAc (B)

## 7.3. Discussion

Here, two homopolymers were identified as components of *H. smyrnensis* EPS content. The first one is an α-(1→4)-Glc polymer and the second polysaccharide is composed of α-(1→3)-GlcNAc. As previously described (See section 7.1.), the *Halomonas* genus is known to produce unique polysaccharides that have promising industrial application. Some new EPS are even named after the bacterium in which they were discovered, as Mauran from *Halomonas maura*. Mauran is an anionic, sulphated heteropolysaccharide with high uronic acid content that have pseudoplastic characteristic[109]. Finding new EPS is hence a promising way to discover new compounds for biotechnology. The occurrence in *H. smyrnensis* of the α-(1→4)-Glc polymer – known as amylose – is interesting as it is mostly produced by higher plants. Moreover, the α-(1→3)-GlcNac polymer is, at our knowledge, a novel polysaccharide. Further studies are needed in order to confirm their structure but those EPS can be specific to *H. smyrnensis*. Nevertheless, this chapter confirms that *H. smyrnensis* is a high EPS producer and synthetize EPS other than Levan.

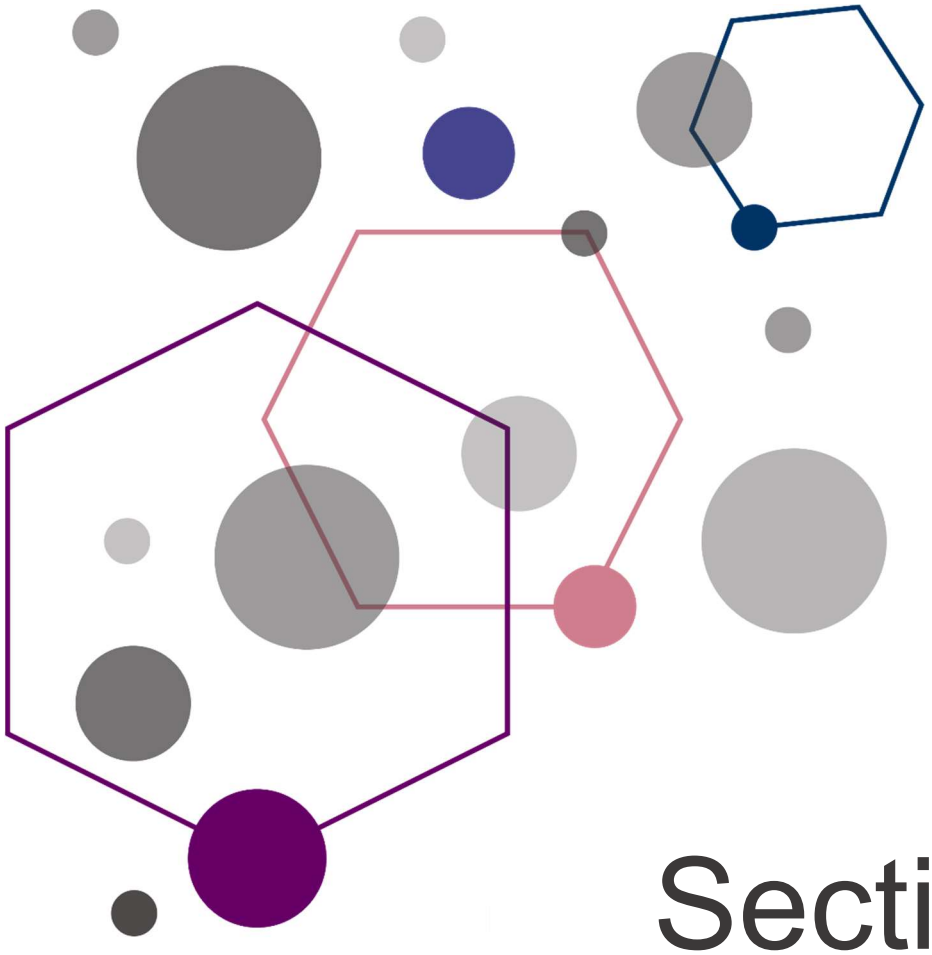

# Section V

## Experimental methods

# Chapter 8: Material and Methods

## 8.1. Bacteria growth

### 8.1.1. Pseudoalteromonas sp1A1

Bacteria cells were provided by Garderes et al.[67], who extracted *Pseudoalteromonas sp1A1* on *S. domuncula*. Sponges were individually cut into small pieces (1 $cm^3$) under sterile conditions. Pieces were washed three times with sterile seawater to remove epibiotic organisms. After incubation for 1 min of pieces from unhealthy specimens in 1 mL of sterile natural seawater, the suspension was spread onto Zobell agar medium (1.30 g $L^{-1}$ yeast extract, 6.61 g $L^{-1}$ peptone, 15.00 g L−1 agar in sea water, pH 7.4) to isolate opportunist bacteria. After 24 h of culture at 20 °C, the most occurring colony morphotype was picked and streaked onto fresh Zobell medium.

### 8.1.2. Spiribacter salinus

Bacteria cells were provided by Dr. Rodolfo Javier Menes[92]. The type strain *S. salinus* M19-40T (LMG 27464T) was obtained from Belgian Coordinated Collections of Microorganisms (BCCM (Gent, Belgium)). The bacterial strain was grown in modified growth medium (MGM18) broth at 30 °C in an orbital shaker (200 rpm) and biomass was harvested after 15 days by centrifugation (10,000 x g).

### 8.1.3. Halopeptonella vilamensis

Bacteria cells were provided by Dr. Rodolfo Javier Menes[101]. Strain SV525T was isolated by serial dilutions in 0.9 % NaCl solution of sediment samples, spread-plated on MGM25 agar and incubated aerobically for 10 days at 30 °C. MGM has the following composition ($l^{-1}$): 5.0 g tryptone (Oxoid), 1.0 g yeast extract (Oxoid) and 600 ml or 833 ml (for MGM18 or

MGM25, respectively) of concentrated salt water (SW30) stock solution (Dyall-Smith 2009). The SW30 solution contained (l−1): 240 g NaCl, 30 g $MgCl_2 \cdot 6H_2O$, 35 g $MgSO_4 \cdot 7H_2O$, 7 g KCl and 5 ml 1 M $CaCl_2 \cdot 2H_2O$. For solid medium 15 g of agar was added. The pH was adjusted to 7.5 ± 0.2, and the medium was autoclaved for 15 min at 121 °C. The strain was routinely grown on MGM18 agar at 30 °C for 5–7 days and maintained at 4 °C for short-term preservation.

### 8.1.4. Halomonas smyrnensis

Bacteria cells were provided by Kazan et al.[110]. Several pond soil samples from the Aegean Region of Turkey, with salt contents in the range 30–50% and pH values of 6.5–7.5, were serially diluted with 0.9% (w/v) saline solution and spread on medium A containing (w/v) 0.5% yeast extract, 0.3% sodium citrate, 2% MgSO4 .$7H_2O$, 0.2% KCl, 25% NaCl and 1% agar. The pH of the medium was adjusted to 6.9 and plates were incubated at 37 °C. After one week of incubation a number of yellow–cream colonies had developed. They were purified using the repeated serial dilution technique followed by restreaking on solid enrichment medium A and the purity of the isolates was examined based on cell shape under a microscope and colony homogeneity on the plates. Four isolates, designated AAD6T, AAD4, AAD17 and AAD21 and belonging to the same genus based on 16S rRNA gene sequence analysis, were studied for phenotypic characteristics. Subculturing was performed on samemediumfor 24 h at 37 °and bacterial isolates were maintained as glycerol stocks at -70 °C for further studies.

## 8.2. Extraction of LOS and LPS

Dried cells were washed three times with water, ethanol and acetone and then lyophilized. The PCP extraction was then performed on the washed cells. A solution of Phenol/Chloroform/Light Petroleum (2:5:8 v/v/v) was prepared. The cells were then dissolved at a concentration of 10 mL/g of cells. The solution was stirred for 1 h at room temperature and then centrifuged for 20 min at 8000 rpm. The supernatant was collected in a round bottom flask and the extraction was repeated twice. The solution was concentrated under vacuum until phenol is the only solvent left in the flask. The solution was then transferred in a falcon, few drops of water were added and a centrifugation was performed for 40 min at 8000 rpm.

The Hot Phenol-Water procedure was hence performed on the remaining cells. A solution of Phenol/Water (1:1) was prepared and the cells were dissolved at a concentration of 40 mL/g of cells. The solution was stirred for 1h at 70 °C. It was then centrifuged for 30 min at 4 °C and 8000 rpm. The water phase was transferred in a Falcon and the extraction was repeated twice. At the end, the Phenol phase was diluted three times in water. Both water and phenol phases were then separately dialysed against distilled water (cut-off 12–14 kDa) and lyophilised.

The water phase underwent an enzymatic treatment. It was first digested by RNase and DNase for 5h at 37°C. Protease were then added and the reaction was let overnight at 56°C. The digested material was extensively dialysed against distilled water (cut-off 12–14 kD) and lyophilised. The partially purified product was analysed by DOC-PAGE, which was followed by gel staining with silver nitrate, using the described procedure[49].

## 8.3. Chemical analysis

### 8.3.1. MGA analysis

An aliquot of LPS/LOS was dried under vacuum for 1 h. It was then dissolved in 300 µL of MeOH/HCl and the reaction was performed overnight at 85 °C. The solvent was then removed under an air flow and the solution neutralised with several washes using MeOH. The product was dried again under vacuum for 30 min. 25 µL of acetic anhydride ($Ac_2O$) and 25 µL of pyridine were then added and the reaction was performed at 85 °C for 30 min. The solvent was is removed under air flow. The product in then diluted in $CHCl_3$ and three washes with water were performed. The $CHCl_3$ phase was dried under air flow. The sample was then diluted in 100 µL of acetone and injected in GC-MS.

### 8.3.2. AAPM analysis

An aliquot of LPS/LOS was dried under vacuum for 1h. It was then dissolved in 500 µL DMSO with NaOH and the solution was stirred for 1h 30 at room temperature. 300 µL of $CH_3I$ was added and the reaction was done overnight at room temperature. The solvent was then removed for 1 h under an air flow. The sample was dissolved in $CHCl_3$ and several washes with water were performed. The $CHCl_3$ was removed under air flow and the sample was dried for 30 min under vacuum. 300 µL of TFA 2M were added and the reaction was done for 2 h at 120 °C. The TFA was removed under air flow and the sample was neutralized with several washes of MeOH. The sample was then diluted in 300 µL of EtOH and one spatula tip of $NaBD_4$ was added. The solution was stirred overnight at room temperature and the reaction was stopped with few drops of HCl. The solvent was removed

under air flow and once again neutralized with several washes with MeOH. The sample was dried 30 min under vacuum and 25 µL of acetic anhydride ($Ac_2O$) and 25 µL of pyridine were added. The reaction was performed at 85 °C for 30 min. The solvent is removed under air flow. The product was then diluted in $CHCl_3$ and washed three times with water. The $CHCl_3$ phase was dried under air flow and the sample is then diluted in 100 µL of acetone. It was then injected in GC-MS.

### 8.3.3. Analysis of Fatty acids Methyl-ester derivatives

An aliquot of LPS/LOS is dried under vacuum for 1 h. The methanolysis is then performed with HCl.MeOH, as described for MGA procedure (8.3.1). The product is then extracted with three time 500 µL of hexane. A fraction of the hexane layer was then injected in GC-MS.

## 8.4. Isolation of Lipid A and Polysaccharides moieties

### 8.4.1. Isolation of *Pseudoalteromonas sp1A1* O-antigen

An aliquot of the extracted LPS (20 mg) was dried under vacuum for 2 h. Hydrazine (1,3 mL) was added and the sample was stirred at 37 °C for 2 h. Cold acetone was added and the solution was centrifuged at 4 °C, 4000 rpm for 15 min. The supernatant was removed and the pellet was washed two other times with acetone. The pellet was dried under air flow and lyophilized. The product was then dissolved in a solution of KOH 4 M (1,3 mL) and the reaction was done overnight at 120 °C. The solution was neutralized with HCl 4 M and extracted three times with HCl. The water

phase was isolated and lyophilized. The salt-containing product was purified using gel filtration chromatography Sephadex G- 10 (GE Healthcare). The de-salted product was further purified by size-exclusion chromatography Bio-Gel P-10 (Bio-Rad). The purified polysaccharide was dissolved in 500 µL $D_2O$ and analysed by NMR spectroscopy.

### 8.4.2. Isolation of *Pseudoalteromonas sp1A1* Lipid A

In order to isolate the lipid A component, an aliquot of pure LPS (20 mg) was treated with acetate buffer (pH 4.4, 5 h, 100 °C) under magnetic stirring. An appropriate mixture of methanol and chloroform was added to the hydrolysate to obtain a methanol/ chloroform/hydrolysate 2:2:1.8 (*v/v/v*) ratio. The mixture was then shaken and centrifuged. The chloroform phase, containing the lipid A, was collected and washed with the water phase of a freshly prepared Bligh/Dyer mixture (chloroform/methanol/water, 2:2:1.8)[114]. This wash step was executed several times and all the organic phases were then collected and dried.

### 8.4.3. Isolation of *Spiribacter salinus* M19-40$^T$ Lipid A

The extracted LOS was further purified by ultracentrifugation (4 °C, 45,000 rpm, 48 h) and then by size-exclusion chromatography on a Sephacryl High Resolution S-200 (GE Healthcare) column. An aliquot of the pellet (10 mg) was then treated by mild acidic hydrolysis as described in paragraph 8.4.2. Another aliquot of lipid A was also treated with 10% ammonium hydroxide, as previously reported[56]. The sample was dried and analyzed by MALDI MS.

### 8.4.4. Isolation of *Halopeptonella vilamensis* polysaccharides

The extracted material was further purified by by size-exclusion chromatography on a Sephacryl High Resolution S-500 (GE Healthcare) column. An aliquot of the product (30 mg) was treated by mild acidic hydrolysis with an acetate buffer (pH 4.4, 2 h, 100 °C). The solution was then centrifuged (4 °C, 7000 rpm, 1 h) and the pellet was washed twice with water. The supernantant were collected and lyophilised. The product was then purified by size-exclusion chromatography on a Sephacryl High Resolution S-100 (GE Healthcare) column. The purified extract was lyophilized, dissolved in 500 µL $D_2O$ and analysed by NMR spectroscopy.

### 8.4.5. Isolation of *Halopeptonella vilamensis* Lipid A

The extracted LOS was further purified by size-exclusion chromatography on a Sephacryl High Resolution S-300 (GE Healthcare) column. An aliquot of the sample (25 mg) was then treated by mild acidic hydrolysis and underwent an ammonium treatment as previously described (See paragraph 8.4.2). Treated Lipid As were dried and analysed by MALDI MS.

### 8.4.6. Isolation of *Halomonas smyrnensis* polysaccharides

An aliquot of the extracted LPS (15 mg) was dried under vacuum and underwent a full de-acylation procedure, as described in paragraph 8.4.1. The salt-containing product was purified using gel filtration chromatography Sephadex G10 (GE Healthcare). The de-salted product was further purified by size-exclusion chromatography Bio-Gel P-2 (Bio-

Rad). The purified polysaccharide was dissolved in 500 µL $D_2O$ and analysed by NMR spectroscopy.

## 8.5. Mass Spectrometry

A reflectron MALDI-TOF MS and $MS^2$ analysis was performed on an ABSCIEX TOF/TOFTM 5800 Applied Biosystems mass spectrometer, equipped with an Nd:YLF laser with a λ of 345 nm, a <500 ps pulse length, and a repetition rate of up to 1000 Hz. The lipid A fraction was dissolved in chloroform/methanol (1:1, *v/v*), as previously described[115]. The matrix was the trihydroxyacetophenone (THAP) dissolved in methanol/0.1%trifluoracetic acid/acetonitrile (7:2:1, *v/v/v*) at a concentration of 75 $mg.mL^{-1}$. The ammonium-treated lipid A was dissolved in chloroform-trifluoroethanol (4:1, v/v) and the matrix used was 2,5-dihydroxy benzoic acid in acetonitrile 0.2% trifluoroacetic acid (7:3, *v/v*)[56]. Lipid A preparation of 0.5 µL and 0.5 µL of the matrix solution were deposited on the MALDI plate and left to dry at room temperature. Each spectrum was a result of the accumulation of 1500 laser shots, whereas 6000–7000 shots were summed for the $MS^2$ data acquisitions[116]. The reported $MS^2$ spectra were all acquired without collision gas. Nevertheless, $MS^2$ experiments were executed with argon or air as the collision gas, and the resulting fragmentation spectra were compared with those that were obtained without collision-induced dissociation. No large differences were observed in all of the cases in the mass range above *m/z* 200. Below this mass, the product ions corresponding to the phosphate fragments at *m/z* 79 and 97 were far more abundant in the collision-induced dissociation spectra, regardless of the collision gas.

## 8.6. NMR spectroscopy

1D and 2D NMR spectra were performed at 298 K in D2O at pD = 7 with a cryoprobe-equipped Bruker 600DRX spectrometer. The spectra were calibrated with internal acetone (H = 2.225 ppm; C = 31.45 ppm). Total correlation spectroscopy (TOCSY) experiments were performed with spinlock times of 100 ms by using data sets (t1 x t2) of 4096 x 512 points. Rotating frame Overhauser enhancement spectroscopy (ROESY) and Nuclear Overhauser enhancement spectroscopy (NOESY) experiments were executed by using data sets (t1 x t2) of 4096 x 512 points with mixing times between 100 and 300 ms. Double-quantum-filtered phase sensitive correlation spectroscopy (DQF-COSY) experiments were executed by using data sets of 4096 x 900 points. The data matrix in all the homonuclear experiments was zero-filled in both dimensions to give a matrix of 4K x 2K points and was resolution-enhanced in both dimensions by a cosine-bell function before Fourier transformation. Coupling constants were determined by 2D phase-sensitive DQF-COSY[117, 118]. Heteronuclear single quantum coherence (HSQC) and heteronuclear multiple bond correlation (HMBC) experiments were executed in $^{1}$H-detection mode by single-quantum coherence with proton decoupling in the $^{13}$C domain using data sets of 2048 x 400 points. HSQC was performed using sensitivity improvement and in the phase-sensitive mode using Echo/Antiecho gradient selection, with multiplicity editing during the selection step[119]. HMBC was optimized on long range coupling constants, with a low-pass J-filter to suppress one-bond correlations, using gradient pulses for selection, and a 60 ms delay was used for the evolution of long-range correlations. The data matrix in all the heteronuclear experiments was extended to 2048 x 1024 points by using forward linear prediction extrapolation[120].

## 8.7. Biological assays

### 8.7.1. ELISA and Quanti-Blue assays with LPS from *Pseudoalteromonas sp1A1*

Those experiments were performed in collaboration with Prof. Bayeart. THP-1 cells were seeded in a 96-well plate at $10^5$ cells $well^{-1}$ in complete medium (140 µL) and were stimulated overnight at 37°C with TPA (12-O-Tetradecanoylphorbol-13-acetate). The next day, cells that did not adhere were removed using complete culture medium, and the plated were left for 1h to recover with complete medium (180 µL). Cells were either stimulated with *Pseudoalteromonas sp1A1 LPS* or *E. coli* LPS (InvivoGen) at the indicated concentrations. The P*seudoalteromonas sp1A1* LPS and *E. coli* LPS were added as solutions in complete medium (20 µL) to reach a 200 mL total volume of the well after stimulation. The cells were incubated overnight at 37°C with 5% CO2. The supernatants were analysed for TNF production by ELISA (BD Biosciences). Data are representative of three independent experiments. Errors bars indicate standard error of the mean of triplicate samples.

Raw-blue-hTLR4 cells were detached with Tripsin then seeded in a 96-well plate at $5.10^4$ cells $well^{-1}$ in complete medium (180µL) and incubated overnight. Cells were simultaneously stimulated with *Pseudoalteromonas sp1A1* LPS and *E. coli* LPS at the indicated concentrations. The *Pseudoalteromonas sp1A1* LPS and *E. coli* LPS were added as solutions in complete medium (20 µL) to reach a 200 mL total volume of the well after stimulation. The cells were incubated overnight at 37°C and 5% CO2, and the supernatants were analysed for Secreted Alkaline Phosphate (SEAP) production by Quanti-blue Assay. Data are

representative of three independent experiments. Error bars indicate standard error of the mean of triplicate samples.

### 8.7.2. Cell culture and ELISA with *H. vilamensis* LOS

Those experiments were performed in collaboration with Prof. Bernardini. HEK293 cell line, stably transfected with human TLR4/MD2-CD14 (InvivoGen) was seeded into 96-well plate at the concentration of 1 × 105 cells/mL. 48 h after seeding the cells were transiently transfected through PolyFect Transfection Reagent (Qiagen) with a reaction mix containing 150 ng of Firefly luciferase reporter constructs, pGL3.ELAM.tk [harboring nuclear factor kappa B (NF-κB) promoter sequences], and 15 ng of *Renilla* luciferase reporter plasmid, pRLTK (as an internal control). The day after the cells were incubated with different concentrations of *H. vilamensis* LOS (1, 10, and 100 ng/mL), or with purified *E. coli* LPS (LPS-EB ultrapure; InvivoGen) or with synthetic lipid IVA used at the same concentrations as above, for 6 h to analyze NF-κB activity (Dual Luciferase Reporter Assay System, Promega) and to measure CXCL-8 release (DuoSet R&D System).

Peripheral blood mononuclear cells were isolated from buffy coats obtained by the blood bank of Sapienza University from healthy adult volunteers (blood donors) following written informed consent. CD14+ monocytes were isolated from PBMCs using the MACS system (Miltenyi Biotec, Bergisch Gladbach, Germany) and cultured in complete RPMI 1640 medium (Lonza, Italy, Milan), supplemented with 10% of heat-inactivated FBS (HycloneTM, Euroclone, Italy, Milan), 1% di l-glutammine (Lonza), 1% of non-essential amino acid solution (NEEA—Lonza), 1% sodium pyruvate (Lonza), penicillin 100 U/mL–streptomycin 100 µg/mL (Lonza), and 0.1% di 2-ME (Gibco, Italy). CD14+ monocytes were seeded at the concentration of



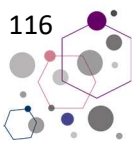

5 × 105 cells/well in 12-multiwell plate and exposed to 1, 10 and 100 ng/mL of LOS from *H. vilamensis* or to commercial E. coli O111:B4 LPS or to synthetic lipid IVA at same concentrations as above for 12 h. Cell supernatants were then collected and processed for ELISA to the levels of TNF and IL-6.

Murine and human cytokines were determined in supernatants of stimulated cells by using R&D Systems DuoSet ELISA kits according to the manufacturers' instructions. Student's paired t test was used to determine the statistical significance of the data.

## 8.8. Molecular Dynamic Simulation

A 128 lipid bilayer was generated using CHARMM-GUI Membrane Builder (http://www.charmm-gui.org/). Each leaflet was composed of a 3:1 ratio of palmitoyloleoyl phosphatidylethanolamine (POPE) and palmitoyloleoyl phosphatidylglycerol (POPG). *Pseudoalteromonas* sp1A1 Lipid A and LOS were built using PyMOL software (http://www.pymol.org) and GLYCAM database (http://www.glycam.org). The atomic partial charges of the residues were calculated with Gaussian and formatted for AMBER14 with antechamber. Atoms and charges were assigned according to AMBER ff11, ff14 and Glycam force fields. Free Lipid A and LOS were immersed in an octaedric box of explicit TIP3P water molecules.

MD simulations were run with AMBER14. All hydrated systems were firstly equilibrated with 1000 steps of steepest descent minimization followed by 7000 steps of conjugate gradient algorithm. They were then heated from 0 to 100 K, with the Langevin thermostat and applying 10 $kcal \cdot mol^{-1}.A^{-2}$ restrain. The systems were then heated until 300 K with no

restrain. After equilibration, 100ns MD simulation was performed at constant temperature (300°C) and pressure (1 atm) at a 2 fs time step. At the end of the simulation, hydrophobic thickness and area per lipid were calculated with the help of the ptraj module of AmberTools 14.

# Conclusion

The investigation of new LPS/LOS structure, and in particular of their Lipid A, is necessary in order to develop new therapies. In this context, the LPS from *Pseudoalteromonas sp1A1* and the Lipid A from *Spiribacter salinus* M19-40$^T$ and *Halopeptonella vilamensis* were characterized.

*Pseudoalteromonas sp1A1* O-antigen possesses an hexa-saccharidic repeating unit with the notable presence of a pyruvate substituent and the KDN. *Pseudoalteromonas sp1A1* also possesses a mixture of two mono-phosphorylated and penta-acylated Lipid A. Its main species is composed of four C12:0 (3-OH) and one C12:0. The secondary species is bearing one C10:0 (3-OH), two C12:0 (3-OH), one C11:0 (3-OH) and one C13:0. The core region from *Pseudoalteromonas sp1A1* is a pentasaccharide containing one Kdo, one heptose, two galactose and one glucose. Concerning its biological properties, *Pseudoalteromonas sp1A1* does not possess significant agonist or antagonist activity. Finally, MDS highlighted that the Outer-membrane of *Pseudoalteromonas sp1A1* possesses a high flexibility due to the asymmetric repartition of its Lipid A. MDS of the LOS in water and with 0.5M of NaCl showed that the presence of salt could influence the conformational angle between the Kdo of the core oligosaccharide and its linked glucosamine. Such properties could be due to the presence of several negatively-charged phosphate groups that can interact with the surrounding $Na^+$. It is worth noticing such difference. Indeed, a change of the LOS conformation can lead to different biological properties in water and in marine environments.

The Lipid A structure from *Spiribacter salinus* M19-40$^T$ was elucidated. It is *mono*-phosphorylated and penta-acylated and contains two C10:0 (3-OH), one C12:0, one C14:0 (3-OH) and one C14:0 (3-oxo). It has

an unusual 2+3 symmetry that is shared with some marine bacteria. The precence of the C14:0 (3-oxo) is also remarkable and had previously been found in *Rhodobacter capsulatus* Lipid A. It is a promising result as this Lipid A inspired the synthetic analogue Eritoran that reached phase III of clinical trials as an anti-sepsis agent. This finding is encouraging for the research of new LPS structure from halophiles. *Halopeptonella vilamensis* lipid A was also characterised, and turned out to be composed of a highly heterogeneous mixture a *bis*-phosphorylated species. It is characterized by a mixture of tri-, tetra-, penta- and hexa-acylated species. Primary fatty acids C12:0 (3-OH) and C10:0 (3-OH) were respectively found as acyloxyamide and acyloaxyl ester directly linked to the di-glucosamine backbone. The Lipid A was also substituted by a mixture of C12:0, C12:1, C14:0 and C14:1 as secondary acyl chains. Immunological assays showed that *H. vilamensis* LOS has a slight agonist activity. Finally, *H. smyrnensis* EPS content was analysed using NMR spectroscopy, two novel homopolymers were found. The first one is formed by α-(1→4)-Glc polymer and the second one by α-(1→3)-GlcNAc units. As for the α-(1→4)-Glc polysaccharide is intriguing to find it produced by a halophilic bacterium. Moreover, the α-(1→3)-GlcNAc polymer is at our knowledge a novel polysaccharide that differ from homologues structure from its linkages.

# ANNEX

## Papers related to this PhD project

- Barrau, C.; Di Lorenzo, F.; Javier Menes R.; Lanzetta R.; Molinaro A.; Silipo A.; *Mar. Drugs* **2018**, 16, 124

- Barrau, C. et. al. Structure and activity of the LPS of *Pseudoalteromonas sp1A1*, *manuscript in preparation*

- Barrau, C. et. al. Structure and activity of the Lipid A from the halophilic bacterium *Halopeptonella vilamensis*, *manuscript in preparation*

## Attended congress, conferences, meeting, and workshop

- 2nd TOLLerant meeting, 24-27/05/2016, Madrid, Spain.
- XV CSCC, 19-22/06/2016, Certosa di Pontignano, Italy
    - Poster communication: Structure of potential agonist and antagonist LPS from extremophile bacteria – Clara Barrau; Flaviana Di Lorenzo; Antonio Molinaro; Alba Silipo
- Structural Glycoscience Workshop, 28-30/06/2016, Grenoble, France
- 3rd TOLLerant meeting, 14-16/12/2016, Ljubljana, Slovenia

- 4th TOLLerant meeting, 5-7/06/2017, Naples, Italy
- EUROCARB, 2-6/07/2017, Barcelona, Spain
    - Poster communication: Structure of potential agonist and antagonist LPS from extremophile bacteria – Clara Barrau; Flaviana Di Lorenzo; Antonio Molinaro; Alba Silipo
- NAPOSAKA meeting, 10/07/2017, Naples, Italy
    - Oral communication: Structure of potential agonist and antagonist LPS from extremophile bacteria – Clara Barrau; Flaviana Di Lorenzo; Antonio Molinaro; Alba Silipo
- 5th TOLLerant meeting, 12-15/12/2017,Ghent, Belgium
- XVI CSCC, 17-20/06/2018, Certosa di Pontignano, Italy
    - Poster communication: Structure of Lipooligosaccharides from halophilic bacteria - Clara Barrau; Flaviana Di Lorenzo; Antonio Molinaro; Alba Silipo
- 2nd NAPOSAKA meeting, 25/06/2018, Naples, Italy
    - Oral communication: Structure of Lipooligosaccharides from halophilic bacteria - Clara Barrau; Flaviana Di Lorenzo; Antonio Molinaro; Alba Silipo
- 29th International Carbohydrate Symposium (ICS 2018), 15-19/07/2018, Lisbon, Portugal
    - Poster communication: Structure of Lipooligosaccharides from halophilic bacteria - Clara Barrau; Flaviana Di Lorenzo; Antonio Molinaro; Alba Silipo
- IASOC, 22-25/09/2018, Naples, Italy
    - Poster communication: Structure of potential agonist and antagonist LPS/LOS from marine and halophilic bacteria - Clara Barrau; Flaviana Di Lorenzo; Antonio Molinaro; Alba Silipo

## Attended internal seminars

| Title | Speaker | Date |
|---|---|---|
| Solid State NMR | Dr. Guido Pintacuda | 22 to 24/02/2016 |
| Basics of detergents formulations and challenges | Dr. Giulia Bianchetti | 16/03/2016 |
| Progettazione risk assessment e controllo qualità del packaging alimentare : il ruolo intteso del consulente chimico | Dr. Vicenzo Benessere | 17/03/2016 |
| Metalloproteins, mimics by design | Dr. Angela Lombardi | 12/10/2016 |
| Chemical Biology and medicinal chemistry of glycoscphingolipid metabolism | Prof. Herman Overkleeft | 19/12/2016 |
| Discovery of novel hyperthermophilic carbohydrate active enzyme for biomass degradation | Prof. Andrea Strazzulli | 8/03/2017 |
| Non-entropic contribution to reinforcement in filled elastomers | Dr. Paul Sotta | 08/06/2017 |
| Structural Bioinformatics: a window to observe new asects of protein behavious | Prof. Neri Niccolai | 8/06/2017 |
| Chemical synthesis of homogeneous glycoproteins | Prof. Yasuhiro Kajihara | 14/11/2017 |

| | | |
|---|---|---|
| Chemical synthesis and characterization of chondroitin sulfate | Prof. Jun-Ichi Tamura | 23/07/2018 |

## Attended courses

| Title | Professor |
|---|---|
| Glycoscience | Prof. Michelangelo Parrilli<br>Dr. Emiliano Bedini |
| Advanced Mass spectrometry | Prof. Pietro Pucci |
| NMR of Biomolecules | Prof. Delia Picone |
| Spettroscopia Intrepretativa NMR Organica | Prof. Antonio Evidente |
| Recombinant production of natural and mutant proteins | Prof. Angela Dulio |
| Ecotoxicology: principles and main applications | Prof. Giovanni Pagano |

## Short stay in European Laboratories

- VIB, Ghent, Belgium (November 2016). Secondment made within Prof. Bayeart's team. Immunological assays of purified LPS. Results are presented in Section II, 3.6.

- CIB-CSIC, Madrid, Spain (April-May 2017). Secondment made within Prof. Martín-Santamaria's team. Molecular Dynamic simulation of LOS and Outer-membrane. Results are presented in Section II, 4.

- DIOMUNE, Madrid, Spain (September 2017). Secondment made within Dr. Llamas's team. Training about sepsis model *in vivo*. Experience in industry and learning about the elaboration of a business plan.

## Acknowledgment

I would like to thank my friend and colleague Mateusz Pallach for his constant help during this project. I would also like to thank Prof. Antonio Molinaro for his advices and his sympathy. I would especially like to thank Prof. Alba Silipo for her excellent scientific expertise and her humanity. I am thankful for the great patience and humanity she had that allowed me to get through a challenging period.

I would like to thank everyone else I worked with in Naples for their kindness. I also would like to thank Prof. Bayeart, Prof. Martin-Santamaria, Dr. Llamas and their team for their nice welcoming during my short stays abroad.

Finally, I would warmly like to thank my parents that have always been by my side despite the distances.

# Bibliography


[1] Woese, C.R.; Kandler, O.; Wheelis M.L.; *Proc. Nati. Acad. Sci.* **1990**, 87, 4576-4579

[2] Pommerville J.C.; Alcamo's fundamentals of microbiology 9th Edition, Chapter 4. (Eds.: Jones & Bartlett Publishers), Burlington, MA, **2010**

[3] Raven P.H., Johnson G.B., Biology 9th Edition, Chapter 34 (Ed.: McGraw Hill), **2011**

[4] Silhavy, T.J.; Kahne, D.; Walker S.; *Cold Spring Harb. Perspect. Biol.* **2010**, 2:a000414

[5] Siegel, S.D.; Liu, J.; Ton-That H.; *Curr. Opin. Microbiol.* **2016**, 34, 31–37

[6] Weidenmaier C.; Peschel A.; *Nat. Rev. Microbiol.* **2008**, 6, 276-287

[7] May, K.L.; Silhavy T.J.; *Biochim. Biophys. Acta.* **2017**, 1386–1393

[8] Raetz, C.R.H.; Whitfield C.; *Annu. Rev. Biochem.* **2002**, 71, 635–700

[9] Lerouge, I.; Vanderleyden J.; *FEMS. Microbiol. Rev.* **2001**, 26, 17-47

[10] Strauss, J.; Burnham, N.A.; Camesano, T.A.; *J. Mol. Recognit.* **2009**, 22, 347–355

[11] Lukáčová, M.; Barák, I.; Kazár J.; *Clin. Microbiol. Infect.* **2008,** 14, 200–206

[12] Holst, O.; *FEMS Microbiol. Lett.* **2007**, 271, 3–11

[13] Molinaro, A; Holst, O; Di Lorenzo, F; Callaghan, M; Nurisso, A; D'Errico, G; Zamyatina, A; Peri, F; Berisio, R; Jerala, R; Jimenez-Barbero, J; Silipo, A; Martin-Santamaria, S.; *Chem. Eur. J.* **2015**, 21, 500 – 519

[14] Rietschel, E.T.; Wollenweber, H.W.; Russa, R.; Brade, H.; Zahringer U.; *Rev. Infect. Dis.* **1984**, 6, 4, 432-438

[15] Kumada, H.; Haishima, Y.; Umemoto, T.; Tanamoto, K.I.; *J. Bacteriol.* **1995**, 177, 8, 2098-2106

[16] Moran, A.P.; Lindner, B.; Walsh, E.J.; *J. Bacteriol.* **1997**, 179, 20, 6453-6463

[17] Kaltashov, I.A.; Doroshenko, V.; Cotter, R.J.; Takayama, K.; Qureshi, N.; *Anal. Chem.* **1997**, 69, 2317-2322

[18] Janeway C.A.Jr; *Cold Spring Harb. Symp. Quant. Biol.* **1989**, 54, 1-13

[19] Alberts B., Johnson A., Lewis J., Raff M., Roberts K., Walter P., Molecular Biology of the Cell, 4th edition (Ed.: Garland Science), New York, chapter 24, **2007**

[20] E Sousa C.R.; *Curr. Opin. Immunol.* **2004**, 16, 21–25

[21] Medzhitov, R.; *Nat Rev Immunol.* **2001**, 1, 135-145

[22] Medzhitov, R.; Preston-Hurlburt, P.; Janeway Jr C.A.; *Nature*, **1997**, 388, 394-397

[23] Hoshino, K.; Takeuchi, O.; Kawai, T.; Sanjo, H.; Ogawa, T.; Takeda, Y.; Takeda, K.; Akira S.; *J. Immunol.* **1999**, 162, 3749-3752

[24] Nagai, Y.; Akashi, S.; Nagafuku, M.; Ogata, M.; Iwakura, Y.; Akira, S.; Kitamura, T.; Kosugi, A.; Kimoto, M.; Miyake, K.; *Nat Immunol.* **2002**, 3, 7 667-672

[25] Huber, R.G.; Berglund, N.A.; Kargas, V.; Marzinek, J.K.; Holdbrook, D.A.; Khalid S.; Piggot, T.J.; Schmidtchen, A.; Bond P.J.; *Structure* **2018**, 26, 1–11

[26] Kieser, K.J.; Kagan J.C.; *Nat. Rev. Immunol.* **2017**, 17, 377-390

[27] Medzhito R.; Horng, T.; *Nat. Rev. Immunol.* **2009**, 9, 692-703

[28] Mayr, F.B.; Yende, S.; Angus, D.C.; *Virrulence*, **2014**, 5:1, 4-11

[29] Kuzmich, N.N.; Sivak, K.V.; Chubarev, V.N.; Porozov, Y.B.; Savateeva-Lyubimova, T.N.; Peri, F.; *Vaccines* **2017**, 5, 34

[30] Brandenburg, K.; Mayer, H.; Koch, M.H.J.; Weckesser, J.; Rietschel E.T.; Seydel U.; *Eur. J. Biochem.* **1993**, 218, 555-563

[31] Netea, M.G.; Van Deuren, M.; Kullberg, B.J.; Cavaillon J.M.; Van der Meer J.W.M.; *Trends Immunol.* **2002**, 23, 3, 135-139

[32] Pulendran, B.; Kumar, P.; Cutler, C.W.; Mohamadzadeh, M.; Van Dyke, T.; Banchereau, J.; *J. Immunol.* **2001**, 167(9), 5067–5076

[33] Saitoh, S.I.; Akashi, S.; Yamada, T.; Tanimura, N.; Kobayashi, M.; Konno, K.; Matsumoto, F.; Fukase, K.; Kusumoto, S.; Nagai, Y.; Kusumoto, Y.; Kosugi, A.; Miyake, K.; *Int. Immunol.* **2004**, 16, 7, 961-969

[34] Ohto, U.; Fukase, K.; Miyake, K.; Satow Y.; *Science.* **2007**, 316, 1632-1634

[35] Park, B.S.; Song, D.H.; Kim, H.M.; Choi, B.S.; Lee, H.; Lee, J.O.; *Nature* **2009**, 458, 1191-1195

[36] Ohto, U.; Fukase, K.; Miyake, K.; Shimizu, T.; *PNAS.* **2012**, 109, 19, 7421-7426

[37] Krüger, C.L.; Zeuner, M.T.; Cottrell, G.S.; Widera, D.; Heilemann, M.; *Sci. Signal.* **2017**, 10, eaan1308

[38] Cochet, F.; Peri, F.; *Int. J. Mol. Sci.* **2017**, 18, 2318

[39] Rothschild, L.J.; Mancinelli, R.L.; *Nature*, **2001**, 409, 1092-1101

[40] Cowan, D.A.; Ramond, J.B.; Makhalanyane, T.P.; De Maayer, P.; *Curr. Opin. Microbiol.* **2015**, 25, 97-102

[41] Krüger, A.; Schäfers, C.; Schröder, C.; Antranikian, G.; *New Biotechnol.* **2018**, 40, 144–153

[42] Bhatnagar, I.; Kim S-K.; *Mar. Drugs.* **2010**, 8, 2673-2701

[43] Leone, S.; Silipo, A.; Nazarenko, E.L.; Lanzetta, R.; Parrilli, M.; Molinaro, A.; *Mar. Drugs.* **2007**, 5, 85-112

[44] Di Lorenzo, F.; Billod, J.M.; Martín-Santamaría, S.; Silipo, A.; Molinaro, A. *Eur. J. Org. Chem.* **2017**, 28, 4055–4073

[45] Leone, S.; Molinaro, A.; Sturiale, L.; Garozzo, D.; Nazarenko, E.L.; Gorshkova, R.P.; Ivanova, E.P.; Shevchenko, L.S.; Lanzetta, R.; Parrilli, M.; Eur. J. Org. Chem. 2007, 1113–1122

[46] Carillo, S.; Pieretti, G.; Casillo, A.; Lindner, B.; Romano, I.; Nicolaus, B.; Parrilli, M.; Giuliano, M.; Cammarota, M.; Lanzetta, R.; Corsaro, M.M.; *Extremophiles* **2016**, 20, 687–694

[47] Di Lorenzo, F.; Paciello, I.; Fazio, L.L.; Albuquerque, L.; Sturiale, L.; da Costa, M.S.; Lanzetta, R.; Parrilli, M.; Garozzo, D.; Bernardini, M.L.; Silipo, A.; Molinaro, A.; *ChemBioChem* **2014**, 15, 2146 – 2155

[48] Westphal O., Jann K., Methods *Carbohydr. Chem.* **1965**, 5, 83-91

[49] Kittelberger R., Hilbink F.; *J. Biochem. Biophys. Methods.* **1993**, 26, 1, 81-86

[50] De Castro, C.; Parrilli, M.; Holst, O.; Molinaro, A.; *Methods. Enzymol.* **2010**, 480, 89-115

[51] Hakomori S.; *J. Biochem.* **1964**, 55, 205-208

[52] Rietschel E.T.; *Eur. J. Biochem.* **1976**, 64, 423-428

[53] Holst O.; *Methods Mol. Biol.* **2000**, 145, 345 –353

[54] Bubb, W.A.; *Concepts Magn. Reson.* **2003**, 19A(1), 1–19

[55] Domon, B.; Costello, C.E. *Glycoconj. J.* **1988**, 5, 397–409

[56] Silipo, A.; Lanzetta, R.; Amoresano, A.; Parrilli, M.; Molinaro, A.; *J. Lipid Res.* **2002**, 43, 2188–2195

[57] Baumann, L.; Baumann, P.; Mandel, M.; Allen R.D.; *J. Bacteriol.* **1972**, 110, 1, 402-429

[58] Gauthier, G.; Gauthier, M.; Christen, R.; *Int. J. Syst. Bacteriol.* **1995**, 45, 4, 755-761

[59] Kalinovskaya, N.I.; Ivanova, E.P.; Alexeeva, Y.V.; Gorshkova, N.M.; Kuznetsova, T.A.; Dmitrenok, A.S.; Nicolau, D.V.; *Curr Microbiol.* **2004**, 48, 441-446

[60] Holmstro, C.; Kjelleberg, S.; *Microbiol. Ecol.* **1999**, 30, 285-293

[61] Bowman J.P.; *Mar. Drugs.* **2007**, 5, 220-241

[62] Ivanova, E.P.; Kiprianova, E.A.; Mikhailov, V.V.; Leavanova, G.F.; Garagulya, A.D.; Gorshkova, N.M.; Vysotskii, M.V.; Nicolau, D.V.; Yumoto, N.; Taguchi, T.; Yoshikawa, S.; *Int. J. Syst. Bacteriol.* **1998**, 48, 247-256

[63] Bohm, M.; Hentschel, U.; Friedrich, A.B.; Fieseler, L.; Steffen, R.; Gamulin, V.; Nuller, I.M.; Muller, W.E.G.; *J. Mar. Biol.* **2001**, 139, 1037-1045

[64] Maaetoft-Udsen, K.; Vynne, N.; Heegaard, P.M.H.; Gram, L.; Frøkiær H.; *Innate Immun.* **2012**, 19, 2, 160-173

[65] Wiens, M.; Korzhev, M.; Krasko, A.; Thakur, N.L.; Perovic´-Ottstadt, S.; Breter, H.J.; Ushijima, H.; Diehl-Seifert, B.; Muller, I.M.; Muller, W.E.G.; *J. Biol. Chem.* **2005**, 280, 30, 27949–27959

[66] Gardères, J.; Bedoux, G.; Koutsouveli, V.; Crequer, S.; Desriac, F.; Le Pennec, G.; *Mar. Drug.* **2015**, 13, 4985-5006

[67] Nadano, D.; Iwasakis, M.; Endo, S.; Kitajima, K.; Inoue, S.; Inoue, Y.; *J. Biol. Chem.* **1986**, 261, 25, 11550-11557

[68] Corsaro, M.M.; Dal Piaz, F.; Lanzetta, R.; Parrilli, M.; *J. Mass. Spectrom*, **2002**, 37, 481-488

[69] Krasikova, I.N.; Kapustina, N.V.; Isakov, V.V.; Gorshkova, N.M.; Solov'eva, T.F.; *Russ. J. Bioorg. Chem.* **2004**, 30, 367–373

[70] Carillo, S.; Pieretti, G.; Parrilli, E.; Tutilo, M.L.; Gemma, S.; Molteni, M.; Lanzetta, R.; Parrilli, M.; Corsaro, M.M.; *Chem. Eur. J.*, **2011**, 11, 7053-7060

[71] Di Lorenzo, F.; *Antonie van Leeuwenhoek*, **2017**, 110, 11, 1401–1412

[72] Sturiale, L.; Garozzo, D.; Silipo, A.; Lanzetta, R.; Parrilli, M.; Molinaro, A.; *Rapid Commun. Mass Spectrom.* **2005**, 19, 1829–1834

[73] Silipo, A.; Leone, S.; Lanzetta, R.; Parrilli, M.; Sturiale, L.; Garozzo, D.; Nazarenko, E.L.; Gorshkova, R.P.; Ivanova, E.P.; Gorshkova, N.M.; Molinaro, A.; *Carbohydr. Res*. **2004**, 35, 1985-1993

[74] Kirschner, K.N.; Lins, R.D.; Maass, A.; Soares, T.A.; *J. Chem. Theory Comput.* **2012**, 8, 4719−4731

[75] Boags, A.; Hsu, P.C.; Samsudin, F.; Bond, P.J.; Khalid, S.; *J. Phys. Chem. Lett.* **2017**, 8, 2513−2518

[76] Patel, D.S.; Qi Y.; Im, W.; *Curr. Opin. Struct. Biol.* **2017**, 43, 131-140

[77] Ma, H.; Irudayanathan, F.J.; Jiang, W.; Nangia, S.; *J. Phys. Chem. B*. **2015**, 119, 14668−14682

[78] Kim, S.; Patel, D.S.; Park, S.; Slusky, J.; Klauda, J.B.; Widmalm, G.; Im, W.; *Biophys. J.* **2016**, 111, 1750-1760

[79] Murzyn, K.; Róg, T.; Pasenkiewicz-Gierula M.; *Biophys. J.* **2005**, 88, 1091-1103

[80] Jo, S.; Kim, T.; Iyer, V.G.; Im, W.; *J. Comput. Chem.* **2008**, 29, 1859-1865

[81] Skjevik, Å.A.; Madej, B.D.; Walker, R.C.; Teigen, K.; *J. Phys. Chem. B*. **2012**, 116, 36, 11124–11136

[82] Dickson, C.J.; Madej, B.D.; Skjevik, Å.A.; Betz, R.M.; Teigen, K.; Gould, I.R.; Walker, R.C.; *J. Chem. Theory Comput.* **2014**, 10, 865−879

[83] Roe, D.R.; III, T.E.C.; *J. Chem. Theory Comput.* **2013**, 9, 3084−3095

[84] Oren, A.; *Curr. Opin. Biotechnol.* **2015**, 33, 119–124

[85] Lanyi, J.K.; *Bacteriol. Rev.* **1974**, 38, 3, 272-290

[86] Roberts, M.F.; *Saline system*, **2005**, 1:5

[87] Mokashe, N.; Chaudhari, B.; Patil, U.; *Int. J. Biol. Macromol.* **2018**, 117, 493-522

[88] Poli, A.; Finore, I.; Romano, I.; Gioiello, A.; Lama, L.; Nicolaus, B.; *Microorganisms* **2017**, 5, 25

[89] Ventosa, A.; De la Haba, R.R.; Sánchez-Porro, C.; Papke, R.T.; *Curr. Opin. Microbiol.* **2015**, 25, 80-87

[90] José León, M.; Rodríguez-Olmos, A.; Sánchez-Porro, C.; López-Pérez, M.; Rodríguez-Valera, F.; Soliveri, J.; Ventosa, A.; Copa-Patin, J.L.; *Int. J. Syst. Evol. Microbiol.* **2015**, 65, 4638–4643

[91] León, M.J.; Vera-Gargallo, B.; Sánchez-Porro, C.; Ventosa, A.; *Int. J. Syst. Evol. Microbiol.* **2017**, 66, 4218–4224

[92] León, M.J.; Fernández, A.B.; Ghai, R.; Sánchez-Porro, C.; Rodriguez-Valera, F.; Ventosa, *Appl. Environ. Microbiol.* **2014**, 80, 13, 3850–3857

[93] León, M.J.; Hoffmann, T.; Sánchez-Porro, C.; Heider, J.; Ventosa, A.; Bremer, E.; *Front Microbiol.* **2018**, 9, 108

[94] Ryhage, R.; Stenhagen, E.; *J.Lipid Res*. **1960**, 361-390

[95] Strittmatter, W.; Weckesser, I.J.; Salimath, P.V.; Galanos, C. *J. Bacteriol.* **1983**, 155, 1, 153-158

[96] Di Lorenzo F.; Palmigiano, A.; Al Bitar-Nehme, S.; Sturiale, L.; Duda, K.A.; Gully, D.; Lanzetta, R.; Giraud, E.; Garozzo, D.; Bernadini, M.L.; et al. *Chem. Eur. J.* **2017**, 23, 3637–3647

[97] Krasikova, I.N.; Kapustina, N.V.; Isakov, V.V.; Dmitrenok, A.S.; Dmitrenok, P.S.; Gorshkova, N.M.; Solov'eva, T.F.; *Eur. J. Biochem.* **2004**, 271, 2895–2904

[98] Vorob'eva, E.V.; Dmitrenok, A.S.; Dmitrenok, P.S.; Isakov, V.V.; Krasikova, I.N.; Solov'eva, T.F.; *Russ. J. Bioorganic Chem.* **2005**, 31, 4, 362–371

[99]Zahr, M.; Fobel, B.; Mayer, H.; Imhoff, J.F.; Campos, V.; Weckesser, J.; *Arch. Microbiol*. **1992**, 157, 6, 499-504

[100] Opal, S.M. ; Laterre, P.; Francois, B.; et al. *JAMA.* **2013**, 309,11,1154–1162.

[101] Menes, R.J.; · Viera, C.E.; Farías, M.E.; *Extremophiles*, **2016**, 20, 19–25

[102] Hornung, V.; Rothenfusser, S.; Britsch, S.; Krug, A.; Jahrsdorfer, B.; Giese, T.; Endres, S.; Hartmann, G.; *J. Immunol.* **2002**, 168, 4531–7

[103] Thomas, K.E.; Galligan, C.L.; Newman, R.D.; Fish, E.N. Vogel, S.N.; *J. Biol. Chem.* **2006**, 281, 41, 31119–30

[104] Carillo, S.; Pieretti, G.; Casillo, A.; Lindner, B.; Romano, I.; Nicolaus, B.; Parrilli, M.; Giulian, M.; Cammarota, M.; Lanzetta, R.; Corsaro, M.M. *Extremophiles* **2016**, 20, 287-294

[105] Di Lorenzo, F.; Palmigiano, A.; Paciello, I.; Pallach, M.; Garozzo, D.; Bernardini, M.L.; La Cono, V.; Yakimov, M.M.; Molinaro, A.; Silipo, A. *Mar. Drugs* **2017**, 15, 201

[106] Kumar, A.S.; Mody, K.; Jha, B. *J. Basic. Microbiol.* **2007**, *47*, 103–117

[107] Casillo, A.; Lanzetta, R.; Parrilli, M.; Corsaro, M.M. *Mar. Drugs* **2018**, *16*, 69

[108] Biswas, J.; Paul, A.K. *Biodivers. Int. J.* **2017**, *1*, 2, 32-39

[109] Arias, S.; Del Moral, A.; Ferrer, M.R.; Tallon, R.; Quesada, E.; Béjar, V. *Extremophiles*, **2003**, *7*, 319-326

[110] Poli, A.; Nicolaus, B. ; Denizci, A.A. ; Yavuzturk, B. ; Kazan, D. *Int. J Syst. Evol. Microbiol.* **2013**, *63*, 10-18

[111] Diken, E.; Ozer, T.; Arikan, M.; Emrence, Z.; Öner, E.T.; Ustek, D.; Arga K.Y. *Springerplus*, **2015**, *4*, 393

[112] Öner, E.T.; Hernández, L.; Combie, J. *Biotechnol Adv.* **2016**, *34*, 827-844

[113] Erkorkmaz, B.A.; Kırtel, O.; Duru, O.A.; Öner, E.T. *Bioprocess. Biosyst. Eng.* **2018**, 41, 9, 1247-1259

[114] Bligh, E.G.; Dyer, W.J.; *Can. J. Biochem. Physiol.* **1959**, 37, 6, 911-917

[115] Silipo, A.; Sturiale, L.; Garozzo, D.; De Castro, C.; Lanzetta, R.; Parrilli, M.; Grant, W.D.; Molinaro, A. *Eur. J. Org. Chem.* **2004**, 10, 2263–2271

[116] Sturiale, L.; Palmigiano, A.; Silipo, A.; Knirel, Y.A.; Anisimov, A.P.; Lanzetta, R.; Parrilli, M.; Molinaro, A.; Garozzo, D. *J. Mass. Spectrom.* **2011**, 46, 1135–1142

[117] Piantini, U.; Sorensen, O.W.; Ernst, R.R.; *J. Am. Chem. Soc.* **1982**, 104, 6800–6801

[118] Rance, M.; Sørensen, O.W.; Bodenhausen, G.; Wagner, G.; Ernst, R.R.; Wüthrich, K.; *Biochem. Biophys. Res. Commun.* **1983**, 117, 479–485

[119] States, D.J.; Haberkorn, R.A.; Ruben D.J.; *J. Magn. Reson.* **1982**, 48, 286–292

[120] Stern, A.S.; Li, K.B.; Hoch, J.C.; *J. Am. Chem. Soc*. **2002**, 124 1982–1993